

POLITECNICO DI TORINO

In collaboration with

Ecole Polytechnique Fédérale de Lausanne (EPFL)

Civil Engineering Master

Degree Course

Master Degree Thesis

PERFORMANCE-BASED DESIGN OF ENERGY PILES IN THE FRAMEWORK OF EUROCODES



Thesis Director:

Prof. Chiaia B.M.

Candidate:

Di Bari Francesco

Thesis Supervisors:

Prof. Laloui L.

Prof. Rotta Loria A. F.

A.A. 2018/2019

A mia nonna N.

A mia nonna M.

A mia madre e mio padre.

Acknowledgements

La prima persona che vorrei ringraziare per il suo ruolo cruciale nello sviluppo della mia tesi di laurea è il mio relatore di tesi, il Prof. Bernardino M. Chiaia. Desidero ringraziarlo, in primo luogo, per avermi dato l'opportunità di lavorare in una delle più famose e ambite università come l'Ecole Polytechnique Fédérale de Lausanne (EPFL) e per essermi stato sempre di supporto durante il mio intero progetto.

I would also to thank Prof. Lyesse Laloui for being a very representative point during my period of stay at EPFL with his charismatic personality and the same time with his vast availability.

Un ringraziamento speciale è dedicato al Prof. Alessandro Francesco Rotta Loria, in primis, per la sua costante disponibilità a fornirmi dei chiarimenti ed avere interessanti confronti; in secundis, per aver suscitato in me la passione per il rigore scientifico e per essere stato un modello da seguire durante il mio lavoro in EPFL.

I wish to thank the entire LMS group (Laboratory of Soil Mechanics) for the interesting discussions we had about energy geostructures.

Ringrazio tutta la mia famiglia per essere stata una fonte inesauribile di incoraggiamento ed in particolar modo tenevo a ringraziare mia madre per essermi stata sempre vicina durante tutto il mio percorso di Laurea.

Ringrazio i miei amici storici per essermi stati sempre vicini: Giuseppe, Vincenzo, Roberto, Riccardo, Vincenzo e Francesco. In egual modo tenevo a ringraziare anche il mio gruppo di "avventure" (Nico, Vittorio, Peter, Julia, Chiara e tutti gli altri) per il loro costante supporto.

Ringrazio tutti miei colleghi con cui ho condiviso questo magnifico percorso, che anche da lontano, non hanno mai mancare il loro supporto: Alessio, Loris, Maurizio, Roberto, Nicola, Pierpaolo, Daniele, Gianclaudio, Marco, Carlo, Michele, Giuseppe, Davide e Michele.

Infine, un profondo ringraziamento è dedicato al mio grande amico e collega Fabrizio per avermi supportato e sopportato durante la nostra esperienza, dimostrando sempre estrema comprensione.

Abstract

The use of geostructures with both structural and storage functions for the extraction and storage of heat represents an effective means of satisfying the needs of human activities since ancient times. This master degree thesis focuses on the thermo-mechanical behavior and performance of these innovative and multi-functional technologies that combine the roles for structural support and energy supply of any type of built environment, in particular geothermal piles (or more commonly called "Energy piles"). The multifunctional role of geothermal poles means that both mechanical and thermal loads are applied to these geostructures. This situation represented an unprecedented challenge for engineers because the variations in temperature, stress, deformation and displacement in the subsoil and within the structures themselves, due to the action of thermal loads, must be considered during the analysis, design and verifications. Prior this work, a considerable amount of design procedures had been made available to be able to quantify the mechanical performance of isolated or group energy piles. However, the foundations composed by energy piles are subjected to thermal loads that have led to the birth of new fields of stress and displacement in the structures. In this context (i) limited applications, if available, have been developed to be able to quantify the thermo-mechanical behavior and the performance of the single energy pole subjected to thermal and mechanical loads; (ii) no simplified procedure was available to perform the design of groups of energy piles against the action of such loads; (iii) absence of a complete framework for the reliability of analytical models for general situations (e.g., layered soil); (iv) no simplified procedure that takes into account the long-term action for several years of thermal load.

To address these challenges, this master thesis was carried out to (i) provide a complete and simplified procedure for designing the group of energy piles in accordance with Eurocodes at SLU (e.g., Geotechnical and Structural) and SLE; (ii) provide an important guideline on the reliability of analytical models in a real design situation; (iii) provide clarity on the effects of long-term effects (e.g., stress and displacement fields) during design situations.

The results presented in this thesis suggest the conclusion that (a) the action of thermal load changes considerably the tension and displacement fields within the pile; (b) *on average* the best analytical model to take into account the piles group effect is the Layer model and (c) the long-term actions have an important role during the stress and displacement checks.

Sommario

L'impiego delle geostrutture con funzione sia strutturale che come serbatoi per l'estrazione e l'immagazzinamento del calore rappresenta un mezzo efficace per soddisfare i bisogni delle attività umane fin dai tempi più antichi. Questa tesi di laurea si concentra sul comportamento termo-meccanico e sulle prestazioni di queste tecnologie innovative e multifunzionali che accoppiano i ruoli per il supporto strutturale e l'approvvigionamento energetico di qualsiasi tipo di ambiente costruito, in particolare dei pali geotermici (o più comunemente chiamati "energy piles"). Il ruolo multifunzionale dei pali geotermici comporta che sia carichi meccanici e che termici siano applicati a tali geostrutture. Questa situazione ha rappresentato una sfida senza precedenti per gli ingegneri perché le variazioni della temperatura, dello stress, della deformazione e dello spostamento nel sottosuolo e all'interno delle strutture stesse, dovuti all'azione dei carichi termici, devono essere considerati durante l'analisi, la progettazione e le verifiche. Prima di questo lavoro, era stata messa a disposizione una notevole quantità di procedure progettuali per poter quantificare le prestazioni meccaniche dei pali energetici isolati o in gruppo. Tuttavia, le fondazioni costituite da pali energetici sono sottoposte a carichi termici che hanno portato alla nascita di nuovi campi di sollecitazione e spostamento nelle strutture. In questo contesto (i) limitate applicazioni, se disponibili, sono state sviluppate per poter quantificare il comportamento termo-meccanico e le prestazioni del singolo palo energetico sottoposto a carichi termici e meccanici; (ii) nessuna procedura semplificata era accessibile per eseguire la progettazione di gruppi di pali energetici contro l'azione di tali carichi; (iii) assenza di un quadro completo per l'affidabilità dei modelli analitici per situazioni generali (ad esempio terreno stratificato); (iv) nessuna procedura semplificata che tenga conto dell'azione a lungo termine per diversi anni di carico termico.

Per affrontare tali sfide, questa tesi è stata eseguita per (i) fornire una procedura completa e semplificata per eseguire la progettazione del gruppo di pile energetici in accordo con gli Eurocodici allo SLU (ad es., Geotecnico e strutturale) e SLE; (ii) fornire un'importante linea guida sull'affidabilità dei modelli analitici in una reale situazione progettuale; (iii) fornire chiarezza sugli effetti degli effetti a lungo termine (ad esempio campi di stress e di spostamento) durante le situazioni di progettazione. I risultati presentati in questa tesi suggeriscono la conclusione che (a) l'azione dei carichi termici cambia notevolmente i campi di tensione e spostamento all'interno del palo; (b) *in media* il miglior modello analitico per tener conto dell'effetto di gruppo dei pali è il Layer model e (c) le azioni a lungo termine hanno un ruolo importante durante le verifiche delle tensioni e spostamenti.

Contents

Introduction.....	1
Scope and challenges.....	1
Solution approach.....	2
Chapter 1 – Energy pile: State of art.....	3
1.1 Energy Geostructures.....	3
1.1.1 Description and technology.....	3
1.1.2 Advantages and possible uses.....	5
1.2 The role of thermal load in the energy piles performance.....	6
1.2.1 Effect of thermal loads on the mechanical behavior of energy piles.....	6
1.2.2 Generalized mathematical formulation of vertical energy pile equilibrium.....	8
1.2.3 Thermo-mechanical schemes for energy piles with no base and head restraints.....	9
1.2.4 Thermo-mechanical schemes for energy piles with base or head restraints.....	11
1.2.5 Thermo-mechanical schemes for energy piles with base and head restraints.....	14
Chapter 2 – Case study.....	17
2.1 Site description.....	17
2.2 Materials and properties.....	19
Chapter 3 – Ultimate Limit State (ULS).....	21
3.1 Semi-probabilistic method.....	21
3.1.1 Introduction.....	21
3.1.2 Actions and design situation.....	22
3.1.3 Design Approaches for deep foundation.....	22
3.2 Geotechnical Ultimate Limit State.....	25
3.2.1 Generalized axial capacity formulation.....	25
3.2.2 Capacity in coarse-grained soil.....	28
3.2.3 Capacity in fine-grained soil.....	29
3.2.4 Verification for energy piles group	31
3.2.5 Design proposed for energy piles group	34
3.2.6 Verification for conventional piles group	36

3.2.7 Design proposed for conventional piles group.....	37
3.3 Structural Ultimate Limit State.....	38
3.3.1 Generalized approach for Structural Ultimate State.....	38
3.3.2 Interaction Domain calculation for circular area.....	43
3.3.3 Design for energy piles.....	44
3.3.4 Design proposed for energy piles to ensure ductility.....	45
3.3.5 Design for conventional piles.....	47
3.3.6 Design proposed for conventional piles to ensure ductility.....	48
3.4 Concluding remarks.....	49
Chapter 4 – Serviceability Limit State (SLS).....	50
4.1 Design and verifications in the framework of Eurocodes.....	50
4.2 Single pile.....	51
4.2.1 Modelling choices.....	51
4.2.2 Combinations.....	53
4.2.3 Influence of the slab.....	55
4.3 Eurocodes dispositions for elastic analysis.....	56
4.3.1 General framework of the influence of Cracked Young’s Modulus on the stress field.....	57
4.3.2 General framework of the influence of Cracked Young’s Modulus on the displacement field.....	59
4.3.3 General framework of the influence of nil Poisson ratio on the stress field.....	60
4.3.4 General framework of the influence of nil Poisson ratio on the displacement field.....	61
4.3.5 Maximum stress trend with the depth.....	62
4.3.6 Influence of Cracked Young’s Modulus in the proposed design.....	63
4.3.7 Influence of nil Poisson ratio in the proposed design.....	66
4.3.8 Concluding remarks.....	67
4.4 Serviceability verifications for both design situations.....	68
4.4.1 Tension Limit State.....	68
4.4.2 Tension Limit State for the real design case.....	69
4.4.3 Cracking Limit State.....	70
4.4.4 Cracking Limit State for the real design case.....	75
4.4.5 Deformation Limit State.....	75
4.4.6 Tension Limit State for the proposed design case.....	76

4.4.7 Cracking Limit State for the proposed design case.....	77
4.5 Comparison between both design situations.....	77
4.6 Concluding remarks.....	80

Chapter 5 – Pile group effect.....81

5.1 Introduction.....	81
5.2 Interaction factor concept.....	83
5.2.1 The problem: a group of two energy piles.....	83
5.2.2 Idealization.....	83
5.2.3 The interaction factor.....	85
5.3 The interaction factor method for energy pile groups based on analytical model.....	87
5.3.1 Idealization, hypothesis and considerations.....	87
5.3.2 The solution approach.....	88
5.4 Layer model.....	90
5.4.1 Soil vertical displacement and approximate pile-soil interaction factor.....	90
5.4.2 Receiver pile vertical displacement and corrected pile-soil-pile interaction factor..	92
5.5 Continuous model.....	95
5.5.1 Soil vertical displacement and approximate pile-soil interaction factor.....	95
5.5.2 Receiver pile vertical displacement and corrected pile-soil-pile interaction factor..	97
5.6 Applications, validation and considerations for both design situations.....	98
5.7 Equivalent pier method.....	101
5.7.1 Hypotheses and considerations.....	101
5.7.2 Geometry for equivalent pier.....	103
5.7.3 Homogenized material properties of the equivalent pier.....	104
5.7.4 Modelling choice.....	106
5.7.5 General framework of the influence of the slab in the Equivalent pier method...	107
5.8 3-D FEM solution.....	111
5.8.1 Modelling solution.....	111
5.8.2 Hypotheses and considerations.....	111
5.9 Findings and discussion.....	113
5.9.1 Energy piles.....	113
5.9.2 Conventional piles.....	118
5.9.3 Deformation limit state verification for energy piles group.....	121
5.10 Concluding Remarks.....	123

Chapter 6 – Cyclic Analysis	124
6.1 Introduction.....	124
6.2 Modelling choice.....	124
6.3 Idealization of cyclic design load.....	126
6.4 Findings and discussion.....	127
6.4.1 Displacement trends obtained in the real design case.....	127
6.4.2 Displacement trends obtained in the proposed design case.....	129
6.4.3 Stress field comparisons between the study cases for Configuration I.....	131
6.4.4 Stress field comparisons between the study cases for Configuration II.....	134
6.4.5 Stress field comparisons between the study cases for Configuration III.....	137
6.4.6 Concluding Remarks.....	140
Chapter 7 – Concluding Remarks	141
7.1 Summary.....	141
7.2 General conclusion	143
Bibliography	146
Curriculum vitae.....	149

Introduction

Scope and challenges

This master thesis focuses on the thermo-mechanical performance of an innovative, multifunctional technology that can be used for energy transfer applications as well as for providing structural support to any type of structure, i.e., energy piles. Energy piles couple the structural support role of conventional pile foundation to the role of conventional geothermal heat exchangers in an unprecedented technology. The operation of energy piles can provide reinforcement to soils for supporting any type of superstructure and at the same time can supply energy for (i) heating and cooling purposes to reach comfort levels in the built environment, (ii) the production of hot water for anthropogenic uses, and (iii) prevention of the icing of pavements and decks of infrastructures.

These kind of technology, that harvest renewable geothermal energy, represent one of the most useful and successful solutions to reduce the amount of carbon emission into the atmosphere in order to build a “sustainable environment”. Despite this potential, relatively limited applications of energy piles are currently observed because of several undiscovered features.

The twofold role of energy piles as structural supports and geothermal heat exchangers involves different types of loads, i.e., mechanical loads and thermal loads, applied to such geostructures. These loads pose unprecedented challenges to engineers because they include variations in the temperature, stress, deformation and displacement fields and consequently a change of strengths. These variations govern the thermal and mechanical behaviour and performance of the energy piles, with a strong impact on the energy, geotechnical and structural response of such foundations. This master thesis addresses the first two aspects of the aforementioned problem, taking into account the change of displacement and stress fields during the design verifications.

In this master project, three main challenges have been addressed in the scope of energy piles:

- i. Prior this work, if available, there was a shortage of application of Eurocodes standards, during serviceability condition verifications, which taking into account the thermo-mechanical behavior of the single isolated pile. The first step has been quantified the effects (e.g. stress and displacement fields) related to thermal load for single isolated pile.
- ii. Energy pile foundations do not consist of single isolated pile but of a group of energy piles that function as a structural support and geothermal heat exchangers. There is a large availability of research which shows for conventional piles subjected to only mechanical loads has proven that when

the piles are located sufficiently close to each other, different mechanical behavior of the piles may be expected compared to when the piles are located sufficiently far from each other. The reason for this phenomenon is that group effects and interactions among the piles occur because of the presence and loading (e.g. mechanical) of the neighboring piles. This effect has also been quantified for energy pile groups subjected to thermal load as well as on the potential presence of group effects caused by the coupled loads (thermo-mechanical) applied on the energy piles (Rotta Loria et al. 2017). Prior this work, there was limited knowledge about a real design situation which taking into account the aforementioned effect (pile group effect due to thermal load).

iii. All of the available analysis and design tools have addressed the behavior of single energy piles but not the behavior of energy pile groups, except for the finite element method in some applications. However, although the latter method provides the most rigorous solutions, the computing time and expertise required to run finite element analyses are often considerable and daunting, especially for engineering purposes. The aim of this master thesis is provide an entire simplified design procedure of energy piles group, in according with Eurocodes, in order to avoid problems related to computational time and sophistication of the modelling.

Solution approach

The findings presented in this master thesis are derived from multidimensional numerical analyses coupled with analytical models being careful to Eurocodes standards during Ultimate Limit State and Serviceability Limit State (cf., Figure I).

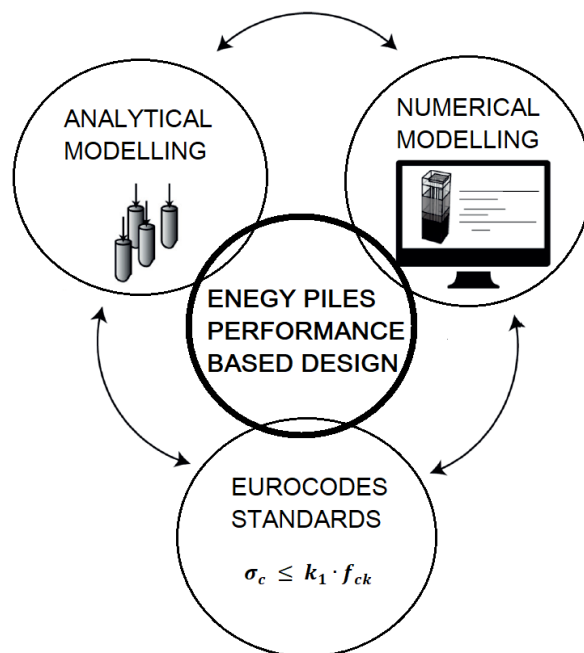


Figure I: Solution approach employed to address challenge of this master thesis

Chapter 1

Energy pile: State of art

1.1 Energy Geostructures

1.1.1 Description of the technology

Energy geostructures, more properly defined in a theoretical sense as thermo-active geostructures and represent an innovative technology that couples the structural support role of conventional structures to the heat exchanger role of shallow geothermal systems. This technology includes all ground-embedded structures that can be used as structural supports while exchanging heat with the ground. Similar to other shallow geothermal systems, energy geostructures work with low enthalpy and exploit the relatively constant temperature field in the superficial subsoil throughout the year for their role as heat exchanger. During the last decades several type of energy geostructures have been developed, in fact in this context deep foundations (e.g., piles, piers), earth retaining structures (e.g., diaphragm walls and sheet pile walls), shallow foundations (e.g., footings, base slabs), tunnel linings and anchors as well as pavements are involved. The resulting geostructures, or the conjunction of support and heat exchanger roles, are so-called energy piles, energy walls, energy slabs, energy tunnels, etc. (Figure 1.1).

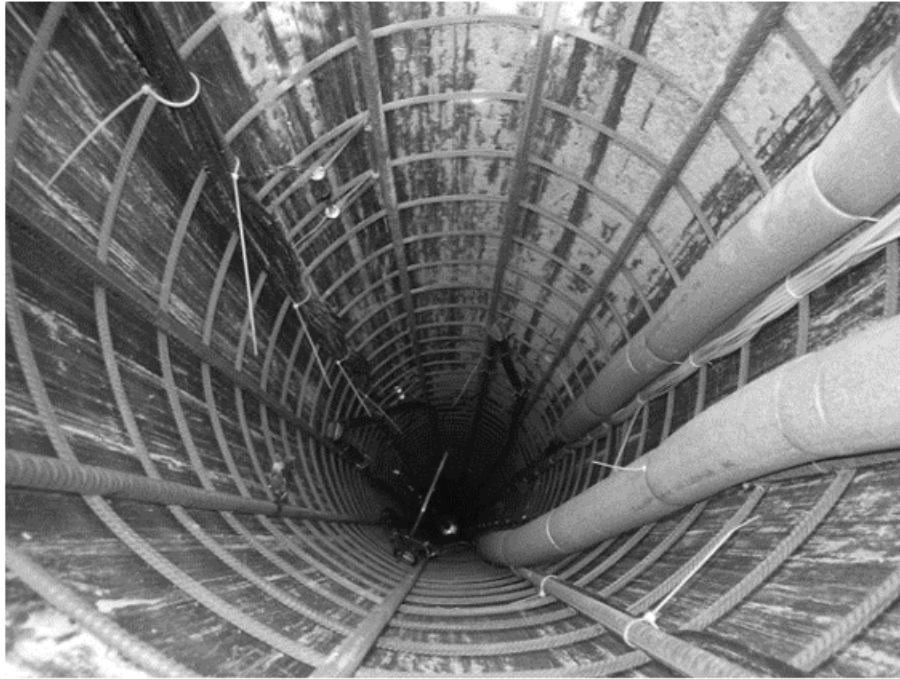


Figure 1.1: Examples of energy piles (Rotta Loria, 2018)

Through these structure several aims can be reached:

- heating and cooling superstructures to reach comfort levels in the built environment;
- contributing to the production of hot water for anthropogenic, agricultural or tank-farming uses;
- providing heat to prevent the icing of pavements and decks of infrastructures such as roads, bridges, station platforms and airport runways.

The employing of energy geostructures for heating and cooling superstructures to reach comfort levels in the built environment can be achieved with a wide number of typologies of energy geostructures, such as energy piles, energy walls, energy slabs and energy tunnels. The use of energy geostructures to provide hot water for anthropogenic purposes can nowadays be achieved based on the lower temperature levels needed for this aim (e.g., 45-55 °C) compared to those needed in constructions built since the 20th century to few decades ago (e.g., 75-85 °C). The most used energy geostructures typologies that can be employed for this purpose, as well as for contributing to the production of hot water for agricultural or tank-farming purposes are energy piles and energy walls. The use of energy tunnels in the vicinity of locations where agricultural or tankfarming activities may be developed is also particularly favorable. The reason for this is that significant amounts of heat, which may be wasted otherwise, can be exchanged with the tunnel environment and the surrounding ground. This heat exchange can be particularly favorable especially when tunnels are characterized

by a significant length or high traffic, and when they are constructed at significant depths or in mountains where noteworthy geothermal gradients are present.

1.1.2 Advantages and possible uses

Similar to other technologies harvesting renewable energy, such as conventional geothermal systems, energy geostructures are an environmentally friendly technology that reduces the need of fossil energy sources and hence the greenhouse gas emissions. For this reason, the use of energy geostructures promotes and respects national and international initiatives, policies, regulations and agreements in order to create multiple beneficial effects.

First of all, an important advantage of energy geostructures must be highlighted: unlike traditional systems of geothermal exchange, energy geostructures also play a role of structural support. This fact entails savings linked to the construction process that could be realized with the separate construction of geostructures and geothermal heat exchangers and coupled thereafter.

Another key difference between energy geostructures and other conventional geothermal systems regard the materials with cui energy geostructures are built: energy geostructures are realized with concrete that has more favorable thermal properties than the filling materials (e.g., bentonite) that constitute conventional geothermal technologies. This peculiarity makes the heat exchange more favorable in the former case compared to the latter. The final difference is that usually the bending radius of the pipes in energy geostructures is greater compared to that characterizing the pipes in conventional geothermal heat exchangers. This features involves a lower flow resistance of the fluid circulating in the pipes, which results in a lower pumping power and, thus, in a lower operation cost. referring to the purposes of the heat exchange that can be established with energy geostructures various are the advantages included with energy geostructures compared to other technological systems. The employing of energy geostructures for heating and cooling superstructures to reach comfort levels in the built environment reduces the environmental impact of any construction and can be exploited to get incentives for the design project and construction of the superstructure. Always referring to the reduction of the environmental impact, the use of energy geostructures for the production of hot water for anthropogenic purposes reduces the costs compared to systems entirely resorting to more conventional technologies. When energy geostructures are employed for contributing to the production of hot water for agricultural or tank-farming uses, cost savings can be achieved via lower operational costs and environmental impacts. The use of energy geostructures for providing heat to prevent the icing of pavements and decks of infrastructures such as roads, bridges, station platforms and airport runways involves reducing the environmental impacts of these

applications because the use of salts or grits is not necessary and numerous disruptions due to this phenomenon.

1.2 The role of thermal load in the energy piles performance

1.2.1 Effect of thermal loads on the mechanical behavior of energy piles

The response of the energy piles subjected upon thermal loads differs from that characterizes conventional piles subjected only to mechanical loads. This response can be idealized within a one-dimensional scheme (Figure 1.2), in which an energy pile of length L and linear thermal expansion coefficient α_{EP} is subjected to a uniform temperature variation ΔT . If an energy pile is free to move both at both at the head and at the base, it is characterized by a thermally induced strain:

$$\varepsilon_f^{th} = -\alpha_{EP}\Delta T \quad (1.1)$$

This thermally induced strain produce a variation in terms of pile length:

$$\Delta L = L' - L = -L\varepsilon_f^{th} = L\alpha_{EP}\Delta T \quad (1.2)$$

where L' is the pile length after the application of the thermal load, (Figure 1.2 (a) and (b)).

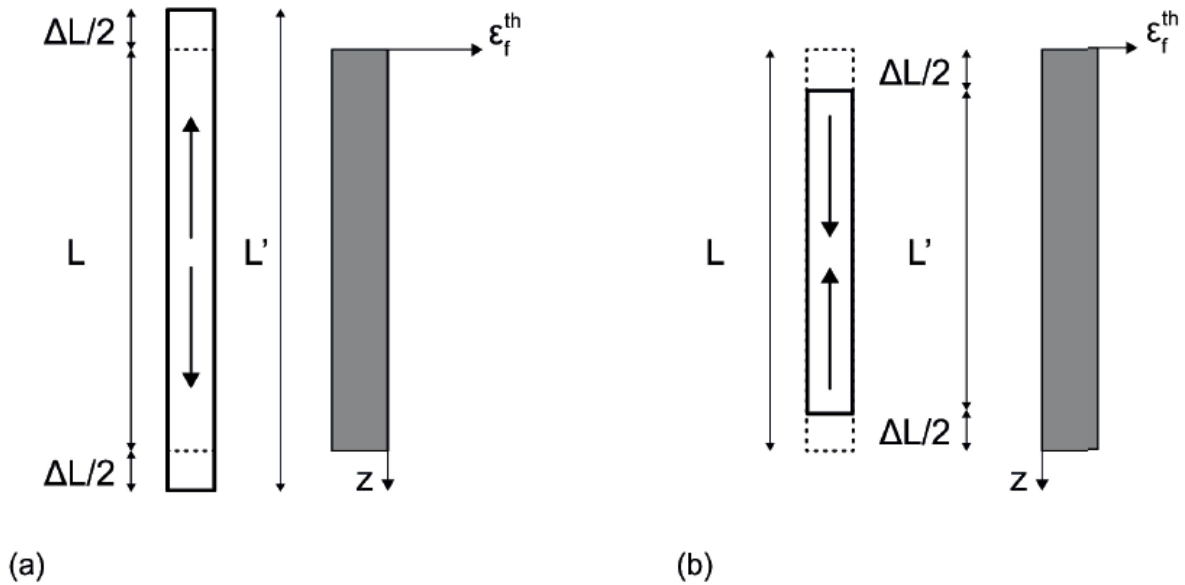


Figure 1.2: Thermally induced strain in the case of thermal action of an energy piles free to deform. Figure 1.2 (a) induced strain due to heating; Figure 1.2 (b) induced strain due to cooling (Rotta Loria, 2018).

Obviously the sign of the length variation is in function of the nature of thermal variation, in fact in the first case (heating) the $\Delta L > 0$, while in the second (cooling) $\Delta L < 0$.

When the thermally induced strain is completely blocked (stuck at the base and at the head) or in other words the pile is not free to deform:

$$\varepsilon_b^{th} = \varepsilon_f^{th} = \alpha_{EP} \Delta T \quad (1.3)$$

and the observed strain is equal to zero:

$$\varepsilon_o^{th} = 0 \quad (1.4)$$

Using the elastic linear relation, there is a thermally induced stress (Figure 1.3 (a) and (b)):

$$\sigma_b^{th} = E_{EP} \varepsilon_b^{th} = E_{EP} \alpha_{EP} \Delta T \quad (1.5)$$

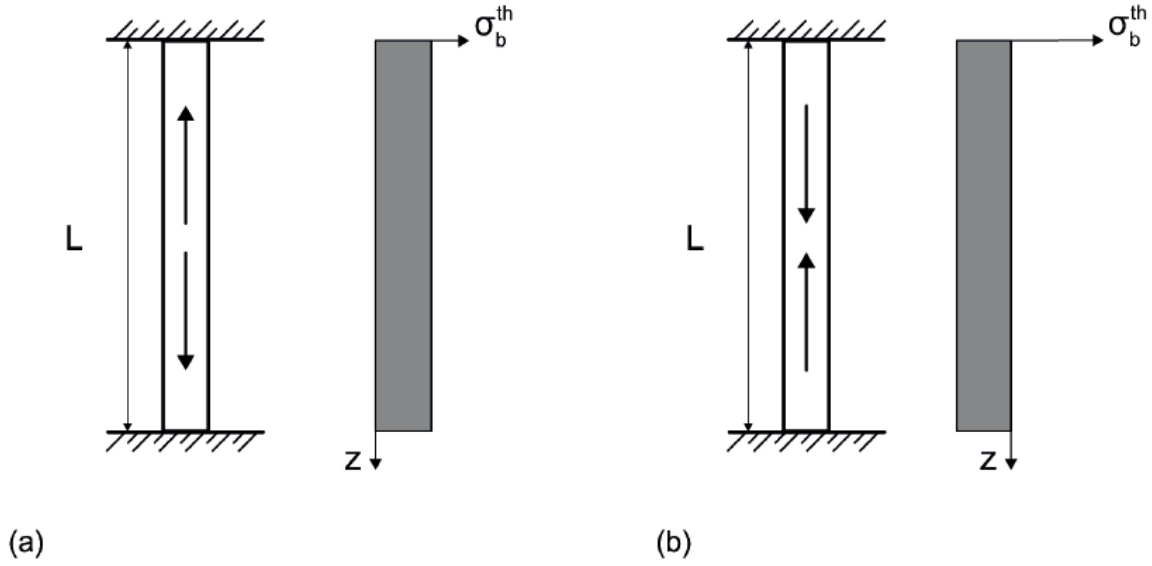


Figure 1.3: Thermally induced stress in the case of thermal action of an energy piles stuck both at the base and at the head. Figure 1.3 (a) induced stress due to heating; Figure 1.3 (b) induced stress due to cooling (Rotta Loria, 2018).

In reality, energy piles are not free to deform because of the presence of surrounding soil and superstructure or of the pier cap (or commonly called slab), hence, the observed strain:

$$\varepsilon_o^{th} \leq \varepsilon_f^{th} \quad (1.6)$$

and this implies that only a part of the strain is blocked.

$$\varepsilon_b^{th} = \varepsilon_o^{th} - \varepsilon_f^{th} \quad (1.7)$$

In the other words, the response of energy piles is governed by a certain degree of freedom, defined as (Rotta Loria, 2018):

$$DOF = \frac{\varepsilon_o^{th}}{\varepsilon_f^{th}} \quad \text{with} \quad 0 \leq DOF \leq 1 \quad (1.8)$$

Using the previous equation (1.8), the thermally induced stress can be calculated as:

$$\sigma_o^{th} = E_{EP}\varepsilon_b^{th} = E_{EP}(\varepsilon_o^{th} - \varepsilon_f^{th}) = E_{EP}(\varepsilon_o^{th} + \alpha_{EP}\Delta T) = E_{EP}\alpha_{EP}\Delta T(1 - DOF) \quad (1.9)$$

The schemes proposed above refers implicitly to energy piles embedded in typical soil deposits for which the soil-pile thermal expansion coefficient ratio is more than one:

$$X = \alpha_{soil}/\alpha_{EP} \leq 1 \quad (2.0)$$

where α_{soil} is the linear thermal expansion coefficient of the soil. In rare cases where

$$X = \alpha_{soil}/\alpha_{EP} > 1 \quad (2.1)$$

and typically at successive stages of geothermal operations, the temperature variation applied to an energy pile and its thermal expansion coefficient do not satisfy the equation (1.6) and consequently:

$$\varepsilon_o^{th} > \varepsilon_f^{th} \quad (2.2)$$

The previous condition occurs because when the linear thermal expansion coefficient of the soil is greater than that of the energy pile, the thermally induced deformation of energy piles is governed by that of the soil rather than by the deformation of the piles. As the temperature changes in the soil regions, this phenomenon becomes more pronounced (Rotta Loria, 2018).

1.2.2 Generalized mathematical formulation of vertical energy pile equilibrium

The general equilibrium equation that govern the vertical equilibrium of energy piles is:

$$P + \frac{\pi D^2}{4} K_h w(z=0) + W + Q_{s,mob} + Q_{b,mob} = 0 \quad (2.3)$$

where P is the applied mechanical load, K_h is the head stiffness of the superstructure or pier cap, $w(z=0)$ is the pile vertical head displacement (with z being the vertical coordinate), W is the pile weight, $Q_{s,mob}$ is the mobilized shaft capacity and $Q_{b,mob}$ is the mobilized base capacity. For a benefit of safety, the pile weight is often neglected in practical analyses and designs.

In case of energy piles mechanical and thermal loads are applied in conjunction, both $Q_{s,mob}$ and $Q_{b,mob}$ can be written in terms of mechanical and thermal contributes:

$$Q_{s,mob} = Q_{s,mob}^m + Q_{s,mob}^{th} \quad (2.4)$$

$$Q_{b,mob} = Q_{b,mob}^m + Q_{b,mob}^{th} \quad (2.5)$$

Energy piles subjected upon thermal load are generally characterized by two portions that displace in opposite directions from the so-called null point of the vertical displacement (located at a depth, $Z_{NP,w}$). Consequently, to ensure equilibrium with the surrounding soil from the so-called null point of the shear stress (generally located at a different depth, $Z_{NP,\tau}$, of that of the vertical displacement), the τ are mobilized in opposite directions at the pile shaft (Rotta Loria, 2018). Referring to what has just been explained the part of the shaft capacity mobilized by the thermal load, $Q_{s,mob}^{th} = Q_{s,mob,up} + Q_{s,mob,down}$, can also be written in terms of two contributions:

$$Q_{s,mob,up} = \pi D \int_0^{Z_{NP,\tau}} \tau dz \quad (2.6)$$

$$Q_{s,mob,down} = \pi D \int_{Z_{NP,\tau}}^L \tau dz \quad (2.7)$$

1.2.3 Thermo-mechanical schemes for energy piles with no base and head restraints

The response of an energy pile free to move in both direction (without both base and head restraints) subjected to an axial mechanical load, a heating or cooling thermal load, is pictured in the Figures 1.4 and Figure 1.5. In the Figure 1.6 the total response of an energy pile subjected to an axial mechanical load in conjunction with both heating thermal and cooling thermal load has been represented. To have a generic idea of the problem, these schemes are referred to an energy piles free at their head and embedded in soft soil that provides negligible end-bearing capacity.

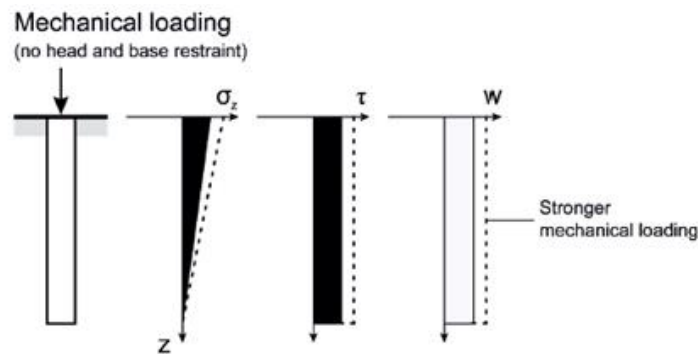


Figure 1.4: Scheme for energy piles free to move both at the head and at the base subjected to mechanical load (Rotta Loria, 2018).

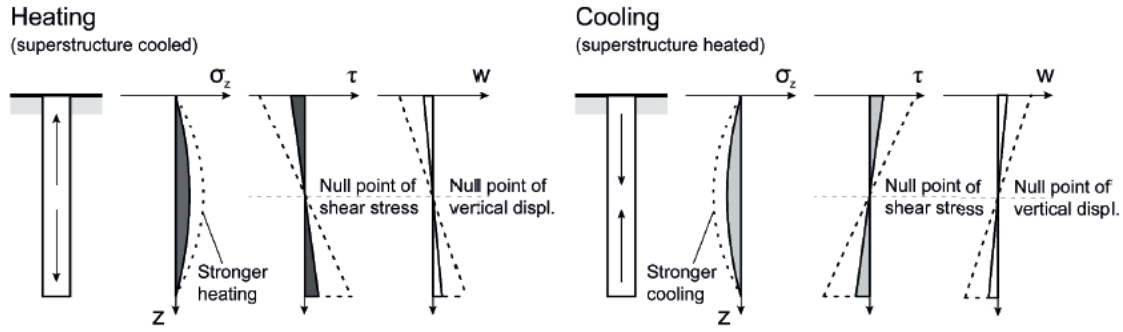


Figure 1.5: Schemes for energy piles free to move both at the head and at the base subjected to thermal load (Rotta Loria, 2018).

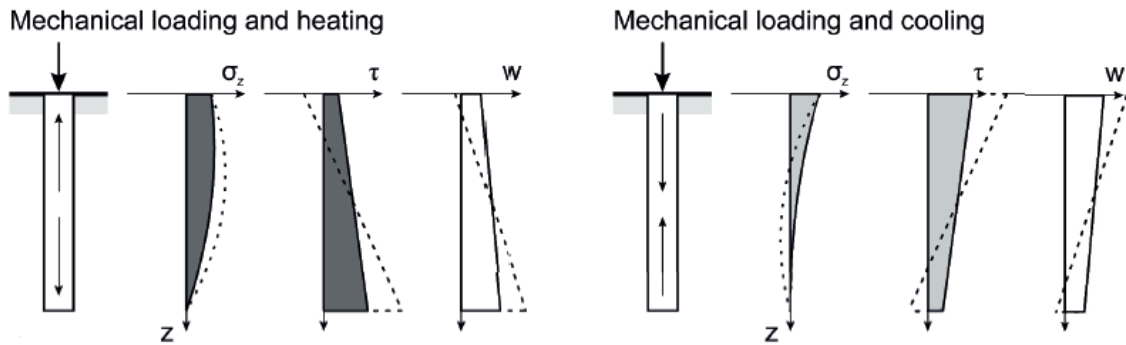


Figure 1.6: Schemes for energy piles free to move both at the head and at the base subjected to mechanical load coupled with heating thermal load (Rotta Loria, 2018).

In the Figure 1.4 are represented the schemes related to normal and tangential stress and vertical displacement for energy piles subjected only to mechanical load. In this case the equation (2.3) can be written as:

$$P + Q_{b,mob}^m = 0 \quad (2.8)$$

The application of an axial mechanical load to the pile head causes a roughly linearly decreasing distribution of compressive vertical stress σ_z within the pile and uniform and roughly constant distributions of positive shear stress τ at the pile-soil interface and downward pile displacement w with depth. As the value of the stiffness of the pile becomes increasingly higher, the distribution of the σ_z becomes more and more uniform and linear; while the distribution of τ and displacements (w) becomes more and more constant and uniform. In the Figure 1.5 are shown the schemes related to normal and tangential stress and vertical displacement for energy piles subjected only to thermal load and in this case the equation (2.3) can be written as (Rotta Loria, 2018)

$$Q_{s,mob}^{th} = Q_{s,mob,up} + Q_{s,mob,down} \quad (2.9)$$

In the previous equation the terms related to mechanical response are neglected because are nil. The application of a heating or cooling thermal load to the pile causes a non-linear distribution of σ_z along the pile length and symmetrical for heating and cooling, which is characterized by a maximum that coincides with the mid-length of the energy pile, where the null points of the vertical displacement and shear stress are also located. The application of a heating thermal load produce negative shear stress and causes an upward shift for the energy pile portion above the null points, while it produces positive shear stress and causes downward shift for the pile portion below the null points. The shear stress and vertical displacement caused by a heating thermal load develop in the opposite direction compared to those caused by a mechanical load above the null points, whereas these develop in the same direction below the null points. The opposite situation occurs in the case of application of cooling thermal load. Shear stress and vertical displacement evolve approximately linearly the pile length. Resuming the aforementioned relation between the pile stiffness and σ_z , τ and w : as the value of the stiffness of the pile becomes increasingly higher, the distribution of σ_z with the depth becomes more uniform with a lower variation for the same applied thermal load. At the same time, as the value of the stiffness of the pile becomes increasingly higher, the trends of τ and w becomes more uniform, but with the higher variation. Stronger thermal loads cause linearly greater stress and displacement variations.

In the Figure 1.6 are pictured the schemes related to normal and tangential stress and vertical displacement for energy piles subjected to an axial mechanical load in conjunction with thermal load. In this case the equation (2.3) can be written as:

$$P + Q_{s,mob} = P + Q_{s,mob}^m + Q_{s,mob}^{th} = 0 \quad (3.0)$$

The distributions of vertical stress and shear stress with depth as well as of vertical displacement can be obtained via superposition of the previous ones. The nature of the total stress along the pile length can be traction when a low mechanical loads and significant cooling thermal load are applied.

1.2.4 Thermo-mechanical schemes for energy piles with base or head restraints

The response of an energy pile with base or head restraints subjected to an axial mechanical load, a heating thermal load have been pictured in the Figures 1.7 and 1.8. In the Figure 1.9 the response of an energy piles with base or head restraints to an axial mechanical load coupled with heating thermal load, obtained from the application of the principle of superposition effects. The base restraint condition may be assumed to characterize energy piles free at their head and bearing on very stiff soil that provides notable end-bearing capacity, not valuable with the conventional formulations. Base

restraint condition may be assumed to characterize energy piles, with a slab at their head, embedded in a soft soil that provides negligible end-bearing capacity (floating piles).

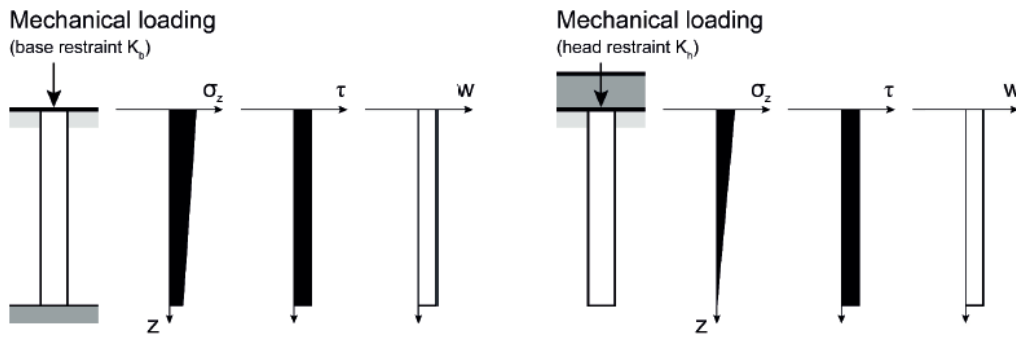


Figure 1.7: Schemes for energy piles with a base or head restraint subjected to mechanical load (Rotta Loria, 2018).

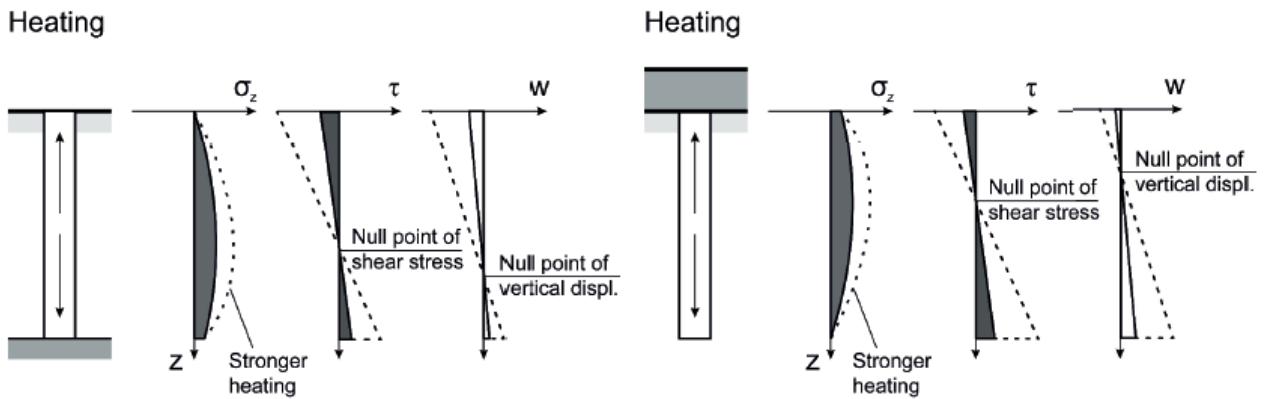


Figure 1.8: Schemes for energy piles with a base or head restraint subjected to thermal load (Rotta Loria, 2018).

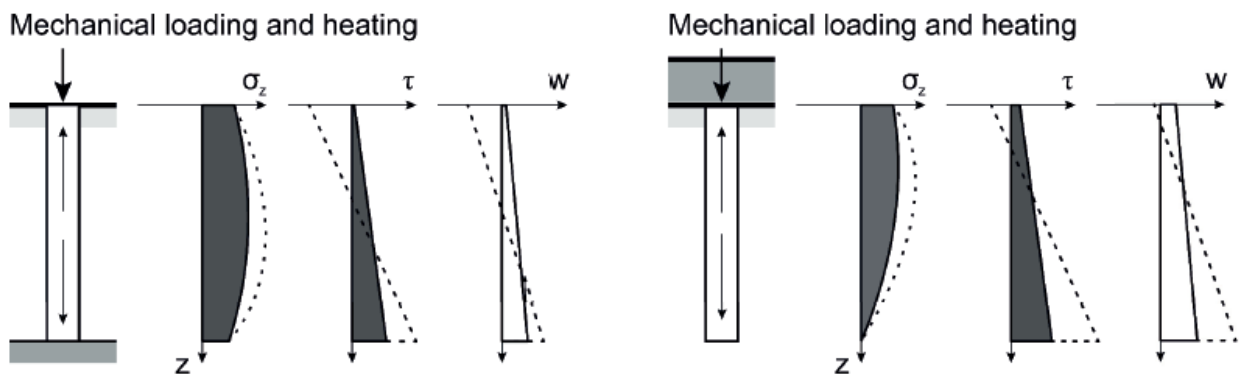


Figure 1.9: Schemes for energy piles with a base or head restraint subjected to mechanical load coupled with heating thermal load (Rotta Loria, 2018).

In the Figure 1.7 are shown the schemes related to normal and tangential stress and vertical displacement for energy piles subjected only to mechanical load. In this case the equation (2.3) can be written as:

$$P + Q_{s,mob}^m + Q_{s,mob}^{th} = 0 \quad (3.1)$$

where only the base restraint is present, whereas

$$P + \pi \frac{D^2}{4} K_h w^m(z=0) + Q_{s,mob}^m = 0 \quad (3.2)$$

where only the head restraint is present.

When a base restraint is present, as the average vertical stress σ_z increases (with a value corresponding to P at the pile head) and the values of shear stress τ and vertical displacement w become lower along the pile length compared to the case of no base and head restraints. This phenomenon arises because of the contribution provided by the base capacity to the vertical pile equilibrium. In these schemes, the base capacity mobilizes at the same time as the shaft capacity for any magnitude of applied load, even though this is not necessarily the case in reality.

When a head restraint is present, the values of the average vertical stress σ_z , the shear stress and vertical displacement variations develop along the pile are smaller compared to the case of no base and head restraints. This phenomenon arises because the head restraint reduces the effect of the downward mechanical load. This effect becomes equal to zero when the interplay between the mechanical load and the head restraint is not considered because the latter term is neglected. The consequence of such an approach is a pile response to mechanical loading equal to that of the case of no base and head restraints (equations (2.3) and (3.2) coincides).

The Figure 1.8 represents the schemes related to normal and tangential stress and vertical displacement for energy piles subjected only to thermal load. In this case the equation (2.3) can be written as:

$$Q_{s,mob}^{th} + Q_{b,mob}^{th} = 0 \quad (3.3)$$

where only the base restraint is present, whereas

$$\pi \frac{D^2}{4} K_h w^{th}(z=0) + Q_{s,mob}^{th} = 0 \quad (3.4)$$

where only the head restraint is present.

Differently from the situation described in the previous chapter (in the case energy piles without restraints both at the head and at the base), when either a base or head restraint is present, vertical stress σ_z is generated at the restrained pile end by the applied thermal load. The vertical stress distribution is greater than that in the case without both base and head restraints, according to the discussed effect of the higher restraint of the system. The null points of the vertical displacement and

shear stress do not coincide but are shifted towards the region of the system characterized by the higher restraint. The vertical displacement developed towards the region of the pile characterized by higher restraint is lower, while a higher displacement is developed towards the region characterized by lower restraint compared to the case where the null points are located at the mid-length of the pile. A cooling thermal load yields a symmetrical response of the energy pile. In reality, the reduction of the compressive stress experienced at the pile toe for the case where a base restraint can reach at most the sum of any vertical mechanical load applied to the pile and its weight. This phenomenon occurs because soils generally cannot withstand tensile stress.

The Figure 1.9 shows the schemes related to normal and tangential stress and vertical displacement for energy piles subjected to an axial mechanical load in conjunction with thermal load. In this case the equation (2.3) can be written as:

$$P + Q_{s,mob}^m + Q_{s,mob}^{th} = 0 \quad (3.5)$$

where only the base restraint is present, whereas

$$P + \pi \frac{D^2}{4} K_h w(z = 0) + Q_{s,mob} = 0 \quad (3.6)$$

where only the head restraint is present.

The total response (Figure 1.9) of energy piles can be obtained by the application of the principle of superposition effects.

1.2.5 Thermo-mechanical schemes for energy piles with base and head restraints

The response of an energy pile with both base and head restraints subjected to an axial mechanical load, a heating thermal load is depicted in the Figures 1.10 and 1.11.

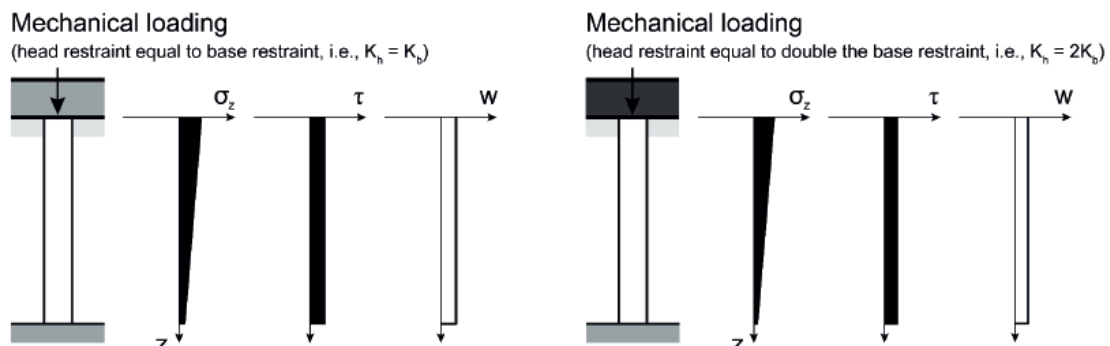


Figure 1.10: Schemes for energy piles with a base and head restraint subjected to mechanical load (Rotta Loria, 2018).

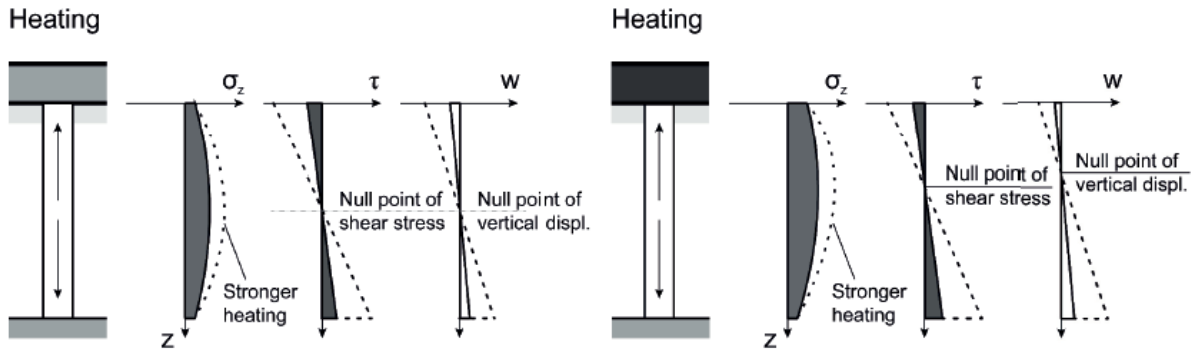


Figure 1.11: Schemes for energy piles with a base and head restraint subjected to thermal load (Rotta Loria, 2018).

In the Figure 1.12 the response of an energy pile with both head and base restraint subjected to mechanical load in conjunction with heating thermal load has been reported.

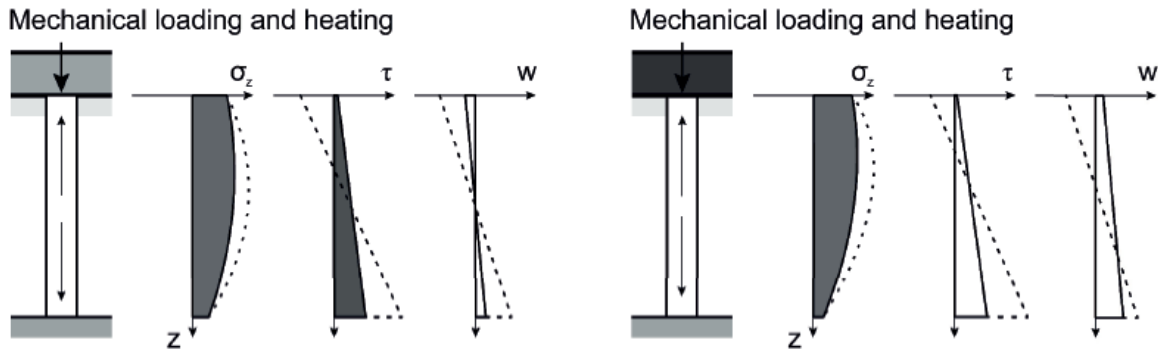


Figure 1.12: Schemes for energy piles with a base and head restraint subjected to mechanical load coupled with heating thermal load (Rotta Loria, 2018).

The previous situation may be assumed to characterize energy piles, with a slab at their head, bearing on stiff soil that provides great end-bearing capacity. Two different cases involving a base restraint equal to the head restraint and a base restraint equal to one-half of the head restraint are considered.

In the case of energy pile subjected only to mechanical load (Figure 1.10), the equation (2.3) can be written as

$$P + \pi \frac{D^2}{4} K_h w^m(z=0) + Q_{s,mob}^m + Q_{b,mob}^m = 0 \quad (3.7)$$

In the proposed schemes, the effect of the presence of the slab on the influence of the mechanical load on the pile response is considered. Hence, lower developments of vertical stress and shear stress as well as of vertical displacement are observed for a higher head restraint, compared to the case of a base restraint only. This behavior may be expected in reality. However, many analyses and designs

usually do not account for the interplay between the action of the mechanical load and the head restraint, neglecting the latter term.

For the case of thermal loading only (Figure 1.11) equation (2.3) can be written as

$$\pi \frac{D^2}{4} K_h w^{th}(z=0) + Q_{s,mob}^{th} + Q_{b,mob}^{th} = 0 \quad (3.8)$$

The distribution of vertical stress σ_z caused by the thermal load is symmetrical along the pile length when the base and head restraints are of the same entity, whereas this distribution is asymmetrical when different magnitudes characterize the end restraints. Higher stress develops towards the region of the system characterized by higher restraint. The higher the restraint provided by the end conditions, the higher the vertical stress and the lower the mobilized shear stress and vertical displacement. The total response (Figure 1.12) of energy piles can be obtained by the application of the principle of superposition effects.

Concluding, this aim of this introductory chapter is that to provide a simplified reference models to explain what happens in the various situations that will then be used in the following chapters.

Chapter 2

Case study

2.1 Site description

The Energy Piles Group Experiment under the Swiss Tech Convention Center of EPFL is full-scale experiment dedicated to the study of group effects within a group of heat exchanger piles. This site was used by Rotta Loria for the in situ experiments collected in his doctoral thesis. The pile foundation that was considered for the entire master thesis is located under the recently built Swiss Tech Convention Centre, Lausanne, Switzerland (cf., Figure 2.1).

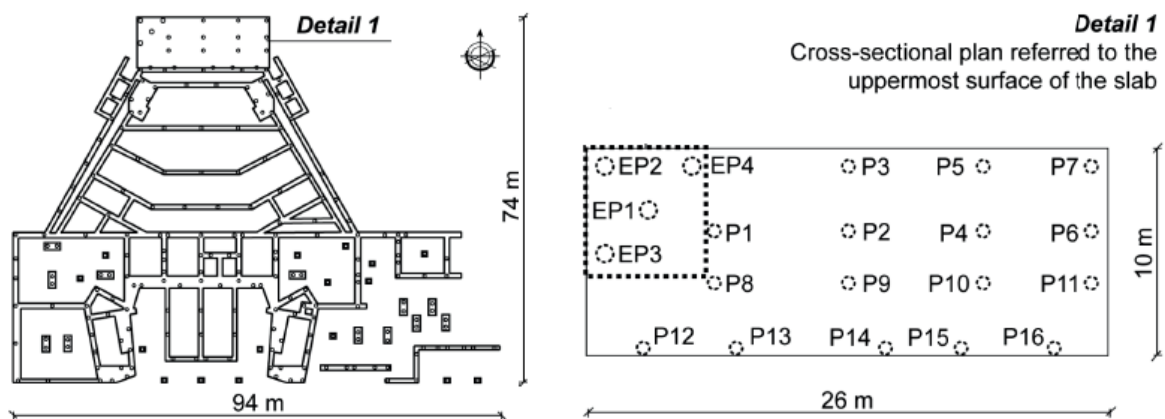


Figure 2.1: Plan view of the EPFL Swiss Tech Convention Center (Rotta Loria, 2018).

The foundation supports a $9 \times 25 \text{ m}^2$ water retention tank and comprises a group of four predominantly end-bearing energy piles (uncalled EP1, EP2, EP3 and EP4 in Figure 2.2) and sixteen predominantly floating conventional piles (uncalled P1-16 in Figure 2.1) below a heavily reinforced 0.9 m-thick slab.

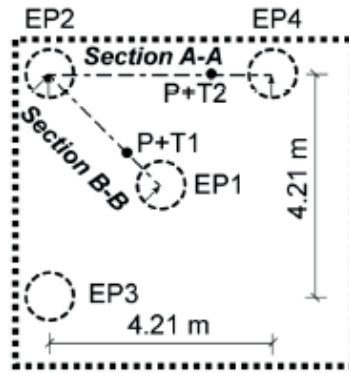


Figure 2.2: Top view of experimental site (Rotta Loria, 2018).

In plan view, the energy piles form a triangle within a 4.21 m square in which the central pile, EP1, is located 3 m from the others, EP2, 3 and 4 (Figure 2.4). The energy piles are 28 m long and 0.9 m in diameter, and the conventional piles are 16 m long and 0.6 m in diameter. All of the piles were bored, cast onsite and are made of reinforced concrete. Vertical loads of 0, 800, 2200 and 2100 kN are applied to energy piles EP1, 2, 3 and 4, respectively. Vertical loads of 300 kN are applied to each of the conventional piles. The values of vertical loads are characteristic values that were calculated by the company involved in the geotechnical and structural designs of the foundation. Throughout the design process, these loads were considered as imposed on the uppermost surface of the slab in correspondence with the area delimited by the cross-sectional surface of the underlying piles. This loading situation is considered in this work (as in that presented by Rotta Loria, 2018).

The energy piles were equipped with four 24-m-long high-density polyethylene U-loops that are connected in series. The inlets and outlets of the absorber pipes were thermally insulated to a depth of 4 m below the pile heads to limit the influence of the climatic conditions on the heat exchange process (Figure 2.3).

The soil stratigraphy of the site (Figure 2.4) was extrapolated based on information that was obtained during the construction of the foundation and data from Rotta Loria (Rotta Loria, 2018) for experimental tests in situ presented in his doctoral thesis (Rotta Loria, 2018). The presented site is located 200 m away, at the Swiss Federal Institute of Technology in Lausanne (EPFL). During the construction of the piles, the groundwater table was located at the top of the deposit, which is estimated to be in an overconsolidated condition. Layers of alluvial soil and sandygravelly moraine were encountered at shallow depths. The upper soil profile of the alluvial soil was inferred to reach a

depth from the uppermost surface of the successively built slab of $z = 8.6$ m. The lower sandy-gravelly moraine layer was located between depths of $z = 8.6$ and 16.6 m (Rotta Loria, 2018). A thin layer of bottom moraine was present below the sandy-gravelly moraine layer between depths of $z = 16.6$ and 20.1 m and laid on a molasse layer. The energy piles were socketed 8.8 m into this bottom molasse layer from a depth of $z = 20.1$ m to a depth of $z = 28.9$ m.

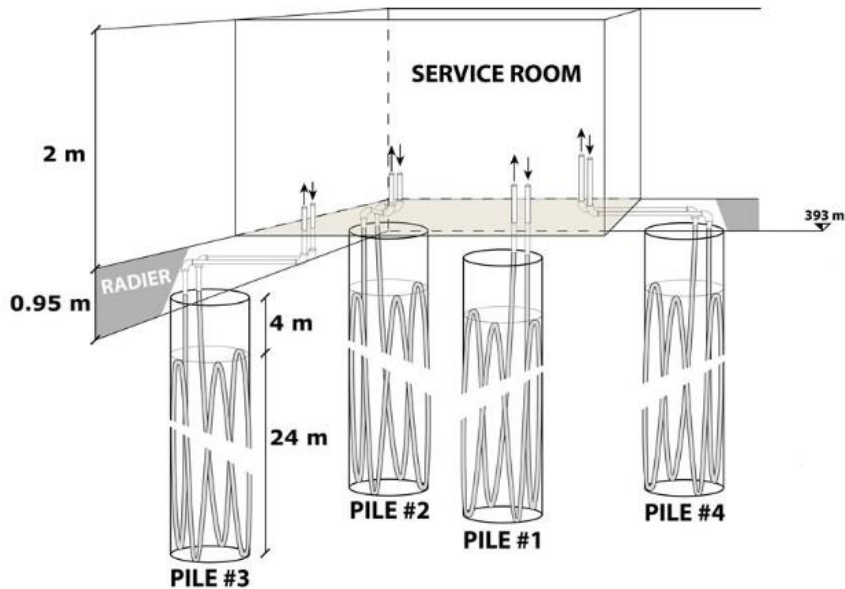


Figure 2.3: Schematic view of the heat exchanger test piles, service room (<https://lms.epfl.ch>)

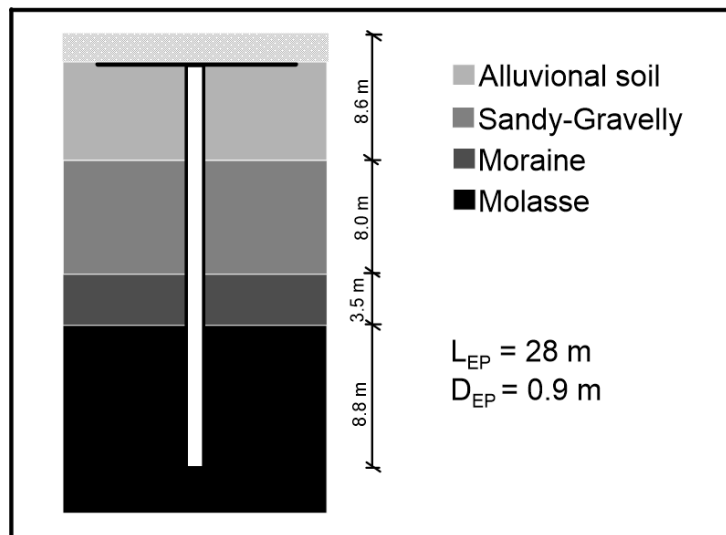


Figure 2.4: Schematic view of the local stratigraphy.

2.2 Materials and properties

Following tables (from Table 2.1 to Table 2.7) summaries all the property of the aforementioned elements of case study (e.g. piles, slab and stratigraphy):

ρ [kg/m ³]	E [MPa]	ν [-]	k [W/(mK)]	C_p [J/(kg * K)]	α [1/K]	L [m]	D [m]
2722	36000	0.20	1.628	837	$1 \cdot 10^{-5}$	28	0.9

Table 2.1: Energy Piles properties (Rotta Loria, 2018)

ρ [kg/m ³]	E [MPa]	ν [-]	k [W/(mK)]	C_p [J/(kg * K)]	α [1/K]	L [m]	D [m]
2722	31500	0.20	1.628	837	$1 \cdot 10^{-5}$	16	0.6

Table 2.2: Conventional Piles properties (Rotta Loria, 2018)

ρ [kg/m ³]	E [MPa]	ν [-]	k [W/(mK)]	C_p [J/(kg * K)]	α [1/K]	L [m]	B [m]
2722	31500	0.20	1.628	837	$1 \cdot 10^{-5}$	26	10

Table 2.3: Slab properties (Rotta Loria, 2018)

ρ [kg/m ³]	E [MPa]	ν [-]	k [W/(mK)]	C_p [J/(kg * K)]	α [1/K]	z [m]
2769	190	0.22	1.49	880	$3.3 \cdot 10^{-6}$	8.6

Table 2.4: Layer A properties (Rotta Loria, 2018)

ρ [kg/m ³]	E [MPa]	ν [-]	k [W/(mK)]	C_p [J/(kg * K)]	α [1/K]	L [m]
2735	84	0.4	3.68	890	$3.3 \cdot 10^{-6}$	8

Table 2.5: Layer B properties (Rotta Loria, 2018)

ρ [kg/m ³]	E [MPa]	ν [-]	k [W/(mK)]	C_p [J/(kg * K)]	α [1/K]	L [m]
2740	90	0.4	3.46	890	$3.3 \cdot 10^{-6}$	3.5

Table 2.6: Layer C properties (Rotta Loria, 2018)

ρ [kg/m ³]	E [MPa]	ν [-]	k [W/(mK)]	C_p [J/(kg * K)]	α [1/K]	L [m]
2167	3000	0.3	3.82	923	$0.23 \cdot 10^{-4}$	8.8

Table 2.7: Layer D properties (Rotta Loria, 2018)

Chapter 3

Ultimate Limit State (ULS)

The action of thermal loads, in conjunction with that of mechanical loads, due to their geothermal and structural support operations, represents a significant challenge. To provide a complete and clear design framework at Ultimate Limit State (ULS), we must clarify that in both Geotechnical and Structural Ultimate Limit State *the effects of thermal loads at ULS can be neglected and can be considered relevant only at serviceability limit states* (Rotta Loria, 2018).

After a brief description of the main aspects of energy piles in the Chapter 1, in according with Eurocodes 7 that provide all standards both from geotechnical and structural perspective, in this chapter the fundamental aspects that regard the energy piles design at Ultimate Limit State (ULS) have been taken into account.

3.1 Semi-probabilistic method

3.1.1 Introduction

The semi-probabilistic method at Limit States already long proposed and widely used for design situations and structural verifications represent, nowadays, the best tool to use during design case. In according with semi-probabilistic method at ULS, the verification in safety of a structural element is satisfied when, section by section, occurs:

$$E_d \leq R_d \tag{3.9}$$

where

- E_d represent the design loading given by the acting forces F_{dj} on the structure, evaluated in function of their own characteristic values and increased by combination factors:

$$F_{dj} = F_{kj} \cdot \gamma_{Fj} \quad (4.1)$$

- R_d represent the calculation value of resisting force developed by the materials constituting the section obtained by the application of combination factors that reduce the values in order to ensure the prefixed safety grade:

$$R_d = \frac{R_{ki}}{\gamma_{Mi}} \quad (4.2)$$

This expression applies to the following ultimate limit states:

- GEO: ‘Failure or excessive deformation of the ground, in which the strength of soil or rock is significant in providing resistance’
- STR: ‘Internal failure or excessive deformation of the structure or structural elements ... in which the strength of structural materials is significant in providing resistance’

3.1.2 Actions and design situation

In according with Eurocode 7 and EN 1990 there are three types of action summaries in the following Table 3.1:

<i>Action</i>	<i>Duration</i>	<i>Examples</i>
Permanent (G)	Likely to act throughout reference period	Self-weight of structures
Variable (Q)		Imposed loads on building floors, beams and roofs; wind*; snow*
Accidental (A)	Usually short	Explosions, vehicle impact*, seismic* (AE, due to earthquake ground motions)

*may be variable or accidental depending on statistical distribution

Table 3.1: Classification of actions (EN 1990).

3.1.3 Design Approaches for deep foundation

According Eurocode 7, Ultimate Limit State (ULS) verifications are carried out with the three possible Design Approaches:

- DA1 – Combination 1: A1 + M1 + R1
- DA1 – Combination 2: A2 + “M1 or M2” + R4 (*)
- DA2: A1 + M1 + R2

- DA3: $A1$ or $A2 + M2 + R3$ (**)

(*) M1 is used for structural actions, instead M2 for that of geotechnical;

(**) A1 is used for structural actions, instead A2 for that of geotechnical;

Where in the latter Design Approach A1 is used for structural actions and A2 is used for those of geotechnical. The factors aforementioned are referred to:

- A1 and A2 are used to symbolize the partial factors on actions;
- R1, R2, R3 and R4 are used to symbolize the partial resistance factors;
- M1 and M2 are used for symbolize the partial factors for soil parameters.

In the following tables (from Table 3.2 to Table 3.5) are summarized the aforementioned factors:

<i>Action</i>		<i>Symbol</i>	<i>A1</i>	<i>A2</i>
Permanent	Unfavourable	γ_G	1.35	1.0
	Favourable		1.0	1.0
Variable	Unfavourable	γ_Q	1.5	1.3
	Favourable		0	0

Table 3.2: Partial factors on the actions (Eurocode 7).

<i>Resistance</i>	<i>Symbol</i>	<i>R1</i>	<i>R2</i>	<i>R3</i>	<i>R4</i>
Base	γ_b	1.00	1.10	1.00	1.30
Shaft (Compression)	γ_s	1.00	1.10	1.00	1.30
Total combined (Compression)	γ_t	1.00	1.10	1.00	1.30
Shaft (Tension)	$\gamma_{s,t}$	1.25	1.15	1.10	1.60

Table 3.3: Partial factors for resistance for driven piles (Eurocode 7).

<i>Resistance</i>	<i>Symbol</i>	<i>R1</i>	<i>R2</i>	<i>R3</i>	<i>R4</i>
Base	γ_b	1.10	1.10	1.00	1.45
Shaft (Compression)	γ_s	1.00	1.10	1.00	1.30
Total combined (Compression)	γ_t	1.10	1.10	1.00	1.40
Shaft (Tension)	$\gamma_{s,t}$	1.25	1.15	1.10	1.60

Table 3.4: Partial factors for resistance for Continuous flight auger (CFA) piles (Eurocode 7).

<i>Resistance</i>	<i>Symbol</i>	<i>R1</i>	<i>R2</i>	<i>R3</i>	<i>R4</i>
Base	γ_b	1.25	1.10	1.00	1.60
Shaft (Compression)	γ_s	1.00	1.10	1.00	1.30
Total combined (Compression)	γ_t	1.15	1.10	1.00	1.50
Shaft (Tension)	$\gamma_{s,t}$	1.25	1.15	1.00	1.60

Table 3.4: Partial factors for resistance for bored piles (Eurocode 7).

<i>Soil Parameter</i>	<i>Symbol</i>	<i>M1</i>	<i>M2</i>
Weight density	γ_γ	1.00	1.00
Effective Cohesion	γ_c	1.00	1.25
Tangent of shear resistance	γ_ϕ	1.00	1.10
Undrained shear strength	γ_{cu}	1.00	1.4
UCS	γ_{qu}	1.00	1.4

Table 3.5: Partial factors for soil parameters (Eurocode 7).

3.2 Geotechnical Ultimate Limit State

3.2.1 Generalized axial capacity formulation

To estimate the response of single energy piles subjected to the mechanical load and perform the verification we need to clarify some aspects related with the base and shaft capacity of the piles. From general perspective the load capacity of the pile is equal to:

$$Q_u = Q_b + Q_s - W \quad (4.3)$$

In the latter equation (4.3) the shaft and base capacity contributions are calculated independently from each other, thus neglecting the different displacement values for which they may be effectively mobilized in practice. *While this assumption simplifies the analysis, it is worth noting that the shaft capacity of piles is mobilized for much smaller pile displacements than the base capacity* (Laloui L. and Rotta Loria, 2019). In practice, it is considered that the axial capacity of the piles is reached for the load for which a further increase in settlement does not induce an increase in the load or for the load that causes a settlement of 10% of the diameter of the pile base. Two failure criteria may be associated with the previous conditions: a *strength failure criterion*, considering the available strength at the pile-soil interface, and a *displacement failure criterion*, considering the allowable settlement of the pile.

Following the approach proposed by Poulos and Davis (1980), which is based on a strength failure criterion, the shaft capacity can be estimated by integrating the pile-soil interface shear strength along the external surface of the pile shaft and the base capacity can be evaluated from bearing capacity theory. This approach yields to the generalized expression for the pile capacity, which can be written as:

$$Q_u = q_s A_s + q_b A_b - W = \left(\bar{c}_a + \overline{\sigma'_v} \bar{K} \tan \delta' \right) A_s + \left(c N_c s_c d_c + \sigma'_{vb} N_q s_q d_q + \frac{1}{2} \gamma D N_\gamma s_\gamma d_\gamma \right) A_b - W \quad (4.4)$$

where:

- q_s is the average shear strength down the pile shaft;
- A_s is the external surface of the pile shaft;
- q_b is the base resistance;
- A_b is the cross-sectional area of the pile base;
- \bar{c}_a is the average pile-soil interface;

- $\bar{\sigma}_v$ is some average vertical stress;
- \bar{K} is some average coefficient of lateral pressure;
- δ is angle of pile-soil interface shear strength;
- c is the soil cohesion;
- σ_{vb} is the vertical stress at level of the pile base;
- γ is the unit weight of the soil;
- D is the pile diameter;
- N_c, N_q and N_γ are bearing capacity factors;
- s_c, s_q and s_γ are shape factors;
- d_c, d_q and d_γ are depth factors.

The bearing capacity, shape and depth factors are summarized in the following tables (from Table 3.6 to Table 3.8).

<i>Term $N_c s_c d_c$</i>				
<i>Author</i>	<i>Cohesion, c [Pa]</i>	<i>Bearing capacity factor, N_c [-]</i>	<i>Shape factor, s_c [-]</i>	<i>Depth factor, d_c [-]</i>
Terzaghi (1943)	Actual value	$(N_q - 1) \cot \varphi$	1.3	-
Meyerhof (1963)	Actual value	Terzaghi (1943)	$1 + 0.2K_p$ $K_p = \tan^2 \left(45 + \frac{\varphi}{2} \right)$	$1 + 0.2\sqrt{K_p} \left(\frac{L}{D} \right)$
Hansen (1970)	Actual value	Terzaghi (1943)	Drained conditions: $1 + \frac{N_q}{N_c}$ Undrained conditions: $(\varphi = 0): 0.2$	Drained conditions: $1 + 0.4k_H$ Undrained conditions $(\varphi = 0):$ $0.4k_H$ $k_H = \tan^{-1} \left(\frac{L}{D} \right)$
Vesic (1977);	Actual value	Terzaghi (1943)	$1 + \frac{N_q}{N_c}$	Hansen (1970)

Table 3.6: Values of expressions of the term Term $N_c s_c d_c$ (Laloui L. and Rotta Loria, 2019)

Term $N_q s_q d_q$				
Author	Vertical stress, σ_{vb} [Pa]	Bearing capacity factor, N_c [-]	Shape factor, s_c [-]	Depth factor, d_c [-]
Terzaghi (1943)	Actual value	$N_q = \frac{\alpha_T^2}{\alpha_T \cos^2 \left(45 + \frac{\varphi}{2}\right)}$	-	-
Meyerhof (1963)	Actual value	$K_p e^{2\pi \tan \varphi}$	Drained conditions: $1 + 0.1K_p$ Undrained conditions: $(\varphi = 0): 1$	Drained conditions: $0.1\sqrt{K_p} \left(\frac{L}{D}\right)$ Undrained conditions: $(\varphi = 0): 1$
Hansen (1970)	Actual value	Meyerhof (1963)	$1 + \sin \varphi$	$1 + 2 \tan \varphi (1 - \sin \varphi)^2 k_H$
Vesic (1977);	Actual value	Meyerhof (1963)	Hansen (1970)	Hansen (1970)

Table 3.7: Values of expressions of the term Term $N_q s_q d_q$ (Laloui L. and Rotta Loria, 2019).

Term $N_\gamma s_\gamma d_\gamma$				
Author	Unit weight, γ [N/m³]	Bearing capacity factor, N_c [-]	Shape factor, s_c [-]	Depth factor, d_c [-]
Terzaghi (1943)	Actual value	$\frac{\tan \varphi}{2} \left(\frac{K_{p\gamma}}{\cos^2 \varphi} - 1\right)$	0.6	-
Meyerhof (1963)	Actual value	$(N_q - 1) \tan(1.4\varphi)$	Drained conditions: $1 + 0.1K_p$ Undrained conditions: $(\varphi = 0): 1$	Drained conditions: $0.1\sqrt{K_p} \left(\frac{L}{D}\right)$ Undrained conditions: $(\varphi = 0): 1$
Hansen (1970)	Actual value	$1.5(N_q - 1) \tan \varphi$	0.6	1
Vesic (1977);	Actual value	$2(N_q + 1) \tan \varphi$	Hansen (1970)	Hansen (1970)

Table 3.8: Values of expressions of the term Term $N_q s_q d_q$ (Laloui L. and Rotta Loria, 2019).

3.2.2 Capacity in coarse-grained soil

For piles embedded in coarse-grained soil, drained conditions may be assumed upon loading so that an effective stress analysis can be considered. Resuming the equation (4.4) in this case some simplifications have been done:

- cohesive components, c , equal to zero;
- neglecting the term $\frac{1}{2} \gamma D N_\gamma s_\gamma d_\gamma$ because small in relation to the term involving N_q ;
- s_q and d_q equal to 1 (conservative approach).

and the generalized equation becomes:

$$Q_u = q_s A_s + q_b A_b - W = \overline{\sigma'_v} \bar{K} \tan \delta' A_s + \sigma'_{vb} N_q A_b - W \quad (4.5)$$

For *displacement piles* the shaft resistance can be expressed as:

$$q_s = \overline{\sigma'_v} \bar{K} \tan \delta' = \overline{\sigma'_v} \beta^f \quad (4.6)$$

This approach is termed “Beta Method”. The coefficient \bar{K} relates the normal stress acting on the pile-soil interface after pile installation, $\overline{\sigma'_n}$, to the in situ vertical effective stress, $\overline{\sigma'_v}$, and is the most important factor, because govern the shaft resistance of displacement piles in coarse-grained soils. In function of pile installation method, \bar{K} depends on the in situ coefficient of earth pressure at rest, K_0 , and the stress change produced by the installation related to the initial soil density (Laloui L. and Rotta Loria, 2019). The values of \bar{K} can vary from values equal to the coefficient of passive earth pressure, K_p , near the ground surface to values equal to the coefficient of the earth pressure at rest, K_0 , near the pile toe.

Typical values of \bar{K}

- for driven cast *in situ* piles are of 1 if wet concrete is placed;
- up to 1.2 if dry concrete is rammed into the pile shaft.

Alternative approaches to quantify \bar{K} have been proposed in a wide number of works over the years. Considering $\bar{K} = K_0$ may be typically appropriate (Laloui L. and Rotta Loria, 2019).

The pile-soil interface angle of shear strength, δ' , is usually assumed to be equal to the angle of shear strength under constant volume conditions of the soil, ϕ'_{cv} , in the absence of interface shear tests results, although the former is generally found to be a little lower than the latter. The approach of considering $\delta' = \phi'_{cv}$ may be justified on the basis that no dilation is to be expected between the soil and the pile shaft at failure (Laloui L. and Rotta Loria, 2019).

When the dilatancy angle of the soil ψ is available, the stress-dilatancy relationship

$$\varphi' = \varphi'_{cv} + 0.8 \psi \quad (4.7)$$

may also be employed to estimate the soil angle of shear strength under constant volume conditions, φ'_{cv} .

For *non-displacement piles* the shaft resistance is generally lower compared to that of displacement piles because during the building process (exactly during excavation) lateral stresses in the ground are reduced and the initial in situ conditions are only partially restored on concrete. Based on investigations (reported in Laloui L. and Rotta Loria, (2019)) an empirical formula for β^f has been proposed (with the limiting value of $\overline{\sigma'_v} \beta^f \leq 200 \text{ kPa}$). A suitable approach to estimate the shaft resistance of non-displacement piles is to consider the typical values of \overline{K}

- for conventional bored piles of 0.7;
- for continuous-flight auger piles of 0.9 in sands and gravels;
- for continuous-flight auger piles from 0.5 to 0.6 in silts and silty sands.

These values are in accordance with the recommendation (Laloui L. and Rotta Loria, 2019) $\overline{K} = 0.7 K_0$. The arguments summarized above for displacement piles about the choice of the pile-soil interface angle of shear strength are also valid for non-displacement piles. To account for potential loosening of the soil during the installation process, values of δ' between φ' and φ'_{cv} may be considered.

3.2.3 Capacity in fine-grained soil

For piles in fine-grained soil, undrained conditions may be assumed upon loading so that a total stress analysis has been historically considered. Resuming the equation (4.4) in this case some simplifications have been done:

- equal to zero the pile-soil interface angle of shear strength δ and $N\gamma$ (considering the undrained angle of shear strength of the soil to be zero);
- and equal to one the shape factors s_c, d_c, s_q and d_q by means of a conservative (when these terms appear in the employed base capacity formulation) as well as the factor N_q , the generalized pile capacity formulation becomes:

$$Q_u = q_s A_s + q_b A_b - W = \overline{c}_a A_s + (c_u N_c + \sigma'_{vb}) A_b - W \quad (4.8)$$

where

- N_C is the bearing capacity proposed by Skempton (1951) for a circular area, which may be taken equal to 9 for depths relevant for piles according to Lancellotta (Lancellotta, 1995) (Laloui L. and Rotta Loria, 2019). Interpolation may be considered from values of 6 to 9 with the increasing penetration depth of the pile up to values of three pile diameters according to Fleming (Laloui L. and Rotta Loria, 2019).
- \bar{c}_a is the pile-soil adhesion varies considerably with many factors including pile type, soil type and method of installation. Many attempts have been made to correlate this parameter with the undrained soil cohesion in the form

$$\bar{c}_a = \alpha^f c_u \quad (4.9)$$

with

$$\alpha^f = \frac{0.5}{\left(\frac{c_u}{\sigma'_v}\right)^{0.5}} \quad \text{for } c_u/\sigma'_v \leq 1 \quad (5.1)$$

$$\alpha^f = \frac{0.5}{\left(\frac{c_u}{\sigma'_v}\right)^{0.25}} \quad \text{for } c_u/\sigma'_v > 1 \quad (5.2)$$

For *displacement piles* to estimate \bar{K} are available some formulations for every different situation:

- For piles in soft normally consolidated or slightly overconsolidated clay, the values \bar{K} of may range between the lower bound $K_0 = 1 - \sin\varphi'$ (5.3) and the value $K_0 = (1 - \sin^2\varphi)/(1 + \sin^2\varphi)$ (5.4);
- For piles in overconsolidated clay, the value of \bar{K} may be considered as $K_0 = (1 - \sin\varphi')\sqrt{OCR}$ (5.5);

In all of the above relationships, the soil angle of shear strength under constant volume conditions φ'_{cv} may be considered for the terms including both φ' and δ' (especially for piles longer than 30-40 m (Lancellotta, 1995)). If the soil angle of shear strength φ' would be available but not that under constant volume conditions φ'_{cv} it may be considered:

$$\varphi'_{cv} = \arctan\left(\frac{\sin\varphi' \cos\varphi'}{1 - \sin^2\varphi'}\right) \quad (5.6)$$

The estimation of the shaft capacity of *non-displacement piles* in fine-grained soil through the effective stress approach is generally more straightforward than that for displacement piles. The shaft resistance of non-displacement piles in fine-grained soils may be accurately estimated assuming $\bar{K} =$

K_0 because little changes of the soil stress state around the pile occur due to pile construction if concrete is promptly poured.

The soil angle of shear strength under constant volume conditions φ'_{cv} may be considered for the terms including both φ' and δ' according to Burland and Twine (1988) for piles in overconsolidated clay (Laloui L. and Rotta Loria, 2019).

3.2.4 Verification for energy piles group

As represented in the Figure 2.6 in the Chapter 2, the case study is built in a layered soil made up by four layers whose properties are summarized in the Tables 2.4-2.7. During the geotechnical ultimate limit state design, the most burdensome situation is that of the EP4 (energy piles) which is loaded with 2200 KN as pictured in the following figure (Figure 3.1):

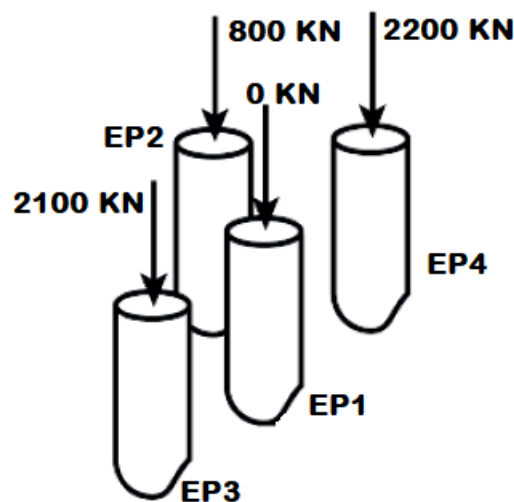


Figure 3.1: Applied mechanical loads to energy piles.

Prior to show all the calculation carried out in order to obtain the design load, this is an important aspect to clarify. In the stratigraphy shows in the Figure 2.6, in this design case, the last soil layer (layer D) is made by molasse, which is classified as a very strong rock. Consequently, the aforementioned formulations to evaluate the shaft and the base capacity are not valid because they may be used only for soils and not rocks. Piles constructed in rock are generally characterised by a *capacity contribution provided by the base that is significantly higher than the contribution provided by the shaft*. In general, both the shaft and base capacity piles in rock are customarily considered proportional to the unconfined compressive strength of the rock, UCS (Horvath et al., 1980; Williams and Pells, 1981; Rowe and Armitage, 1987; Zhang and Einstein, 1998).

Most approaches indicate that the **shaft resistance** is proportional to the square root of the rock unconfined compressive strength (Laloui L. and Rotta Loria, 2019). At the same time, a remarkable discontinuity in the transition zone between hard soils and soft rocks is highlighted by Fleming et al. (2008), providing the following expressions:

$$q_s = p_a \Psi \left(\frac{c_u}{p_a} \right)^{0.5} \quad \text{for hard soils} \quad (5.7)$$

$$q_s = p_a \Psi \left(\frac{UCS}{p_a} \right)^{0.5} \quad \text{for rocks} \quad (5.8)$$

where p_a is the atmospheric pressure, $\psi=0.5$ for the fine-grained soil data and $\psi=2$ for the main soft rock data. According to Zhang and Einstein (1998), the **base resistance** of piles resting on rock (e.g., associated with a normalized displacement of 10% of the pile diameter) is proportional to the square root of the rock unconfined compressive strength as:

$$q_b = 15 \left(\frac{UCS}{p_a} \right)^{0.5} \quad (5.9)$$

For the combinations for the calculation of the design load, the following loads have been supposed:

- $G_k = 0.7 N_k$;
- $Q_k = 0.3 N_k$;

Resuming the design approaches summarized in the Chapter 3.1.3 the design loads have been calculated as

$$N_d = G_k \gamma_G + Q_k \gamma_Q = 0.7 N_k \gamma_G + 0.3 N_k \gamma_Q \quad (6.1)$$

and presented in the following table (Table 3.9):

<i>Design approaches</i>	<i>Design load [KN]</i>
DA1 – Combination 1: A1 + M1 + R1	3069
DA1 – Combination 2: A2 + M1 + R4	2398
DA2: A1 + M1 + R2	3069
DA3: A1 + M2 + R3	3069

Table 3.9: Design loads for each design approach for energy piles.

For layer A, B and C the shaft resistance is evaluated following the equation (4.6) where the single contribute are:

- $\bar{K} = 0.7 K_0 = 0.7(1 - \sin \varphi'_{d,cv})$;
- Resuming equation (4.7) $\varphi'_{k,cv}$ has been calculated;
- σ'_{vb} is the average stress between two following layers;

For layer D the contribute of shaft capacity should be calculated assuming the equation (5.7), but this equation can be used when the soil layer is in drained condition and in this case the layer D is in undrained condition. In this way, to avoid mistakes related to the use of the formulations, the contribute of Layer D in the context of the shaft capacity is neglected.

The results for each design approach are shows in the Table 3.10:

<i>Layer</i>	<i>DA1 – c1: A1 + M1 + R1</i>	<i>DA1 – c2: A2 + M1 + R4</i>	<i>DA2: A1 + M1 + R2</i>	<i>DA3: A1 + M2 + R3</i>
	<i>Shaft capacity, Q_s</i>	<i>Shaft capacity, Q_s</i>	<i>Shaft capacity, Q_s</i>	<i>Shaft capacity, Q_s</i>
	<i>[KN]</i>	<i>[KN]</i>	<i>[KN]</i>	<i>[KN]</i>
<i>A</i>	196.48	196.48	196.48	173.3
<i>B</i>	532.03	532.03	532.03	458.58
<i>C</i>	349.50	349.5	349.5	307.84
<i>D</i>	-	-	-	-

Table 3.10: Values of shaft capacity in KN for each layer.

The total shaft capacity will be given by the following equation:

$$Q_{s,tot} = \frac{Q_{s,A} + Q_{s,B} + Q_{s,C}}{\gamma_R \xi_1} \quad (6.2)$$

where ξ_1 is the recommended correlation factor to determine characteristic pile resistance from pile load test results, related to number of piles tested. Their values are summarized in the following table:

<i>n</i>	<i>1</i>	<i>2</i>	<i>3</i>	<i>4</i>	<i>≥ 5</i>
ξ_1	1.4	1.3	1.2	1.1	1.0

Table 3.11: Correlation factor values (Eurocode 7).

The total values of shaft capacity are shown in the table 3.12:

<i>DA1 – c1: A1 + M1 + R1</i>	<i>DA1 – c2: A2 + M1 + R4</i>	<i>DA2: A1 + M1 + R2</i>	<i>DA3: A1 + M2 + R3</i>
<i>Shaft capacity,</i>	<i>Shaft capacity,</i>	<i>Shaft capacity,</i>	<i>Shaft capacity,</i>
<i>Q_{s,tot} [KN]</i>	<i>Q_{s,tot} [KN]</i>	<i>Q_{s,tot} [KN]</i>	<i>Q_{s,tot} [KN]</i>
770.01	592.32	700.01	610.21

Table 3.12: Values of the total shaft capacity for each design approach.

The total values of base capacity is calculated assuming the following equation:

$$Q_{b,tot} = \frac{Q_b}{\gamma_R \xi_1} \quad (6.3)$$

where Q_b is calculated with equation (5.9). The total values of base capacity are shown in the table 3.13:

<i>DA1 – c1: A1 + M1 + R1</i>	<i>DA1 – c2: A2 + M1 + R4</i>	<i>DA2: A1 + M1 + R2</i>	<i>DA3: A1 + M2 + R3</i>
<i>Base capacity, Q_b</i>	<i>Base capacity, Q_b</i>	<i>Base capacity, Q_b</i>	<i>Base capacity, Q_b</i>
<i>[KN]</i>	<i>[KN]</i>	<i>[KN]</i>	<i>[KN]</i>
5756.82	4497.52	6541.84	6081.75

Table 3.13: Values of base capacity for each design approach.

According to Eurocode 7, the Geotechnical ultimate limit state verification is satisfied when:

$$Q_u = Q_{b,tot} + Q_{s,tot} \geq N_{Ed} \quad (6.4)$$

The verification is satisfied for all design approaches.

3.2.5 Design proposed for energy piles group

Even tough during the geotechnical verifications for energy pile with length equal to 28 m we have neglected the shaft capacity of layer D, the checks for all design approach are satisfied. *This means that even having designed a pile with a length of 19.2 m would have satisfied the checks, not penetrating the layer D by 8.8 m, but resting only the base on it, in order to guarantee a much larger base capacity.*

A less length of 19.2 m (15.7m) would not have ensured that the verification was satisfied, since the base of the pile would not have rested on layer D, but on layer C. This means that the equation (5.9) is no longer valid and to calculate the base capacity we should use the Hansen's equation:

$$Q_{b,tot} = \frac{q_b A_b}{\gamma_R \xi_1} = \frac{(\sigma'_{vb} N_q d_q) A_b}{\gamma_R \xi_1} \quad (6.5)$$

where the term σ'_{vb} has been calculated until the layer B (because the pile rest on layer C). In the following table are shown the results:

<i>DA1 - c1: A1 + M1 + R1</i>	<i>DA1 - c2: A2 + M1 + R4</i>	<i>DA2: A1 + M1 + R2</i>	<i>DA3: A1 + M2 + R3</i>
<i>Base capacity, Q_b</i>	<i>Base capacity, Q_b</i>	<i>Base capacity, Q_b</i>	<i>Base capacity, Q_b</i>
<i>[KN]</i>	<i>[KN]</i>	<i>[KN]</i>	<i>[KN]</i>
793.25	619.75	901.45	667.26

Table 3.14: Values of base capacity for each design approach.

The verification is not satisfied for all design approaches. In the following figures is summarized the situation:

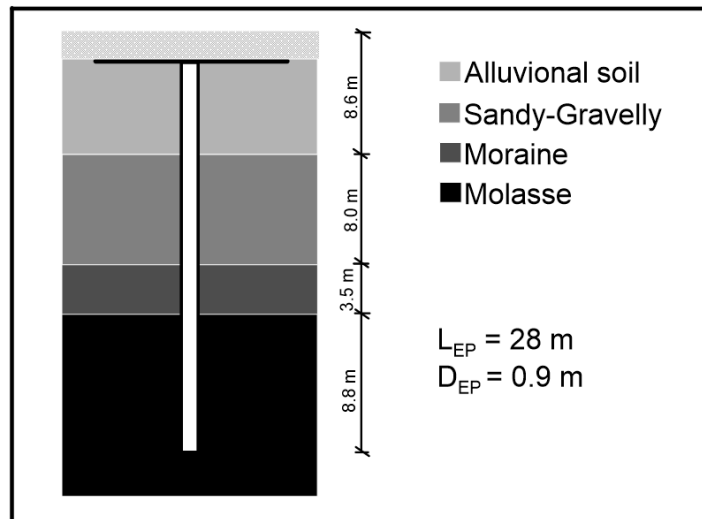


Figure 3.2: Schematization of real case.

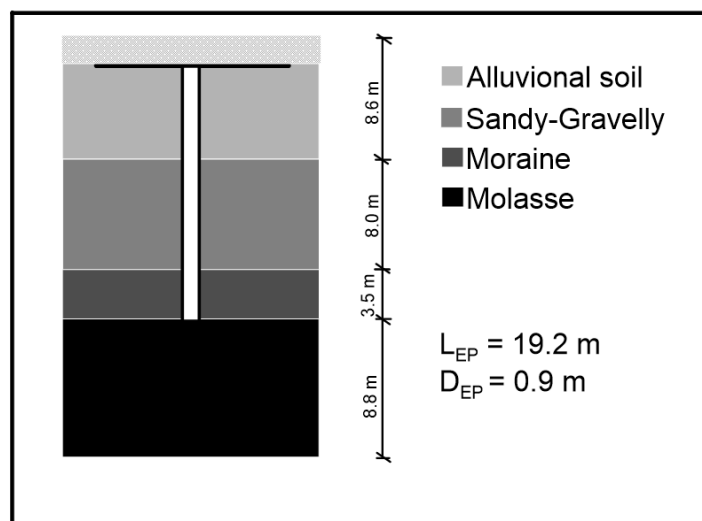


Figure 3.3: Schematization of the following design.

3.2.6 Verification for conventional piles group

Following the aforementioned combinations and verifications and noting that each conventional pile is loaded with 300 KN:

<i>Design approaches</i>	<i>Design load [KN]</i>
DA1 – Combination 1: A1 + M1 + R1	418.5
DA1 – Combination 2: A2 + M1 + R4	327
DA2: A1 + M1 + R2	418.5
DA3: A1 + M2 + R3	418.5

Table 3.15: Design loads for each design approach for conventional piles.

The results for each design approach are shows in the Table 3.16:

<i>Layer</i>	<i>DA1 – c1: A1 + M1 + R1 Shaft capacity, Q_s [KN]</i>	<i>DA1 – c2: A2 + M1 + R4 Shaft capacity, Q_s [KN]</i>	<i>DA2: A1 + M1 + R2 Shaft capacity, Q_s [KN]</i>	<i>DA3: A1 + M2 + R3 Shaft capacity, Q_s [KN]</i>
<i>A</i>	130.99	130.99	130.99	115.54
<i>B</i>	354.69	354.69	354.69	305.71
<i>C</i>	18.31	18.31	18.31	16.13

Table 3.16: Values of shaft capacity in KN for each layer.

The total shaft capacity will be given by the equation (6.2). The total values of shaft capacity are shown in the table 3.17:

<i>DA1 – c1: A1 + M1 + R1 Shaft capacity, $Q_{s,tot}$ [KN]</i>	<i>DA1 – c2: A2 + M1 + R4 Shaft capacity, $Q_{s,tot}$ [KN]</i>	<i>DA2: A1 + M1 + R2 Shaft capacity, $Q_{s,tot}$ [KN]</i>	<i>DA3: A1 + M2 + R3 Shaft capacity, $Q_{s,tot}$ [KN]</i>
359.99	281.26	327.26	285.26

Table 3.17: Values of the total shaft capacity for each design approach.

The total values of base capacity is calculated assuming the equation (6.5)

The total values of base capacity are shown in the table 3.18:

<i>DA1 – c1: A1 + M1 + R1</i>	<i>DA1 – c2: A2 + M1 + R4</i>	<i>DA2: A1 + M1 + R2</i>	<i>DA3: A1 + M2 + R3</i>
<i>Base capacity, Q_b</i>	<i>Base capacity, Q_b</i>	<i>Base capacity, Q_b</i>	<i>Base capacity, Q_b</i>
<i>[KN]</i>	<i>[KN]</i>	<i>[KN]</i>	<i>[KN]</i>
360.13	281.36	409.25	302.93

Table 3.18: Values of base capacity for each design approach.

The Geotechnical ultimate limit state verification is satisfied when the equation (6.4) is satisfied.

The verification is satisfied for all design approaches.

3.2.7 Design proposed for conventional piles group

The previous verifications have been carried out taking into account the conventional pile length equal to 16 m.

In this proposed design for the conventional piles group has noted that the verifications are satisfied even when the pile length is equal to 15 m. The results are summarized in the following tables:

<i>Layer</i>	<i>DA1 – c1: A1 + M1 + R1</i>	<i>DA1 – c2: A2 + M1 + R4</i>	<i>DA2: A1 + M1 + R2</i>	<i>DA3: A1 + M2 + R3</i>
	<i>Shaft capacity, Q_s</i>	<i>Shaft capacity, Q_s</i>	<i>Shaft capacity, Q_s</i>	<i>Shaft capacity, Q_s</i>
	<i>[KN]</i>	<i>[KN]</i>	<i>[KN]</i>	<i>[KN]</i>
<i>A</i>	130.99	130.99	130.99	115.54
<i>B</i>	316.04	316.04	316.04	272.40

Tabel 3.19: Values of Shaft capacity in KN for each layer

The total shaft capacity will be given by the equation (6.2)

The total values of shaft capacity are shown in the table 3.20:

<i>DA1 – c1: A1 + M1 + R1</i>	<i>DA1 – c2: A2 + M1 + R4</i>	<i>DA2: A1 + M1 + R2</i>	<i>DA3: A1 + M2 + R3</i>
<i>Shaft capacity,</i>	<i>Shaft capacity,</i>	<i>Shaft capacity,</i>	<i>Shaft capacity,</i>
<i>$Q_{s,tot}$ [KN]</i>	<i>$Q_{s,tot}$ [KN]</i>	<i>$Q_{s,tot}$ [KN]</i>	<i>$Q_{s,tot}$ [KN]</i>
319.30	249.47	362.85	253.02

Table 3.20: Values of Shaft capacity for each design approach

The total values of base capacity is calculated assuming the equation (6.5) neglecting the following contributes:

- (i) s_c, d_c and s_q are equal to one;

(ii) the cohesion is nil;

(iii) the term $\frac{1}{2} \gamma D N_{\gamma} s_{\gamma} d_{\gamma}$ (in the equation 4.4) is neglected because is small.

The total values of base capacity are shown in the table 3.21:

<i>DA1 – c1: A1 + M1 + R1</i>	<i>DA1 – c2: A2 + M1 + R4</i>	<i>DA2: A1 + M1 + R2</i>	<i>DA3: A1 + M2 + R3</i>
<i>Base capacity, Q_b</i>	<i>Base capacity, Q_b</i>	<i>Base capacity, Q_b</i>	<i>Base capacity, Q_b</i>
<i>[KN]</i>	<i>[KN]</i>	<i>[KN]</i>	<i>[KN]</i>
227.70	177.90	258.76	191.54

Table 3.21: Values of Base capacity for each design approach.

The verification, following the equation (6.4), is satisfied for all design approaches.

3.3 Structural Ultimate Limit State

3.3.1 Generalized approach for Structural Ultimate State

The ultimate limit state is the design for the safety of a structure and its users by limiting the stress that materials experience. In order to comply with engineering demands for strength and stability under design loads, ULS must be fulfilled as an established condition. The ULS are associated with the extreme value of bearing capacity or other forms of structural failure that may endanger people's safety. Some examples of the causes that can lead to the ULS are:

- loss of stability of part or of the whole structure;
- breaking of critical sections of the structure;
- transformation of the structure into a mechanism;
- instability due to excessive deformation;
- deterioration following fatigue;
- deformations or cracks, which produce a change in geometry that requires the replacement of the structure.

The overcoming of a last limit state is irreversible and is defined as *collapse*.

Resuming the equation (3.9) to satisfy the ULS verification the acting force must be less or equal than the resisting one as:

$$N_{Ed} \leq N_{Rd} \tag{6.6 (a)}$$

$$M_{Ed} \leq M_{Rd} \tag{6.6 (b)}$$

where N_{Rd} and M_{Rd} are the resisting forces respectively for axial force and bending moment. In the general framework the verification is satisfied when the point with coordinates $(N_{Ed}; M_{Ed})$ is inside the *interaction domain* (Figure 3.4). In general piles foundation are subjected to axial force and bending moment and the conjunction of these two forces is the reason for which it needs to verify both the actions.

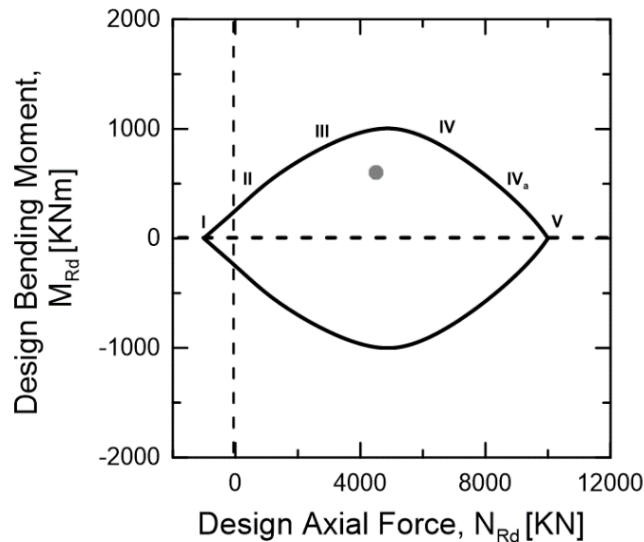


Figure 3.4: General example of the satisfied verification.

The boundary curve of the limit domain is the set of $M-N$ couples that they correspond to diagrams of limit deformations (from field I to field V as pictured in the aforementioned figure).

In other words diagrams of ε that they reach the maximum deformation of the material at a point and do not exceed this value at no other point. For the concrete it is usually adopted in the calculation a constitutive bond represented by a parabolic tract and a constant tract (Figure 3.5 (a)); for partialized section the deformation limit is given by the ε_{cu} value, equal to $3.5 \cdot 10^{-3}$. In the case of a fully compressed section the limit is instead constituted by the achievement of the deformation ε_{c1} (equal to $2 \cdot 10^{-3}$) at a point located at 3/7 of the height, measured from the most compressed edge. For the steel the bond constitutive has a linear stroke and a constant stretch (Figure 3.5(b))

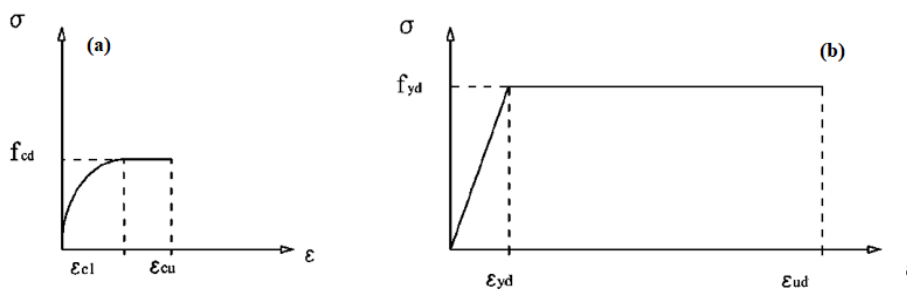


Figure 3.5: (a) Concrete constitutive bond; (b) Steel constitutive bond (Eurocode 2).

Furthermore the following hypotheses have been formulated:

- preservation of the flat sections, in fact considering the beam no deformable to shear stresses, it is possible at analytical level to have sections orthogonal to the axis line of the beam and to obtain calculation models for linear deformations.
- Perfect adherence between steel and concrete, even if it is not locally satisfied, it appears to be global.

By using the constitutive bonds of the materials, the values of the deformation can be pictured in univocal way to the values of the stresses in concrete and steel, σ_c and σ_s ; Note the stresses you can derive the values of N and M from their definition itself:

$$N = \int \sigma_c dA_c + \int \sigma_s dA_s = N_c + N_s \quad (6.7)$$

$$M = \int \sigma_c y dA_c + \int \sigma_s y dA_s = M_c + M_s \quad (6.8)$$

Note that, despite the non-linearity of the constitutive bonds, the contribution of the reinforcement varies with linear law with A_s if all the reinforcement is proportionally increased. The construction of the domain takes place by sweeping all the breaking fields of the section, where each of them describes the internal stress-deformation state based on the position of the neutral axis. By evaluating the stress state, the tensions acting on the sections can be defined and therefore the forces obtained by integration into the area. As displayed in the previous figure (Figure 3.4) there six breaking fields:

- *FIELD I*

The field I is between the two deformed planes which pass through the final deformation of the steel: the first plane corresponds to having all the fibers of the section that work on the last deformation of the steel and the second plane at the lower reinforcement level works at last deformation and the upper concrete that works at 0. Any deformed configuration passes for the last deformation point between the two planes is a field configuration I. Therefore a configuration belong to field I when the steel works at last deformation, while the less stretched fiber works with a deformation that lies between 0 and the last deformation. These sections will be subject to tensile stresses with small eccentricities and maximum exploitation of the lower steel is achieved, which also reaches the ULS (Figure 3.6):

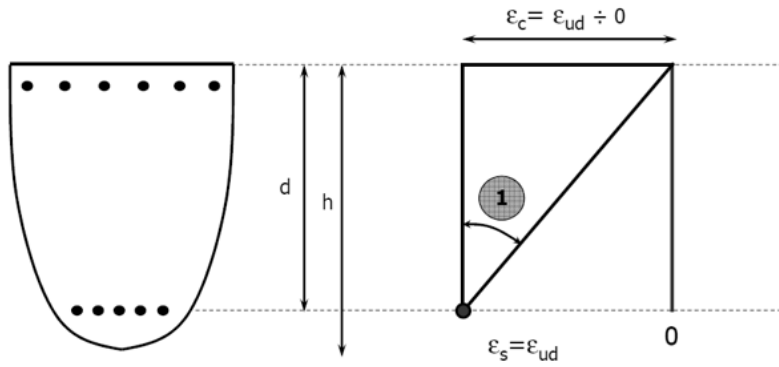


Figure 3.6: Breaking field I scheme (Giordano L., 2016).

- FIELD II

Varying the deformation of the concrete between zero and the maximum deformation and the field configurations II always start from the maximum steel deformation which will then be responsible for the last limit state configuration. The neutral axis is internal and divides the partially compressed and stretched section. The field configurations 2 will be subject to normal stresses with large eccentricities and simple bending with small armatures placed in the stretched area (Figure 3.7):

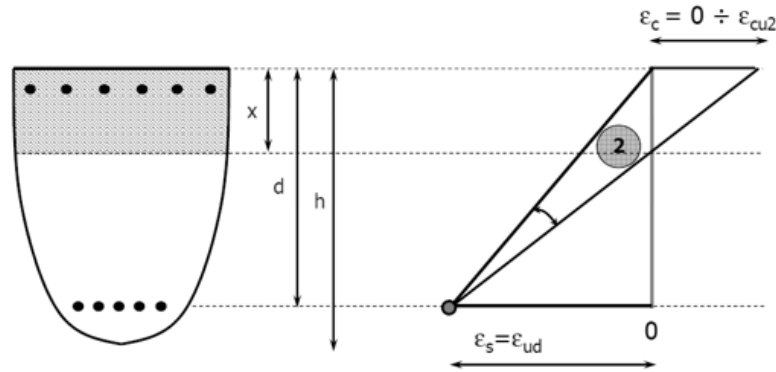


Figure 3.7: Breaking field II scheme (Giordano L., 2016).

- FIELD III

In field III the concrete deformation is maximum, while that of the steel varies between the maximum and the ϵ_{yd} . The neutral axis is always internal and the ultimate limit state is reached by the concrete and the maximum exploitation of both steel and concrete has been reached (Figure 3.8):

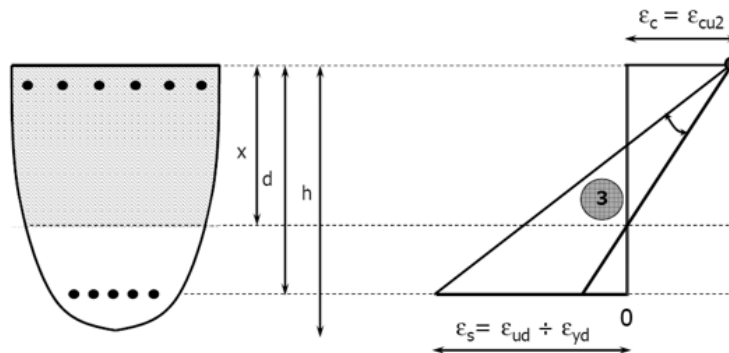


Figure 3.8: Breaking field II scheme (Giordano L., 2016).

- *FIELD IV*

The deformation of the concrete is always maximum, while that of the steel varies between 0 and ϵ_{yd} . Neutral axis still internal and the configurations are subject to normal stresses with large eccentricities and simple bending with large quantities of reinforcement (Figure 3.9):

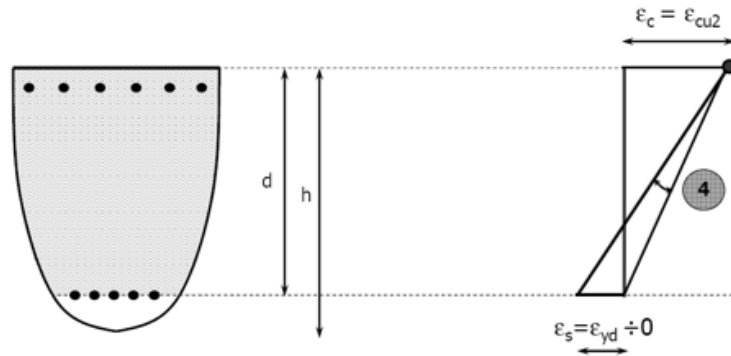


Figure 3.9: Breaking field IV scheme (Giordano L., 2016).

- *FIELD IVa*

In field IVa the deformation of the steel becomes negative and therefore of compression and ends when the section is compressed. The same considerations of field IV apply (Figure 3.10)

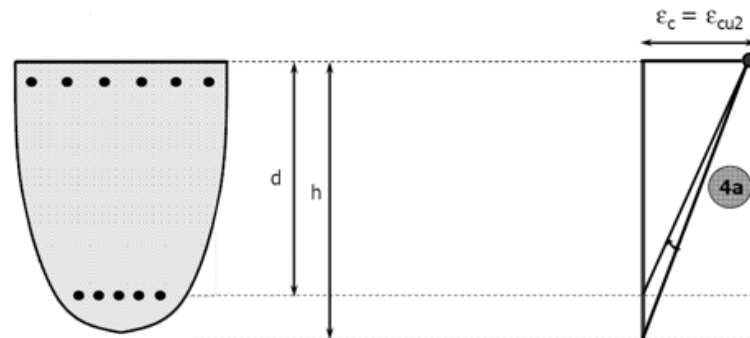


Figure 3.10: Breaking field IVa scheme (Giordano L., 2016).

- *FIELD V*

The pole in field V changes again and the becomes that in correspondence of the section that has at the beginning of field 5 the fiber which has the deformation ϵ_{c2} , and at the height of this fiber we will have the depth of the neutral axis ($3/7$ of the height if the maximum concrete deformation is 0.35% and is $\epsilon_{c2} = 0.2\%$). In field V there is a decrease in the compressed upper fiber, while the lower fiber varies from 0 to ϵ_{c2} . The section is subject only to compression efforts (Figure 3.11):

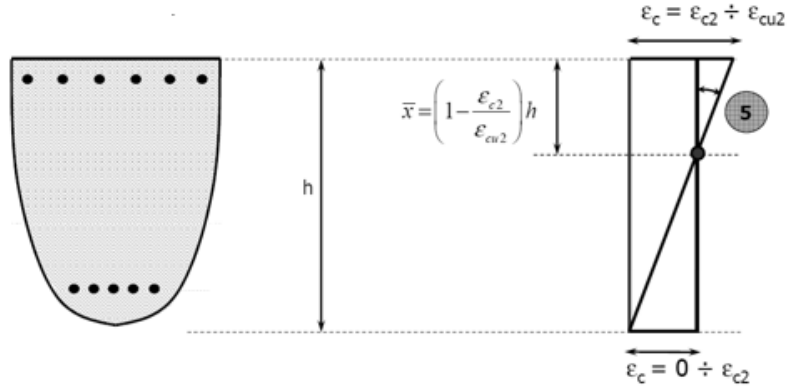


Figure 3.11: Breaking field V scheme (Giordano L., 2016).

3.3.2 Interaction Domain calculation for circular area

To calculate the interaction domain for the circular area (because the piles foundation area is circular) is different from the calculation done for the interaction domain for square or rectangular area. An iterative procedure has been implemented for the solution of the equilibrium equation:

$$F(y_c) = N_c(y_c) + N_s(y_c) - N_{Ed} = 0 \quad (6.9)$$

where

$$N_s(y_c) = \sum_{i=1}^{n_s} A_{s,i} \cdot \sigma_{s,i}(y_c) \quad (7.1)$$

The iterative procedure will be conducted with the aid of the Tangent Method which, starting from two values of y_c in which $F(y_c)$ assumes a different sign, proceeds in consecutive linear approximations to narrow the interval between these y_c values. For this reason it is first necessary to find an initial range of values of y_c in which the function $F(y_c)$ increasing with y_c , assumes different sign values.

With the possible value of neutral axis, the contribute of Resisting axial force of the concrete has been calculated as:

$$N_c(y_c) = 2 \cdot \left(\frac{D}{2}\right)^2 \cdot [\theta(y_c) - \sin\theta(y_c) \cdot \cos\theta(y_c)] \cdot f_{cd} \quad (7.2)$$

where

$$\theta(y_c) = \arccos \frac{D/2 - 0.8 \cdot y_c}{D/2} \quad (7.3)$$

To evaluate $N_s(y_c)$ the elastic relations have been used: firstly the deformations $\varepsilon_{s,i}$ have been calculated through the proportion (in function of the breaking field) and then:

$$\text{if } \varepsilon_{s,i} \geq \varepsilon_{y,d} \quad \text{then} \quad \sigma_{s,i} = \varepsilon_{y,d} \cdot E_s$$

$$\text{if } \varepsilon_{s,i} < \varepsilon_{y,d} \quad \text{then} \quad \sigma_{s,i} = \varepsilon_{s,i} \cdot E_s$$

There is only one value of y_c which satisfy the equation (6.9). Then the calculation of the resisting moment (both for concrete and steel side) have been evaluated with the obtained value of y_c :

$$M_{R,d} = N_c(y_c) \cdot y_{c,G} \quad (7.4)$$

where $y_{c,G}$ is the distance between the center of gravity of the compressive zone and the center of the section, given by the following equation:

$$y_{c,G} = \frac{2}{3} \cdot \frac{\sin^3 \theta(y_c)}{\theta(y_c) - \sin \theta(y_c) \cdot \cos \theta(y_c)} \cdot R \quad (7.5)$$

The resisting contribute of the reinforcement is given by:

$$M_{s,Rd} = \sum_{i=1}^{n_s} A_{s,i} \cdot \sigma_{s,i}(y_c) \cdot \left(\frac{D}{2} - y_{s,i} \right) \quad (7.6)$$

where $y_{s,i}$ is the perpendicular distance between the edge of the section and the center of gravity if each reinforcement bar. This procedure must be repeated for each breaking field in order to be able to draw the complete interaction domain.

3.3.3 Design for energy piles

Resuming that explained in the chapters 3.3.1 and 3.3.2 the interaction domain for the real case situation has been drawn and in this case the values of the acting forces is summarized in the following table:

Acting Force	Value
N_{Ed}	3069 [KN]
V_{Ed}	0 [KN]
M_{Ed}	0 [KN]

Table 3.22: Values of acting forces for energy piles.

As summarized in the previous table, the design case is that of concentrated force applied in the center of gravity; these values has been given by the construction company that have realized the whole structure. The concrete used by the construction company is C45/50 and a class of steel B500B. In according with Eurocode 2 (EN 1992, 2004) the minimum reinforcement required is in function of pile area as summarized in the following table (Table 3.23):

<i>Nominal pile cross section: A_c</i>	<i>Area of longitudinal reinforcement: $A_{s,bpmin}$</i>
$A_c \leq 0.5 \text{ m}^2$	$A_s \geq 0.5 \% A_c$
$0.5 \text{ m}^2 < A_c \leq 1 \text{ m}^2$	$A_s \geq 0.0025 \text{ m}^2$
$A_c > 0.5 \text{ m}^2$	$A_s \geq 0.25 \% A_c$

Table 3.23: Recommended minimum reinforcement area in non-displacement piles (EN 1992, 2004)

and in this case:

$$0,5 \text{ m}^2 \leq A_c \leq 1 \text{ m}^2 \quad \rightarrow \quad A_{s,min} = 0,0025 \text{ m}^2 \quad \text{and} \quad A_{s,min} = 2544 \text{ mm}^2 = 10\Phi 18;$$

The result is pictured in the following Figure:

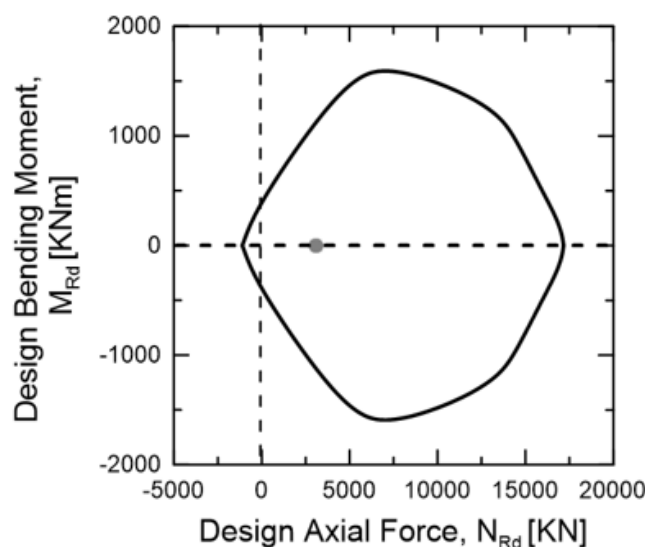


Figure 3.12: Interaction domain in the real design situation for energy piles.

The verification at ULS is widely satisfied.

3.3.4 Design proposed for energy piles to ensure ductility

The following procedure has been applied on the design proposed case, when the pile length is equal to 19.2 m. According with standards (UNI 11104, 2016) the concrete class has been chosen in function of exposure class: in this case (Switzerland) the exposure class is XC2 and the concrete class is C25/30. In this case of proposed design the concrete cover has also been evaluated following the recommendations given by the aforementioned standard. From general point of view, during the design of foundations, the concrete cover can varies between 40 mm and 70 mm. In the case of piles foundations the concrete cover must also respect the tie spacing (spacing between the bars) in order to facilitate construction operations (e.g., the vibration of concrete).

To ensure adequate ductility capacity of reinforced concrete members, some points must be respected:

- the resisting axial force of the reinforced concrete cross-sections needs to be greater than or equal to the axial force needed to crack them in view of potential strain localization effects,
- the reinforcement has to be characterized by a large deformation capacity and
- the ratio f_t/f_{yd} has to respect a lower bound (where f_{yd} is the tensile strength of the reinforcement steel).

In general, the first condition implies that:

$$N_R \geq N_{cr} \quad (7.7)$$

Equivalently,

$$f_y \rho_r A_{EP} \geq f_{ct} A_{EP} [1 + \rho_r (n_r - 1)] \approx f_{ct} A_{EP} \quad (7.8)$$

Simplifying the previous equation, the minimum reinforcement ratio can be expressed as (Rotta Loria, 2018)

$$\rho_{r,min} = \frac{f_{ctm}}{f_{yd}} \quad (7.9)$$

where:

$$f_{ctm} = 0.3 \cdot f_{ck}^{2/3} \quad (8.1)$$

$$f_{yd} = \frac{f_{yk}}{\gamma_s} \quad \text{where} \quad \gamma_s = 1.15 \quad (8.2)$$

And obtaining:

$$A_{s,min} = 4561,59 \text{ mm}^2 = 12\Phi 22$$

The aforementioned equations (7.9) and (8.1) have been reported following the recommendations given by Eurocode 2.

The first verification necessary is:

$$\rho_{r,min} \leq \rho_{r,eff} \quad (8.3)$$

With the amount of reinforcement obtained from the previous calculation the new interaction domain has been calculated, noting that the shape is different from that calculated with the old standards.

The result is pictured in the following Figure:

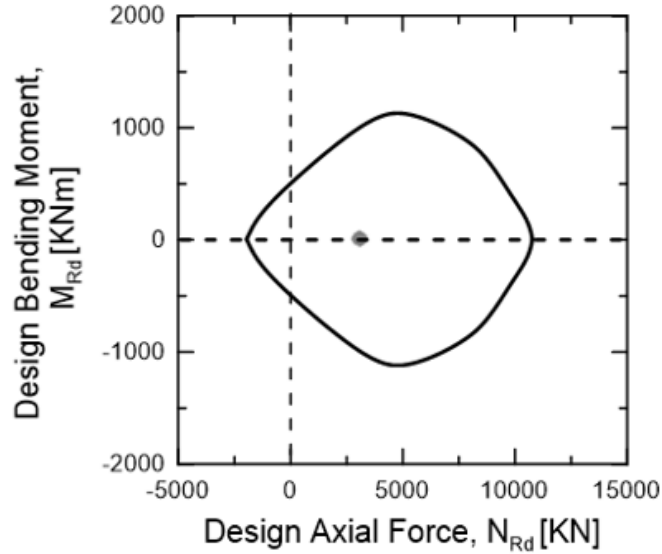


Figure 3.13: Interaction domain in the proposed design situation for energy piles.

Even in this case the verification is widely satisfied. In the proposed design has been also verificated the tie spacing, in the other words, the space between the bars. According with Eurocodes:

$$Tie\ spacing = \theta(y_c) \left(\frac{D - 2d'}{2} \right) = 188\ mm < 200\ mm \quad (8.4)$$

3.3.5 Design for conventional piles

For the conventional piles group, made by 16 piles identical (in diameter and length) and loaded equally (300 kN), the procedure applied is the same summarized in the chapter 3.3.3. In this case the acting force are:

Acting Force	Value
N_{Ed}	418.5 [kN]
V_{Ed}	0 [kN]
M_{Ed}	0 [kN]

Table 3.24: Values of acting forces for conventional piles.

Resuming the Table 3.23, in this case the diameter of each conventional pile is 0.6 m and consequently the following reinforcement has been calculated, by reference of the old standards:

$$0\ m^2 \leq A_c \leq 0.5\ m^2 \rightarrow A_{s,min} = 0.005 \cdot A_c = 1413.72\ mm^2$$

and

$$A_{s,min} = 1608.5\ mm^2 = 8\Phi 16;$$

Drawing in the same way shown previously the interaction diagram, the verification is widely satisfied:

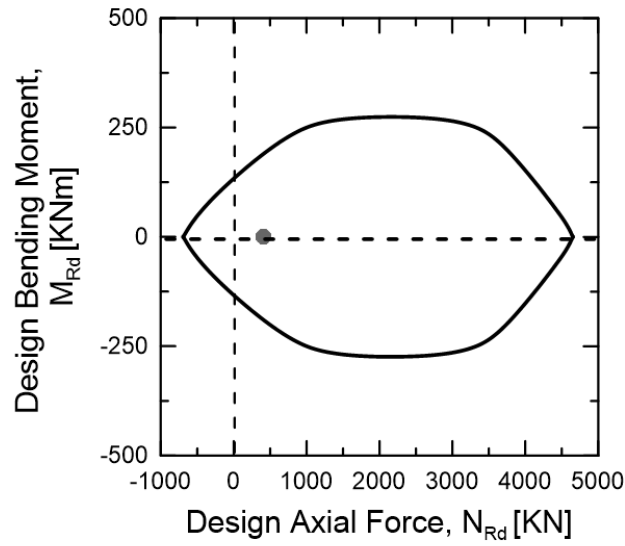


Figure 3.14: Interaction domain in the real design situation for conventional piles.

3.3.6 Design proposed for conventional piles to ensure ductility

Resuming the procedure shown in the chapter 3.3.4 and adapting it for the proposed design for conventional piles (with $L_{EP} = 15\text{ m}$), the verification is widely satisfied (Figure 3.15) with the minimum reinforcement equal to:

$$A_{s,min} = 2035.75\text{ mm}^2 = 8\Phi 18$$

that respect the equation (8.3).

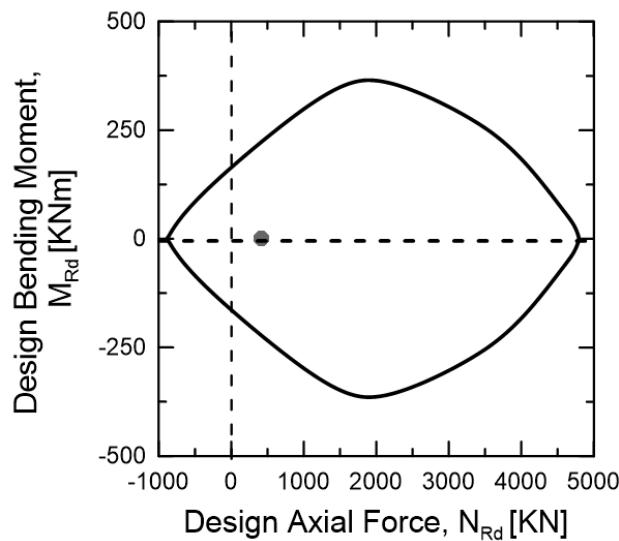


Figure 3.15: Interaction domain in the proposed design situation for conventional piles.

In this calculation the same concrete and steel class used for the proposed design for energy piles has been utilized (C25/30 and steel B500B). Also in this case the tie spacing has been verified:

$$Tie\ spacing = \theta(y_c) \left(\frac{D - 2d'}{2} \right) = 188\ mm < 200\ mm$$

3.4 Concluding remarks

To provide a basis for a novel performance-based design framework of energy piles subjected to mechanical and thermal loads, e.g., in the context of the *ultimate limit state* according with Eurocodes, the main conclusions have been pointed out:

- Thermal loads involve effects that can be neglected in the performance-based design of energy piles at ultimate limit states, both from a geotechnical and a structural perspective, and that can only be considered relevant at serviceability limit states (Rotta Loria, 2018);
- Geotechnical ultimate state verification is satisfied for the proposed case design despite the pile length has been decreased and not penetrating the molasse for 8.8 m but only resting the pile base on it to ensuring a great base capacity. This could be advantageous for economic perspective and a shorter length could avoid some problems related with serviceability conditions;
- Structural ultimate limit state verification is also satisfied for both design case (real case design and the proposed one) but in the latter case the safer method has been used, to ensure ductility. Moreover the first conclusion holds when a minimum longitudinal reinforcement for the pile concrete cross-sectional area that can ensure sufficient ductility capacity is employed.

Chapter 4

Serviceability Limit State (SLS)

4.1 Design and verifications in the framework of Eurocodes

Serviceability Limit State (SLS) is defined as any condition that results in the loss of functionality or the rapid deterioration of the structural system. Once reached a limit state during the life of the structure, the structural system no longer possesses the requirements for its correct use, also in terms of durability and aesthetics. In the general framework, the exceeding of this limit during the life of the structure can produce:

- Local damage that can reduce the durability of the structure, its efficiency or its appearance;
- Movements and deformations that may limit the use of the construction, its efficiency and its appearance;
- Displacements and deformations that may compromise the efficiency or appearance of non-structural elements, plants and machinery;
- Vibrations that may compromise the use of the construction;
- Fatigue damage which may compromise the durability of the structure;
- Corrosion and / or excessive degradation of the materials in use of the exposure environment.

For reinforced concrete structures the most important SLS are:

- *Tension limit state*: high compressive stresses in concrete can cause longitudinal cracks with consequent problems of durability or excessive viscous deformations; High tensions in stretched steel can induce too much injury wide and permanently open with possible durability problems;
- *Cracking limit state*: great crack appearing that compromise the correct use of the structure;
- *Deformation limit state*: deformations and excessive displacements can induce damage excessive in non-structural elements such as partitions and finishes.

To guarantee the satisfaction of the SLS verifications the following checks must be carried out:

- Tension check (both for compressive and tensile stresses);
- Cracking check;
- Deformability verification.

4.2 Single pile

In this chapter the SLS checks have been carried out to avoid the aforementioned problems during the life of the structure. In this particular case, for energy piles foundation the main problems can be:

- Exceeding of the maximum differential and average settlement allowed, according with Eurocodes (Eurocode 2);
- Exceeding of the maximum compressive stress (Eurocode 2);
- Exceeding of the maximum tensile stress, because during the life of energy piles they are also subjected to a negative thermal variation that produce a tensile stress within the pile. That could be the most burdensome situation for concrete, knowing that the concrete tensile strength is much lower than the compressive one (Eurocode 2);
- Exceeding of the maximum crack opening, according with Eurocodes (Eurocode 2).

In order to perform these checks and to verify the most burdensome situation, a stationary analysis on a single pile has been performed. In this case the single pile could be for benefit of safety because the tension are higher than when a complete and rigorous analysis has been carried out, because the displacement increase and the tension decrease in the latter case. Another important advantage for these checks is the saving of the computational time, because for single pile is not required a high computational time.

4.2.1 Modelling choices

A 2-D axisymmetric finite element model of the site was developed using the software COMSOL Multiphysics (COMSOL, 2014) (Figure 4.1). The model reproduces the single pile as if it were isolated and it does not accounts for the presence of the pipes in the energy piles in which a heat carrier fluid is assumed to flow.

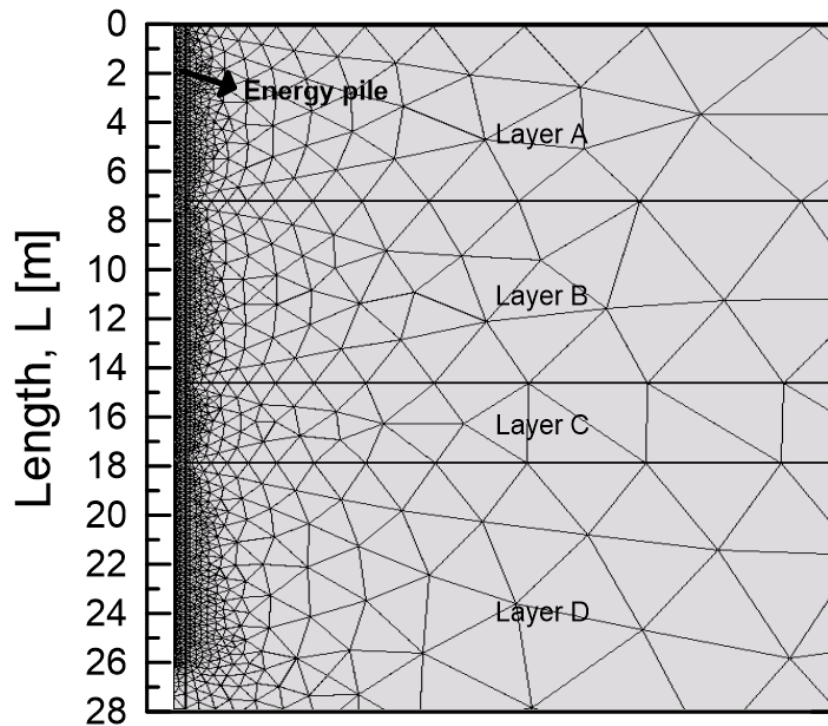


Figure 4.1: 2-D Axisymmetric model performed.

The parameters of the layers are summarized in the chapter 2. In this simulation is important to say that the linear thermal expansion coefficients of the layers (α_{soil}) are equal to zero and the thermal variation has been applied on the whole pile because the pipes have not been modelled in this analysis. The numerical analysis of the response of the reinforced concrete foundation in the soil under mechanical and thermal loads is based on the following assumptions:

- the displacements and deformations of all of the materials can be representatively described through a linear kinematic approach under quasi-static conditions (i.e., negligible inertial effects);
- the materials that constitute the pile foundation are considered to be isotropic with pores that are fully filled by air and are assumed to be purely conductive domains with equivalent thermo-physical properties that are given by the fluid and the solid phases;
- the materials that make up the soil layers are assumed to be isotropic;
- the loads that are associated with this problem have a negligible impact on the variation of the hydraulic field in the soil;
- all the materials are considered to be representatively described by linear thermo-elastic behaviors.

Restrictions are applied to both the vertical and horizontal displacements on the base of the model (i.e., pinned boundary) and to the horizontal displacements on the sides (i.e., roller boundaries).

4.2.2 Combinations

As mentioned in the previous chapter, the checks for SLS have been carried out considering a design load given by three different combinations: characteristic, quasi-permanent and frequent. In this case the classic combination formula (equation (8.6)) needs to be employed while considering the following (Eurocode (EN 1990, 2002)):

$$E_d = \sum_{j \geq 1} \gamma_{G,j} G_{k,j} + \gamma_{Q,1} Q_{k,1} + \sum_{i \geq 1} \gamma_{Q,i} \Psi_{0,i} Q_{k,i} \quad (8.6)$$

(i) For heating thermal loads, it is not known *a priori* whether the involved effects make them the dominant load. Thus, *different design combinations* must be considered. One combination assumes that the effects of the thermal loads make them the dominant load ($\Delta T_k = Q_{k,1}$), (Rotta Loria, 2018):

$$E_d = \sum_{j \geq 1} \gamma_{G,j} G_{k,j} + \gamma_{Q,1} \Delta T_k + \gamma_{Q,2} \Psi_{0,2} Q_{k,2} + \dots + \gamma_{Q,i} \Psi_{0,i} Q_{k,i} \quad (8.7)$$

The other combinations assume that the effects of the thermal loads do not make them the dominant load, (Rotta Loria, 2018):

$$E_d = \sum_{j \geq 1} \gamma_{G,j} G_{k,j} + \gamma_{Q,1} Q_{k,1} + \gamma_{Q,2} \Psi_{0,2} \Delta T_k + \dots + \gamma_{Q,i} \Psi_{0,i} Q_{k,i} \quad (8.8)$$

(ii) For cooling thermal loads, a *unique design combination* must be considered, where, ($\Delta T_k = Q_{k,1}$), (Rotta Loria, 2018):

$$E_d = \sum_{j \geq 1} G_{k,j} + \gamma_{Q,1} \Delta T_k \quad (8.9)$$

The reason for the above is that the coefficients $\Psi_{0,i}$ and $\gamma_{G,j}$ are equal to zero and one, respectively, for loads the effects of which are favourable for the performance verification, such as (variable and permanent) compressive loads with respect to cooling thermal loads (which cause a decrease in energy pile compression). In the context of this study, the considered approach results in one load combination.

In the context of the partial factor ψ_i , since the considered building represent a congregation area, the partial factors ψ_i for mechanical loads are chosen with reference to the values predicted by the Eurocode (EN 1990, 2002) for “Category B”. Accordingly:

- $\psi_0 = 0.7$
- $\psi_1 = 0.7$
- $\psi_2 = 0.6$

According to Rotta Loria (2018) the partial factors ψ_i for thermal loads:

- $\psi_0 = 0.6$
- $\psi_1 = 0.5$
- $\psi_2 = 0.5$

In the case study the piles are not equally loaded and when the calculation of the combinations have been carried out, the maximum load (2200 KN) has been used. The results of the combinations are summarized in the following tables (Table 4.1-Table 4.8):

<i>Characteristic combination</i>							
Heating Thermal Loads - Dominant Mechanical						E_d	
γ_G	G_k	γ_Q	Q_k	ΔT	Ψ_0	[KN]	[°C]
1	1540	1	660	15	0.6	2200	9

Table 4.1: Characteristic combination, mechanical load dominant.

<i>Characteristic combination</i>							
Heating Thermal Loads - Dominant Thermal						E_d	
γ_G	G_k	γ_Q	Q_k	ΔT	Ψ_0	[KN]	[°C]
1	1540	0.7	660	15	1	2002	15

Table 4.2: Characteristic combination, heating thermal load dominant.

<i>Characteristic combination</i>							
Cooling Thermal Loads - Dominant Thermal						E_d	
γ_G	G_k	ΔT	γ_Q	Q_k	[KN]	[°C]	
1	1540	-10	0.7	660	2002	-10	

Table 4.3: Characteristic combination, cooling thermal load dominant.

<i>Frequent combination</i>							
Heating Thermal Loads - Dominant Mechanical						E_d	
γ_G	G_k	Ψ_1	Q_k	ΔT	Ψ_2	[KN]	[°C]
1	1540	0.7	660	15	0.5	2002	7.5

Table 4.4: Frequent combination, mechanical thermal load dominant.

<i>Frequent combination</i>							
Heating Thermal Loads - Dominant Thermal						E_d	
γ_G	G_k	Ψ_1	Q_k	ΔT	Ψ_2	[KN]	[°C]
1	1540	0.7	660	15	0.6	1936	10.5

Table 4.5: Frequent combination, heating thermal load dominant.

<i>Frequent combination</i>							
Cooling Thermal Loads - Dominant Thermal						E_d	
γ_G	G_k	Ψ_1	Q_k	ΔT	Ψ_2	[KN]	[°C]
1	1540	0.5	660	-10	0.6	1931	-6

Table 4.6: Frequent combination, cooling thermal load dominant.

<i>Quasi-Permanent combination</i>							
Heating Thermal Loads - Mechanical Loads						E_d	
γ_G	G_k	Ψ_1	Q_k	ΔT	Ψ_2	[KN]	[°C]
1	1540	0.6	660	15	0.5	1936	7.5

Table 4.7: Quasi-permanent combination, mechanical load dominant.

<i>Quasi-Permanent combination</i>							
Cooling Thermal Loads - Dominant Thermal						E_d	
γ_G	G_k	Ψ_1	Q_k	ΔT	Ψ_2	[KN]	[°C]
1	1540	0.5	660	-10	0.6	1936	-5

Table 4.8: Quasi-permanent combination, cooling thermal load dominant.

The most burdensome combination is the *characteristic combination*.

4.2.3 Influence of the slab

The stiffness characterizing the pile-structure interaction can finally be determined with reference to a rigid rectangular plate resting vertically loaded on a semi-infinite isotropic elastic half-space as (Gorbunov-Posadov and Serebrjanyi, 1961) (Laloui L. and Rotta Loria, 2019):

$$K_h = \frac{E_{soil} \sqrt{B_{slab} L_{slab}}}{(1 - \nu_{soil}^2) \rho_0} \quad (9.1)$$

where B_{slab} and L_{slab} the dimensions of the slab or general structural element connected at the pile head and ρ_0 is a displacement factor that can be evaluated as a function of the length to breadth ratio of the considered element $\chi = L_{slab}/B_{slab}$ (cf., Figure 4.2).

When layered (i.e., non-uniform) soil deposits are encountered and the variation of the deformation moduli between successive layers is not large, equation (9.1) may be approximately applied by considering average values of the Young's modulus and Poisson's ratio characterizing the soil deposit determined as follows:

$$\overline{E_{soil}} = \frac{1}{\sum_{k=1}^N l_k} \sum_{k=1}^N E_{soil,k} l_k \quad (9.2)$$

$$\overline{v_{soil}} = \frac{1}{\sum_{k=1}^N l_k} \sum_{k=1}^N v_{soil,k} l_k \quad (9.3)$$

where $E_{soil,k}$ and $\nu_{soil,k}$ are the Young's modulus and Poisson's ratio of the soil layer k . According to Poulos and Davis (1980), variations of v_{soil} along piles may be ignored because the displacement of such foundations is slightly dependent on the Poisson's ratio of the soil.

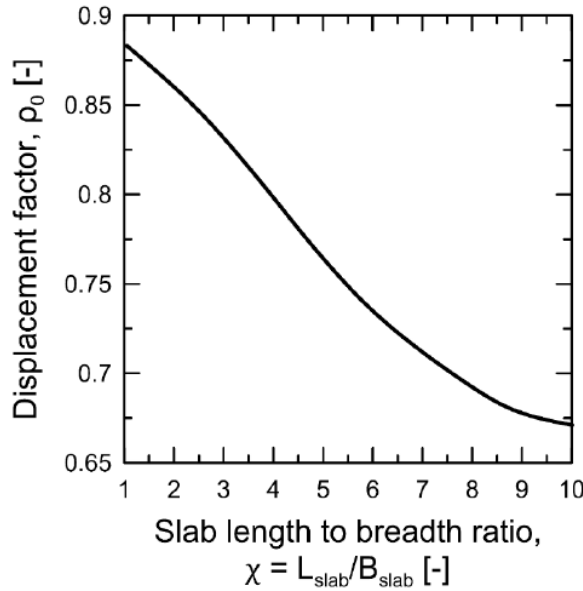


Figure 4.2: Relationship between length to breadth ratio and displacement factor of an infinitely rigid plate resting on a semi-infinite elastic half space (redraw after (Gorbunov-Posadov and Serebrjanyi, 1961)) (Laloui L. and Rotta Loria, 2019).

The value provided by the equation (9.1) is a lower bound because it has been developed taking into account the fact that below the slab there are only present the layers of soil, hence, not taking into account the effect of the piles (that stiffen the pile-slab structure).

In the real case design, when the equations (9.2 and 9.3) have been used, the average values of E_{soil} and ν_{soil} have been calculated not taking into account the parameters of the layer D, because they are completely different from that of the other layers avoiding the overestimated values.

The value of K_h calculated taking into account the previous assumptions has been applied on the pile head in the 2-D axisymmetric model, choosing the item “spring foundation”.

4.3 Eurocodes dispositions for elastic analysis

The constitutive law chosen, as mentioned before, is a thermo-mechanical elastic linear law; in fact during the FEM analysis all the components of the model (soil layers, pile and slab) have been

modelled as elastic. Since the goal of this work is adapt the conventional design procedure for energy piles, according with Eurocode, during elastic analysis, must use different values of Young's Modulus and Poisson ratio. For Young's Modulus the recommended value is equal to the Young's Modulus of the cracked section; regarding the Poisson ratio the recommended value is equal to zero.

The value of the Young's Modulus of the cracked section is calculated as:

$$E_{cr} = \frac{E_{cm}}{3} \quad (9.4)$$

Unfortunately the Eurocode do not provide the exact value of Young's Modulus of the cracked section. The previous equation has been formulated so as to take into account the long-term deformation of the concrete, knowing that precisely in the long term and therefore once the concrete has cracked, the deformation of the concrete becomes about a third of that in the short term.

In the following chapters the influence of the Young's Modulus of the cracked section has been evaluated both for mechanical and thermal load to quantify the variation within the displacement and stress fields.

4.3.1 General framework of the influence of Cracked Young's Modulus on the stress field

To understand the role and the influence of the Young's Modulus of the cracked section a sensitive analysis has been performed to quantify the effect on the stress and displacement field under thermal and mechanical load. Within this general framework two different situation have been studied: single pile with and without infinite rigid slab.

The influence of E_{cr} has been evaluated by vary the two ratios:

- L/D where L is the pile length and D represent the pile diameter;
- $\Lambda = E_{EP}/G_{soil}$ where E_{EP} is the Young's Modulus of the concrete and G_{soil} is the shear modulus of the soil. The definition of this ratio (*pile-soil stiffness ratio*) is based on the work of Randolph and Wroth (1978) for the analysis of conventional piles subjected to solely mechanical loads and has been extended to the analysis of energy pile groups subjected to both mechanical and thermal loads (Rotta Loria, 2018). It considers the shear modulus of the soil (which is preferred to the Young's modulus) because in pile-related problems the soil deforms primarily in shear and because the shear modulus is usually assumed to be unaffected by whether the loading is drained or undrained.

In the Figures 4.3 and 4.4 the comparisons (in terms of stresses) between the mean Young's Modulus and Young's Modulus of the cracked section for an energy pile subjected both upon mechanical and

thermal load, in both study cases have been pictured.

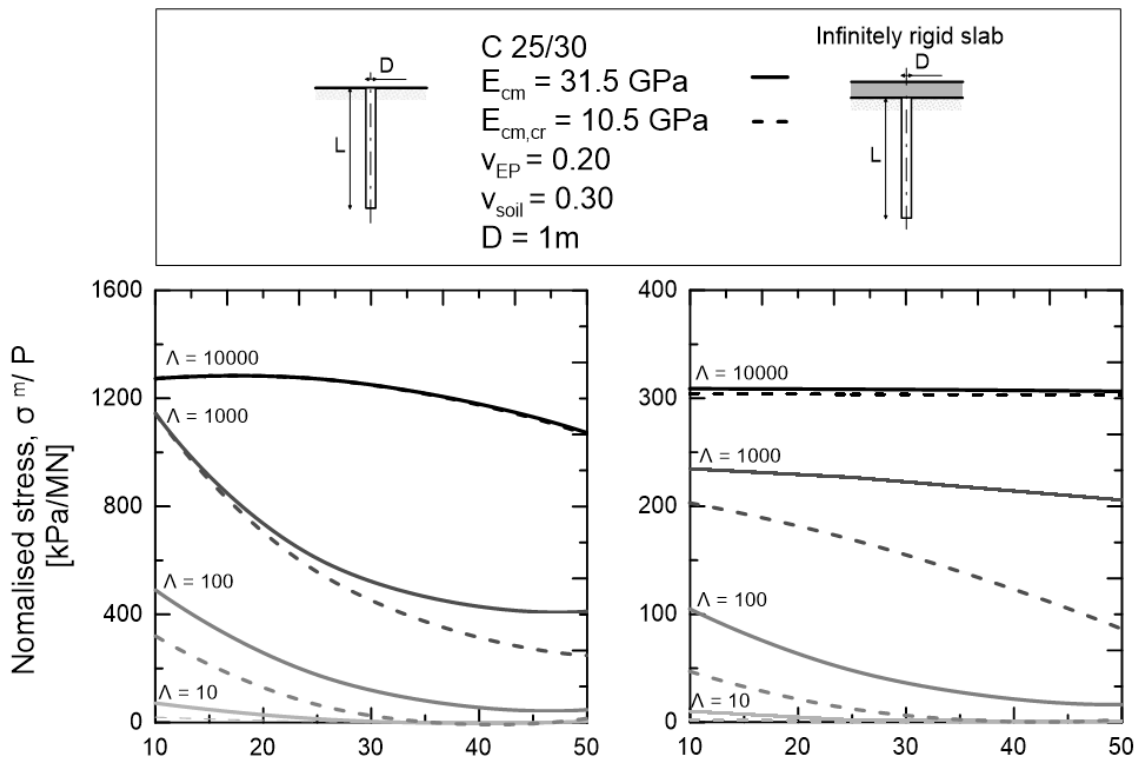


Figure 4.3: General framework of stress field variation for single pile subjected upon mechanical load.

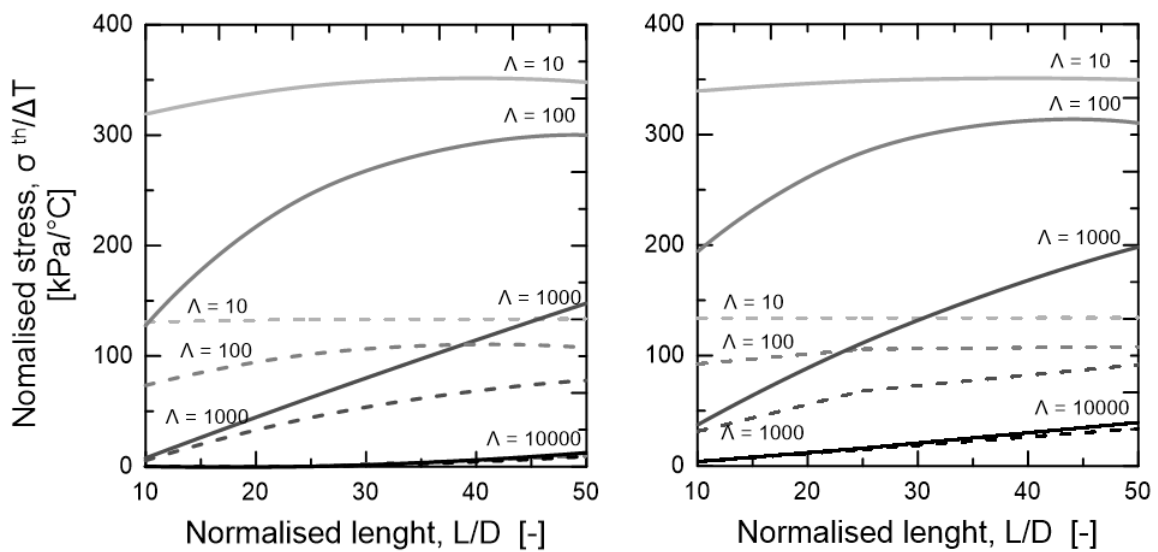


Figure 4.4: General framework of stress field variation for single pile subjected upon thermal load.

In the figure (Figure 4.3) is pictured the effect on the stress field of the Young's Modulus of the cracked section for free head pile and pile with a head restraint under mechanical load. As the value of the pile-soil stiffness ratio increase the difference between the stress fields given by the two values

of Young's Modulus tend to zero, in both study situation (free head pile and pile with an head restraint).

In the figure (Figure 4.4) is pictured the effect on the stress field of the Young's Modulus of the cracked section for free head pile and pile with a head restraint under thermal load. As the value of the pile-soil stiffness ratio decrease the difference between the stress fields given by the two values of Young's Modulus increase, in both study situation (free head pile and pile with an head restraint). In fact for $\Lambda = 10$ the values of the stresses given by E_{cm} and those given by E_{cr} are much far.

Regarding the stress field, there are some important differences between mechanical and thermal load:

- The value of pile-soil stiffness ratio play an important role: when the single pile is subjected upon mechanical load as the soil become stiffer the values of stress increase, instead the opposite happens for single pile subjected upon thermal load;
- The difference between the values of the stresses given by the given by E_{cm} and those given by E_{cr} are more remarkable in the case of the single pile subjected upon thermal load: this means that using E_{cr} underrate so much the values of the stresses and the disposition given by the equation (9.4) that is valid for mechanical load is not for thermal load.

4.3.2 General framework of the influence of Cracked Young's Modulus on the displacement field

In the Figures 4.6 and 4.7 the comparisons (in terms of displacements) between the mean Young's Modulus and Young's Modulus of the cracked section for an energy pile subjected both upon mechanical and thermal load, in both study cases have been pictured.

There are some points that must be highlighted:

- In the both case study (single pile subjected upon thermal load and mechanical load) and in the both situation (free head pile and pile with an head restraint), as the pile-soil stiffness ratio increase the values of the displacements increase;
- The difference between the displacements field given by E_{cr} and that of E_{cm} , in the both case study, is less remarkable than the difference between the stresses field given by the two values of Young's Modulus.

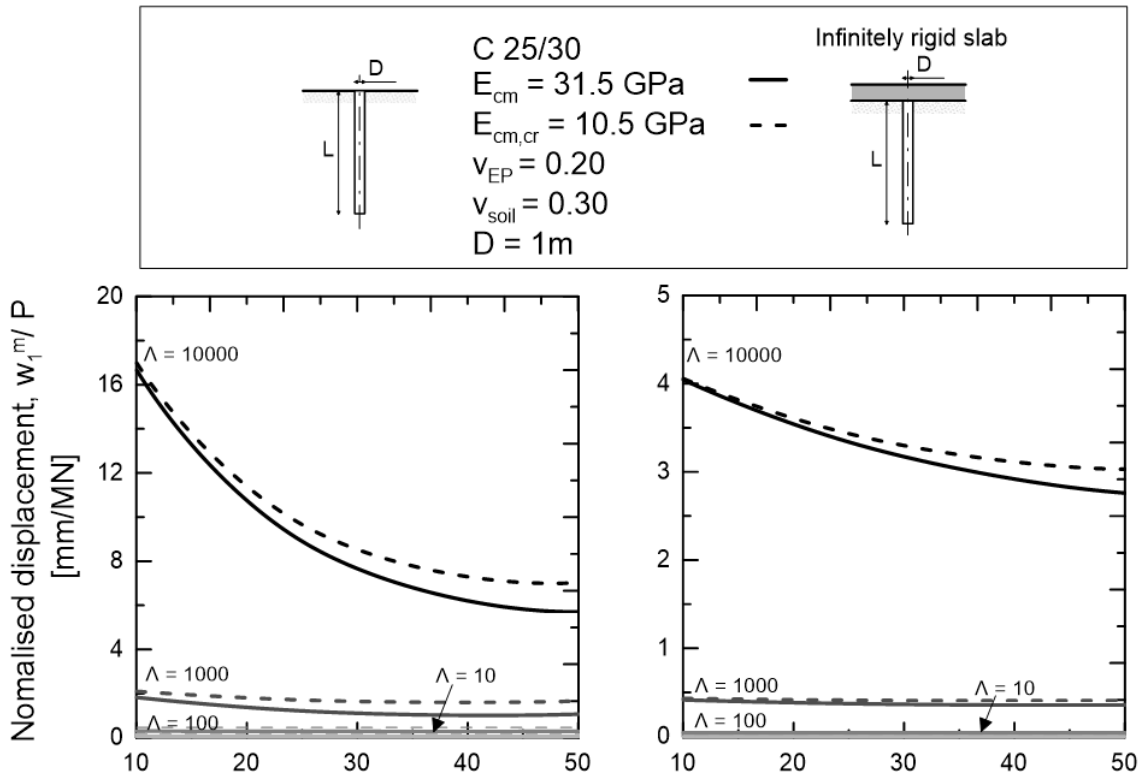


Figure 4.5: General framework of displacements field variation for single pile subjected upon mechanical load

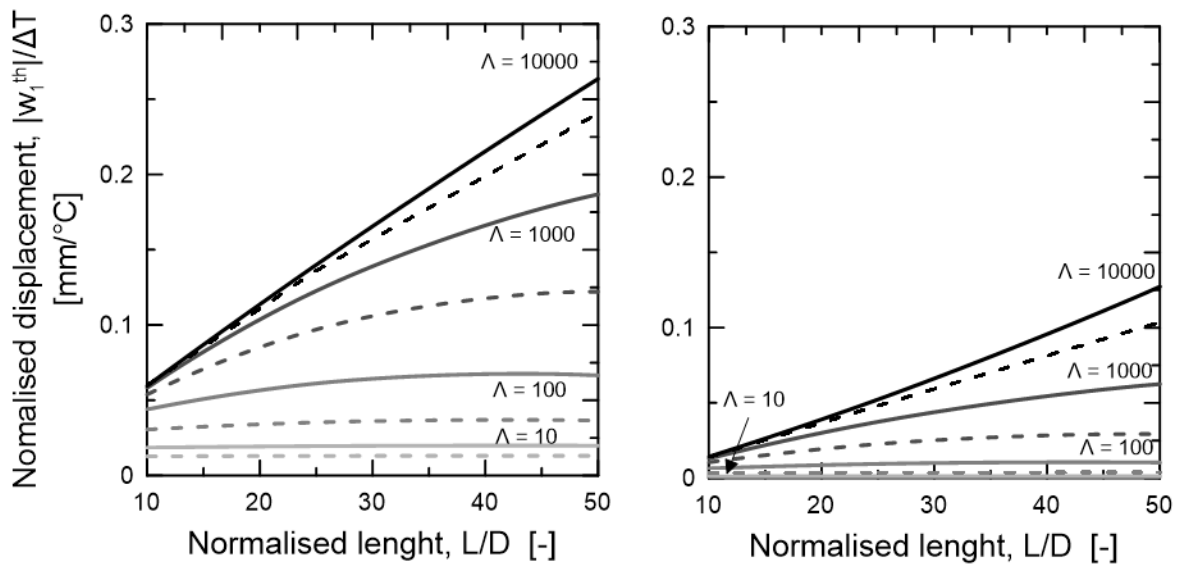


Figure 4.6: General framework of displacements field variation for single pile subjected upon thermal load.

4.3.3 General framework of the influence of nil Poisson ratio on the stress field

In the Figures 4.7 and 4.8 the difference between the two stress fields given by the values of Poisson ratio ($\nu = 0.2$ and $\nu = 0$) is pictured. There are some points that must be highlighted:

- The variation of stress fields given by the nil Poisson ration in both cases study is negligible;
- This analysis has been performed using a value of Young's Modulus equal to E_{cm} .

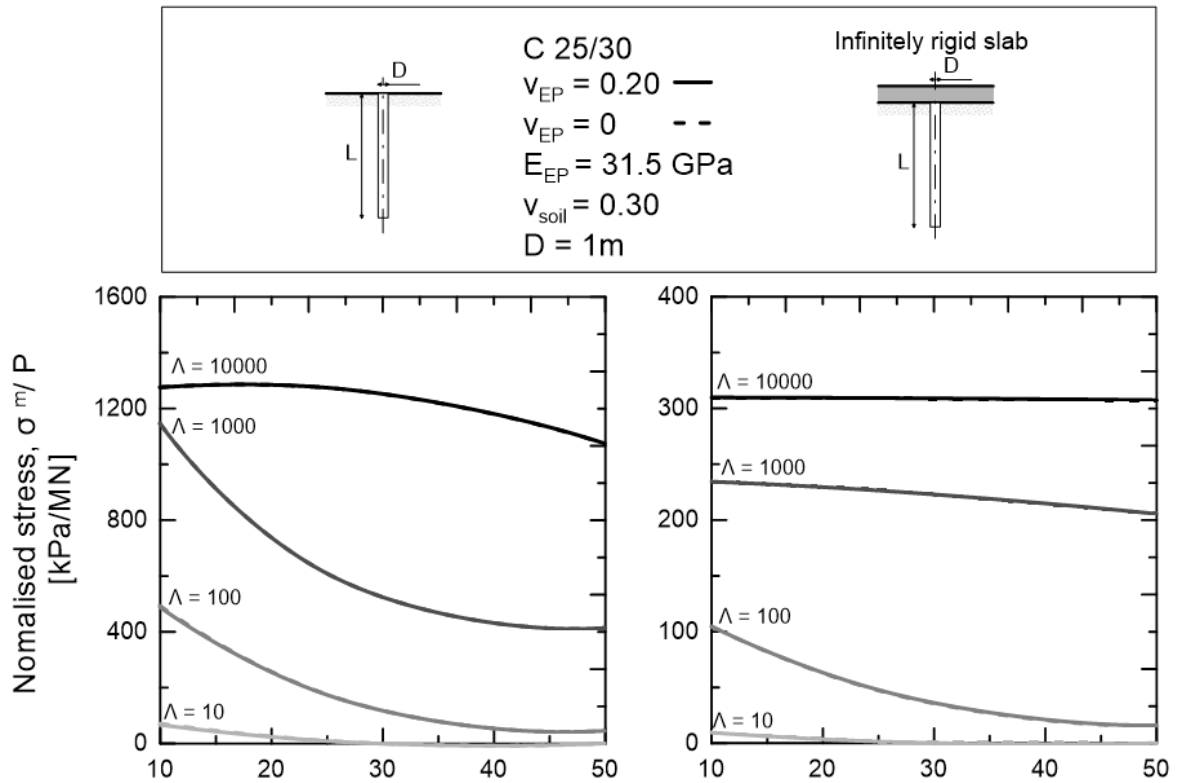


Figure 4.7: General framework of stress field variation for single pile subjected upon mechanical load.

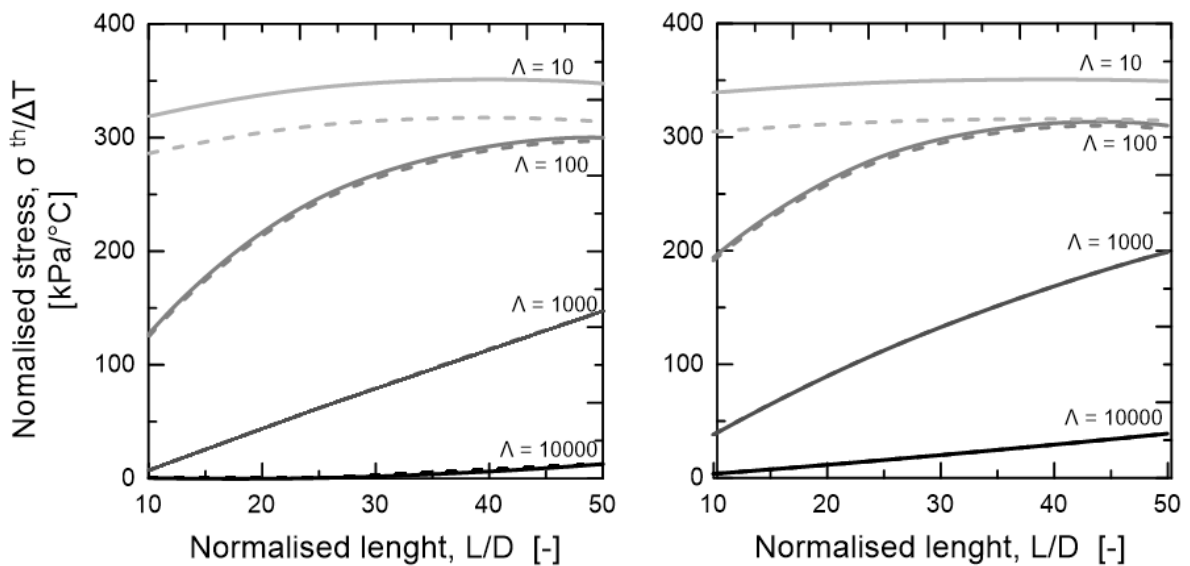


Figure 4.8: General framework of stress field variation for single pile subjected upon thermal load.

4.3.4 General framework of the influence of nil Poisson ratio on the displacement field

In the Figures 4.9 and 4.10 the difference between the two displacement fields given by the two values of Poisson ratio ($\nu = 0.2$ and $\nu = 0$) is pictured. The variation of the values of displacements both in the case of mechanical and thermal load, for both case studies, is negligible.

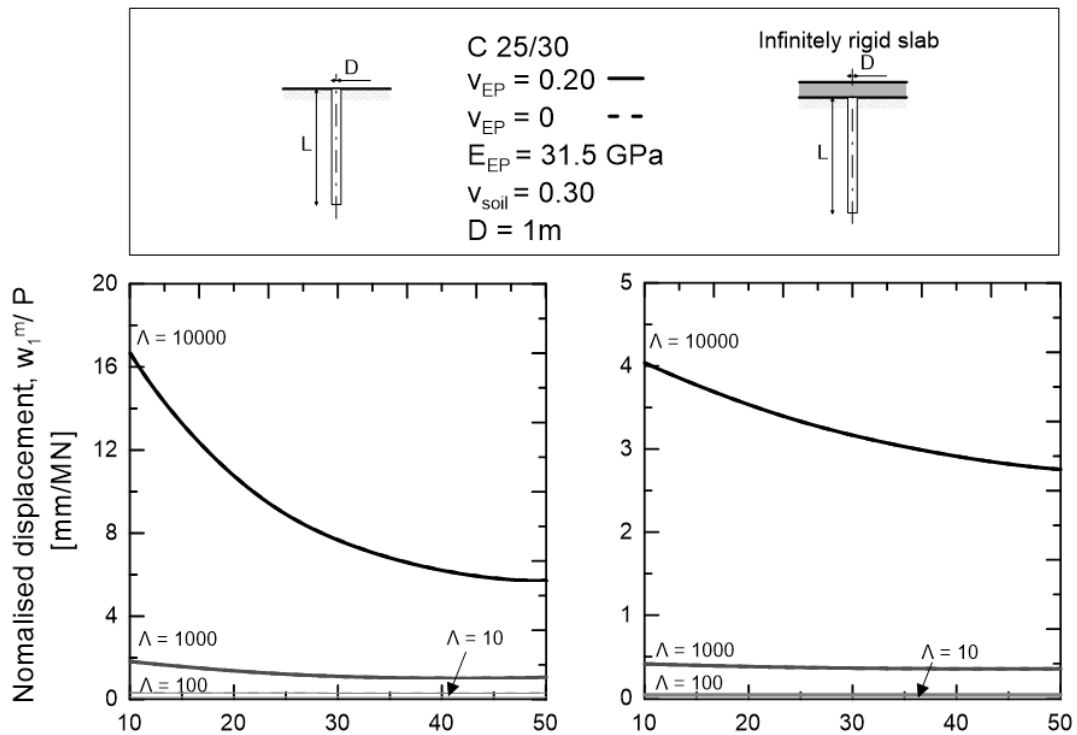


Figure 4.9: General framework of displacements field variation for single pile subjected upon mechanical load

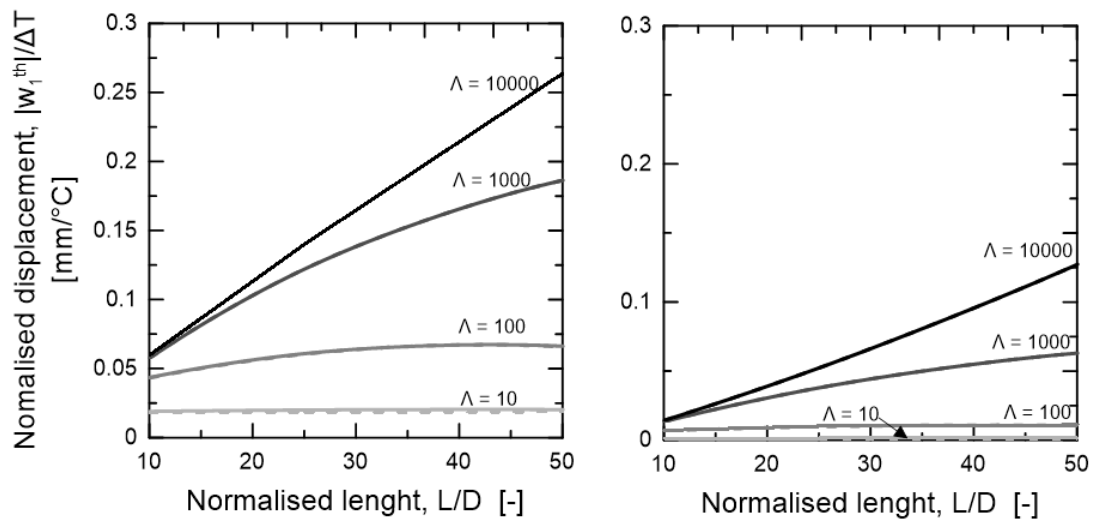


Figure 4.10: General framework of displacements field variation for single pile subjected upon thermal load.

4.3.5 Maximum stress trend with the depth

After the previous discussions it was also considered appropriate to evaluate, in function of the L/D and Λ , how the position of the maximum total stress along the pile varies. First of all, in the case study with the slab (therefore not free in the head) the values of the depth of the maximum total stress are always in the upper half of the pole (Figure 4.11) unlike the case without slab. Moreover in both cases that as the ground becomes less and less rigid the point of maximum total stress tends to rise

(in fact for $\Lambda = 10000$ indifferently from L/D , the depth of the maximum total stress approaches the head of the pile). The dotted line represents the trend of the depth of the maximum total stress obtained with a E_{cr} : in the case of a free pile in the head, the difference with the E_{cm} is much more marked than in the pile stuck in the head.

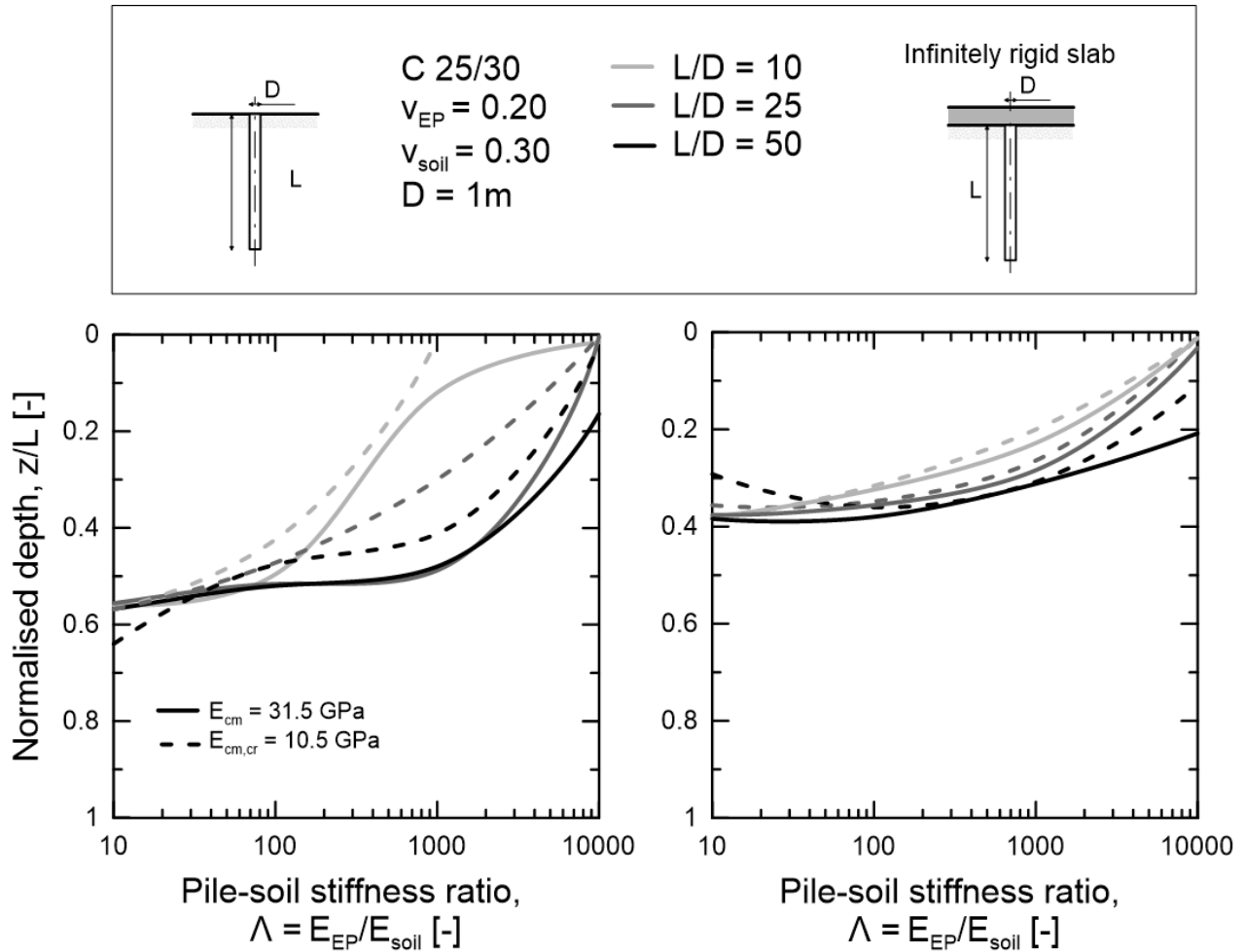


Figure 4.11: Trends of the the depth of the maximum total stress in the case of free head pile and pile with head restraint.

4.3.6 Influence of Cracked Young's Modulus in the proposed design

As in the general case, the influence of the cracked Young's Modulus and the nil Poisson ratio was also seen in our real case study in the proposed design ($L_{EP} = 19.2\text{ m}$). In the Figure 4.12 the trends of the mechanical (Figure 4.12 (a-c)) and thermal (Figure 4.12 (b-d)) stress have been portrayed. Despite the presence of the slab on the pile head, the influence of the cracked Young's Modulus is more or less the same in both situation (free head pile and pile with head restraint): in fact, the values

of the maximum thermal and mechanical stresses obtained with E_{cm} are always two times bigger than those obtained with E_{cr} .

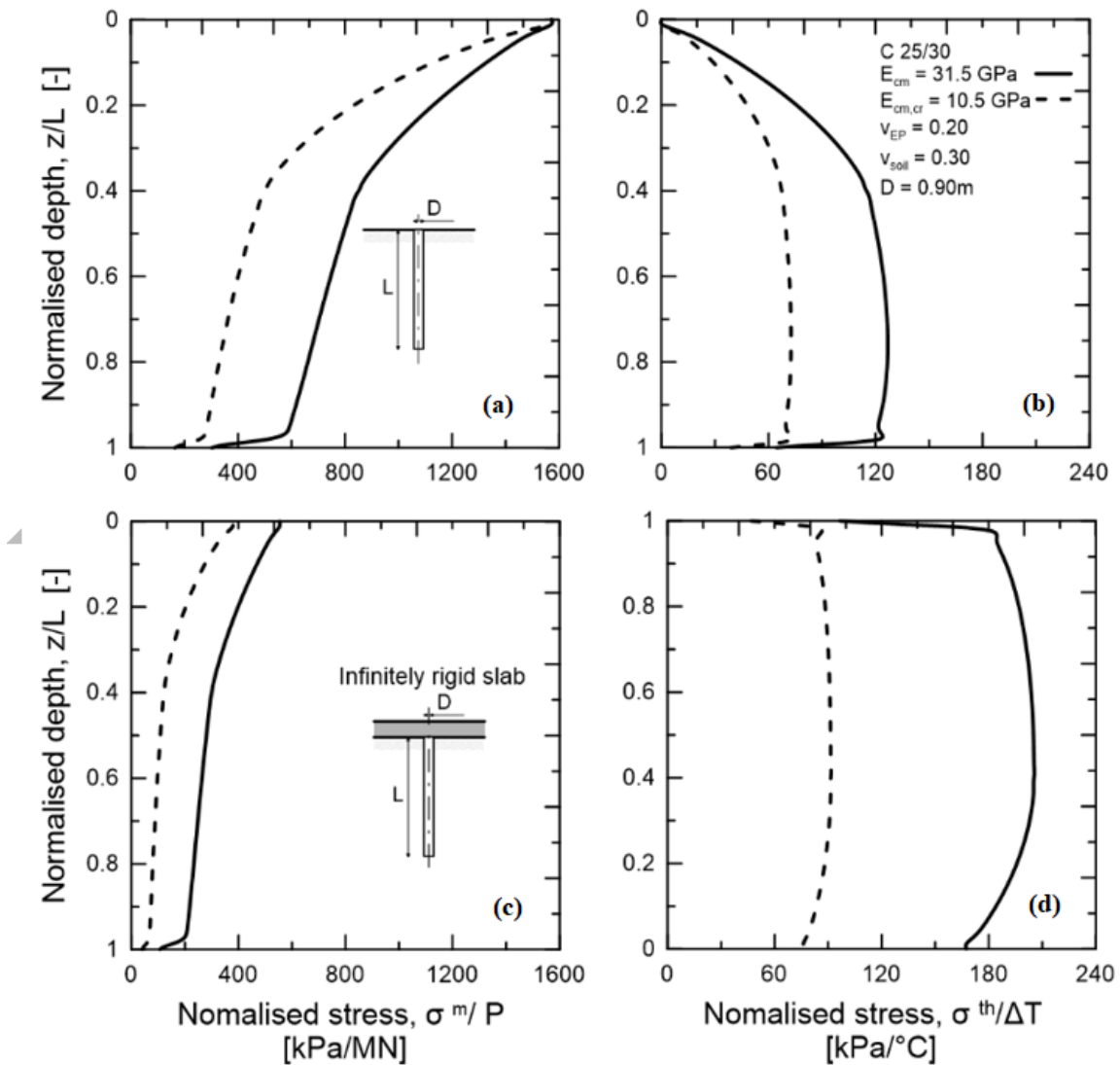


Figure 4.12 (a):Influence of the cracked Young's Modulus in the case of free head pile subjected upon mechanical load; (b) case of free head pile subjected upon thermal load; (c) case of pile with a head restraint subjected upon mechanical load; (d) case of pile with head restraint subjected upon thermal load.

In the Figure 4.13 (a-d) the trends of mechanical and thermal displacements in the case of free head pile and pile with head restraint are shown. The values of thermal displacements in both cases (piles subjected upon mechanical and thermal load) tends towards the positive part of the graph when the cracked Young's Modulus is used, but this effect is less remarkable in the pile with head restraint (Figure 4.13 (d)). In the case of pile subjected upon mechanical load the values of displacements rise in both cases but is more remarkable in the free head pile case (Figure 4.12(a)).

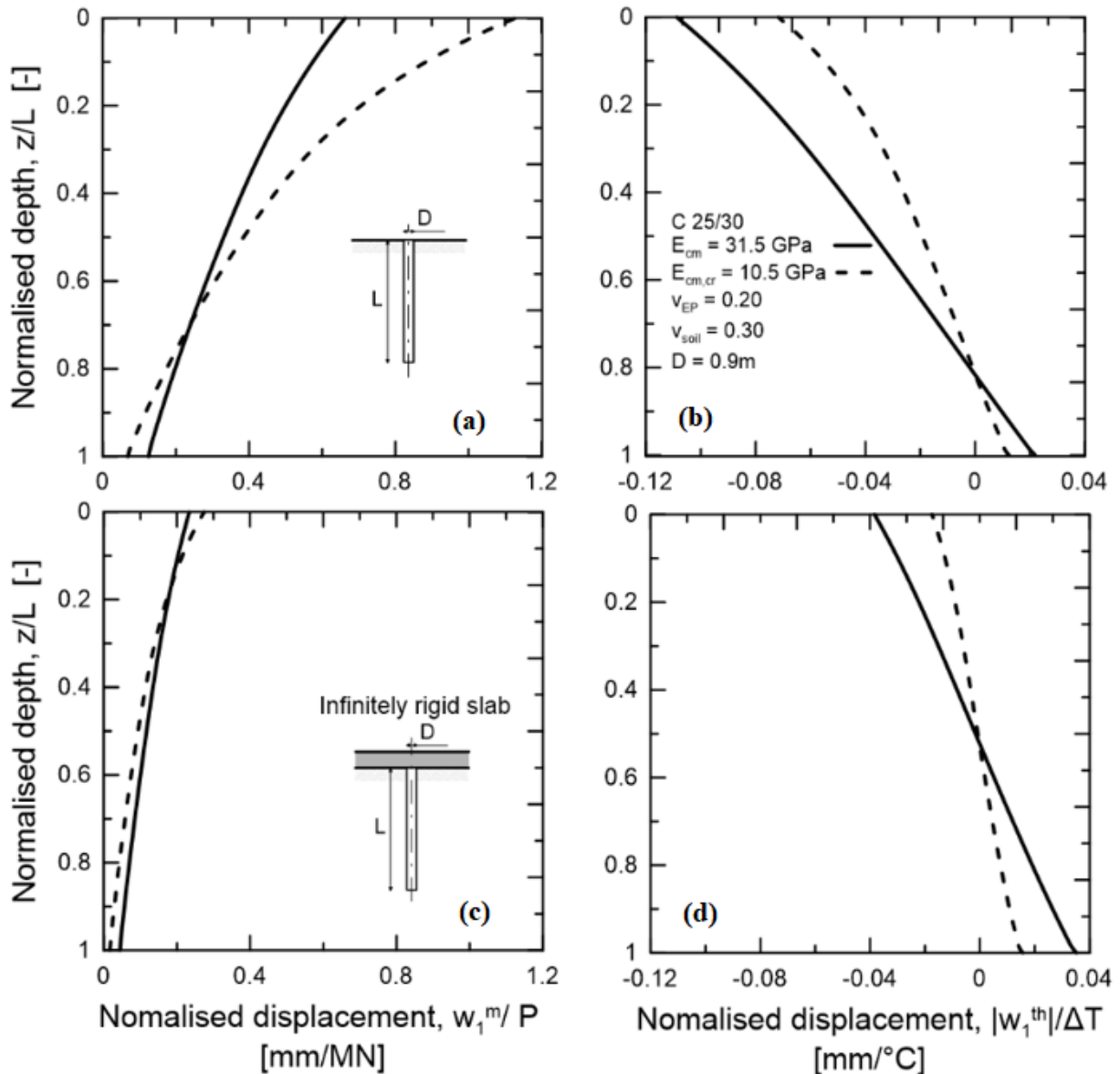


Figure 4.13 (a): Influence of the cracked Young's Modulus in the case of free head pile subjected upon mechanical load; (b) case of free head pile subjected upon thermal load; (c) case of pile with a head restraint subjected upon mechanical load; (d) case of pile with head restraint subjected upon thermal load.

During the displacement checks, it must be verified that the total movement is less than the allowed limit. In the case of a free head pile, the best solution to adopt would be to perform analysis with the cracked Young's Modulus because it gives us higher values. Our case study instead, consists of pile with head restraint: in this case, the best choice to adopt is to perform analysis with E_{cm} because it gives us higher values.

4.3.7 Influence of nil Poisson ratio in the proposed design

In the Figures 4.14 and 4.15 are summarized the trends of the stresses (Figure 4.14) and displacements (Figure 4.15) with a Poisson ratio equal to 0.20 and zero. The differences given by the value of the Poisson ratio is negligible, as in the general framework.

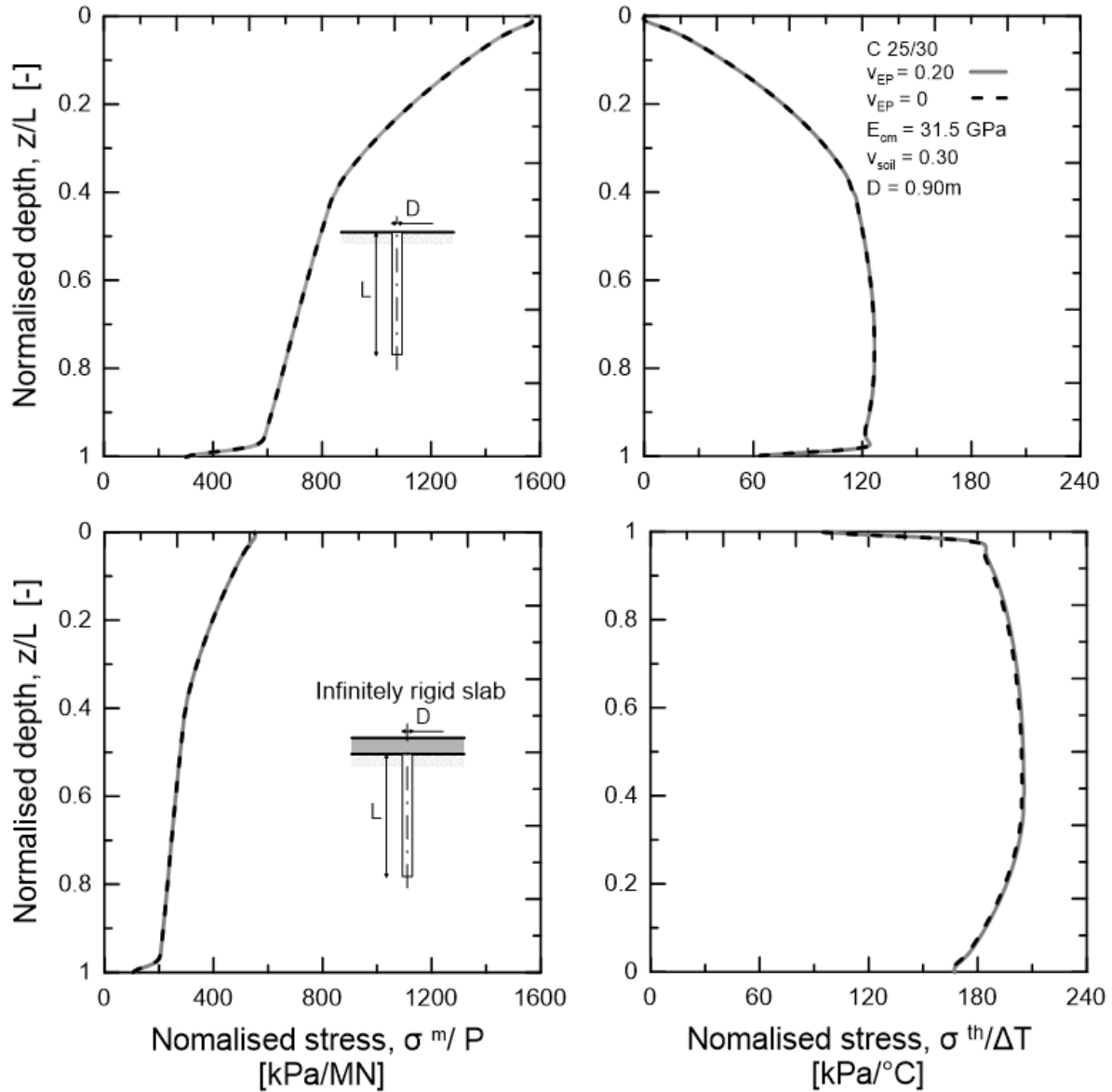


Figure 4.14 (a): Influence of the cracked Poisson ratio in the case of free head pile subjected upon mechanical load; **(b)** case of free head pile subjected upon thermal load; **(c)** case of pile with a head restraint subjected upon mechanical load; **(d)** case of pile with head restraint subjected upon thermal load.

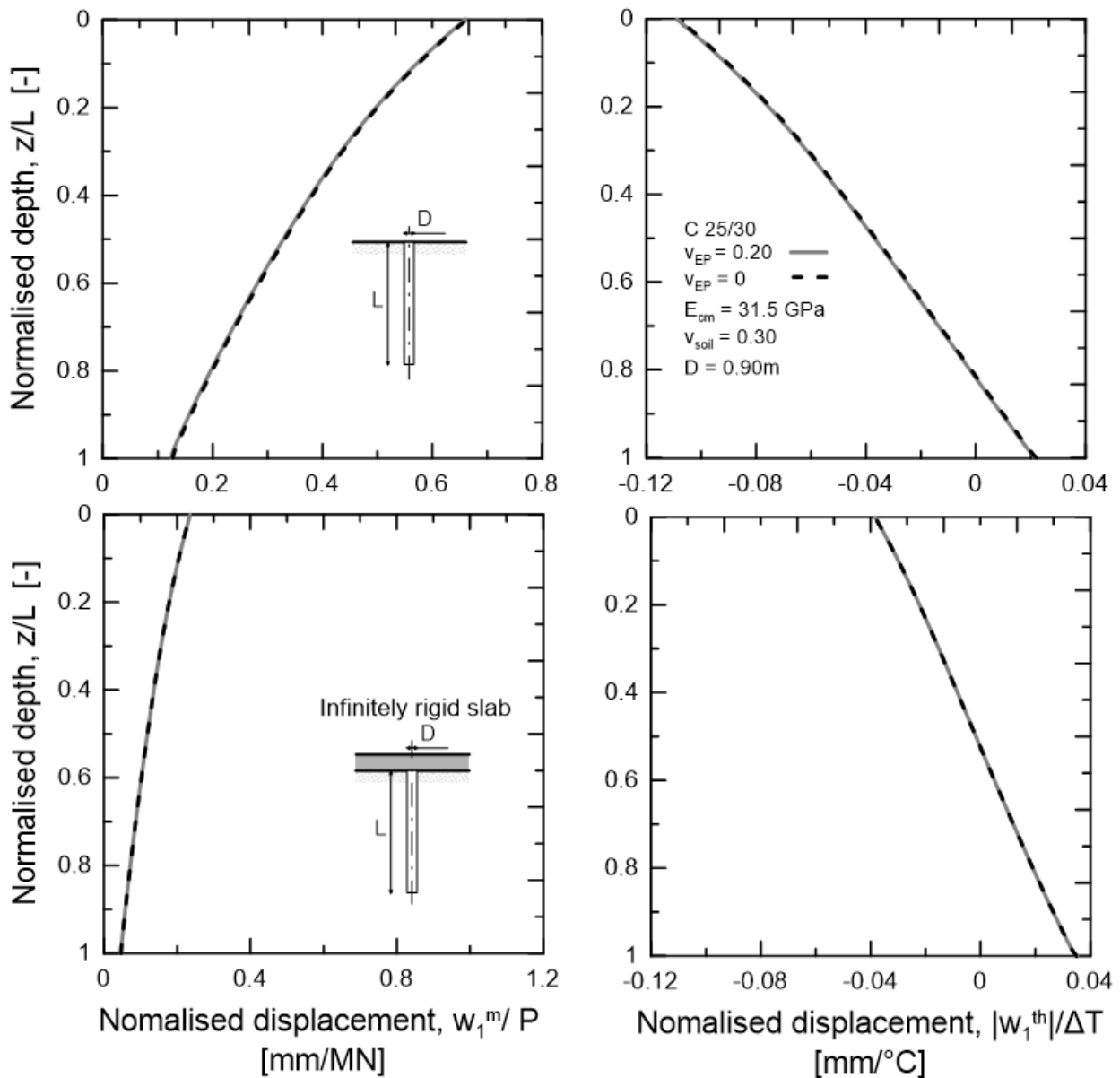


Figure 4.15 (a): Influence of the cracked Poisson ratio in the case of free head pile subjected upon mechanical load; **(b)** case of free head pile subjected upon thermal load; **(c)** case of pile with a head restraint subjected upon mechanical load; **(d)** case of pile with head restraint subjected upon thermal load.

4.3.8 Concluding remarks

To perform a single pile analysis in order to verify the serviceability condition there are some points that must be highlighted:

- The Eurocode recommendation to use a cracked Young's Modulus it is not a safety advantage for single piles subjected upon thermal load because they underestimate the value of the stresses;

- The Eurocode recommendation to use a nil Poisson ratio does it does not provide substantial differences in terms of displacements and stresses.

4.4 Serviceability verifications for both design situations

4.4.1 Tension Limit State

As mentioned in the chapter 4.1 the the compressive strength in the concrete must be limited in order to avoid longitudinal cracks, micro-cracking or high viscosity levels, where these may have unacceptable effects on the functionality of the structure. Experimentally it has been noticed that when:

- If the compression stress level in the concrete under the characteristic combination exceeds a critical value longitudinal cracks may arise. In the absence of adequate measures (such as increasing the concrete cover in the compression or confinement area by transverse reinforcement) it may be appropriate to limit the compression stress to the value

$$\sigma_c = k_1 \cdot f_{ck} \quad (9.5)$$

where for k_1 the recommended value is 0.6 for environmental class XD, XF and XS;

- A linear visco-elastic behavior can be assumed if the stress in the concrete below the almost permanent loads is less than:

$$\sigma_c = k_2 \cdot f_{ck} \quad (9.6)$$

where for k_2 the recommended value is 0.45. If the stress in the concrete exceeds this value, it is recommended to consider a non-linear visco-elastic behavior;

- It can be admitted that the appearance of cracks or unacceptable displacement are avoided when, under the combination of characteristic loads, the traction tension in the armature does not exceed

$$\sigma_s = k_3 \cdot f_{yk} \quad (9.7)$$

where for k_3 the recommended value is 0.8. If the stress is due only to imposed deformations, as in the case of impeded shrinkage, it is recommended that the traction stress does not exceed

$$\sigma_s = k_4 \cdot f_{yk} \quad (9.8)$$

where for k_4 the recommended value is 1.

The above reported recommendations (according to Eurocode 2 (EN 1992, 2004)) have been estimated following some hypothesis:

- Preservation of the flatness of the sections;

- Equal deformations between steel and surrounding concrete, both in traction and in compression;
- Linear elastic behavior of concrete in compression: both steel and concrete have a linear elastic behavior and in fact the steel reaches a maximum tension equal to f_{yk} , while for concrete we consider a linear elastic behavior, as we take stress values very low until reaching $0.6f_{ck}$;
- The section is considered as not cracked when the tensile stress induced by the bending does not exceed (Eurocode 2 (EN 1992, 2004)):

$$f_{ct,eff} = f_{ctm} = 0.3 \cdot f_{ck}^{2/3} \quad (9.9)$$

- Linear elastic behavior of the steel both in traction and in compression.

In other words, the checks that must be carried out are following the equations (9.6) and (9.8).

4.4.2 Tension Limit State for the real design case

Resuming the load combinations for thermal loads (equations (8.7)-(8.9)) the most burdensome combination is the characteristic one in the case of single pile modelled with slab on its head (in COMSOL model is called “spring foundation”). The checks for the real design case (pile with length equal to 28 m) are summarized in the following tables:

<i>Serviceability check – Mechanical load dominant combination - Heating</i>					
$\sigma_{c,max,m+th}$ [kPa]	f_{ck} [Mpa]	f_{ck} [Kpa]	k_2	$k_2 \cdot f_{ck}$ [Kpa]	check
2922.23	45	45000	0.6	27000	✓
$\sigma_{s,max,m+th}$ [kPa]	f_{yk} [Mpa]	f_{yk} [KPa]	k_4	$k_4 \cdot f_{yk}$ [Kpa]	check
-16441.45	-500	-500000	1	-500000	✓

Table 4.10: Serviceability check for *characteristic combination* in case of mechanical load dominant during heating.

<i>Serviceability check – Thermal load dominant combination - Heating</i>					
$\sigma_{c,max,m+th}$ [kPa]	f_{ck} [Mpa]	f_{ck} [Kpa]	k_2	$k_2 \cdot f_{ck}$ [Kpa]	check
4833.76	45	45000	0.6	27000	✓
$\sigma_{s,max,m+th}$ [kPa]	f_{yk} [Mpa]	f_{yk} [KPa]	k_4	$k_4 \cdot f_{yk}$ [Kpa]	check
-27196.37	-500	-500000	1	-500000	✓

Table 4.11: Serviceability check for *characteristic combination* in case of thermal load dominant during heating.

<i>Serviceability check – Thermal load dominant combination - cooling</i>					
$\sigma_{s,max,m+th}$ [kPa]	f_{yk} [Mpa]	f_{yk} [KPa]	k_4	$k_4 \cdot f_{yk}$ [Kpa]	check
-805479.15	-500	-500000	1	-500000	✘

Table 4.12: Serviceability check for *characteristic combination* in case of thermal load dominant during cooling.

Even if the most burdensome combination is the characteristic one, but is not directly related with the opening cracks because is not directly related with the displacement. The combination suitable to these type of checks is the quasi-permanent one. In the following tables are summarized the results:

<i>Serviceability check – Heating thermal load</i>					
$\sigma_{c,max,m+th}$ [kPa]	f_{ck} [Mpa]	f_{ck} [Kpa]	k_2	$k_2 \cdot f_{ck}$ [Kpa]	check
2488.25	45	45000	0.45	20250	✔
$\sigma_{s,max,m+th}$ [kPa]	f_{yk} [Mpa]	f_{yk} [KPa]	k_4	$k_4 \cdot f_{yk}$ [Kpa]	check
-13999.74	-500	-500000	1	-500000	✔

Table 4.13: Serviceability check for *quasi-permanent combination* in case of heating thermal load.

<i>Serviceability check – Cooling thermal load</i>					
$\sigma_{s,max,m+th}$ [kPa]	f_{yk} [Mpa]	f_{yk} [KPa]	k_4	$k_4 \cdot f_{yk}$ [Kpa]	check
-406768.96	-500	-500000	1	-500000	✔

Table 4.14: Serviceability check for *quasi-permanent combination* in case of cooling thermal load.

With the quasi-permanent combination values all the tension limit state verifications are satisfied.

4.4.3 Cracking Limit State

The importance of limiting cracks is one of the central aspects of the behavior of reinforced concrete structures in operation, as excessive cracks can irreversibly compromise not only the aesthetics of the structural elements, but in the long term, even its static function . In aggressive environments, in fact the corrosion of the reinforcements could strongly reduce the resistant area of the same thus decreasing the resistance of the entire element and modifying the calculation models seen so far.

Analyzing a tie of reinforced concrete subjected to traction:

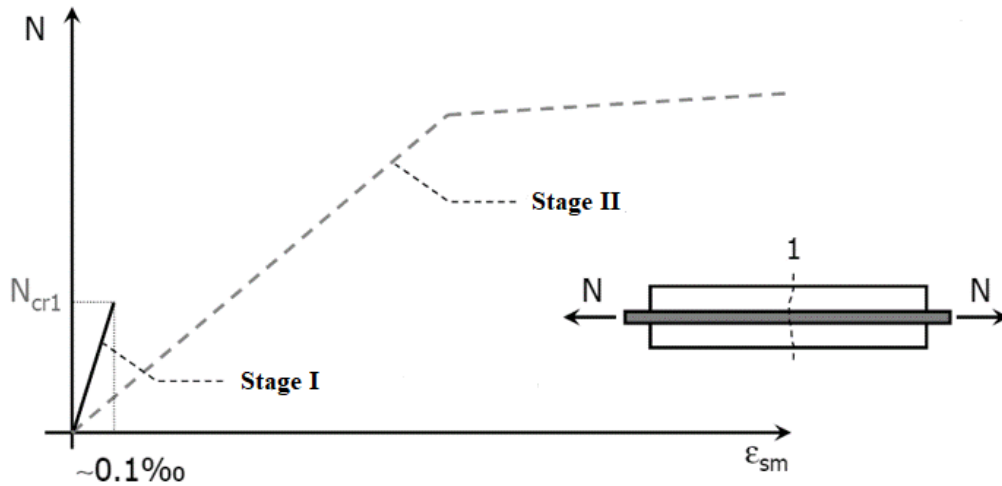


Figure 4.16: Load –deformation law, in which is described the 1st stage of crack opening (Giordano L.,2016)

The deformation in a cracked element, however, depends on the area in which it is evaluated and in the case 1) the deformation can be evaluated as described above, but in case 2) no.

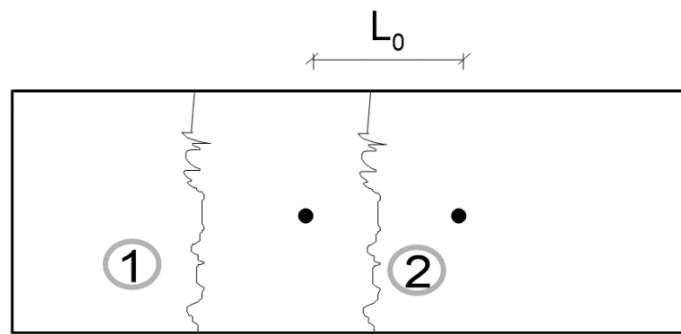


Figure 4.17: Representative scheme of the zone of crack openings.

Therefore starting from the fact that the base on which the deformation moves is large and therefore we can take more cracks, we will define the average deformation, ϵ_{sm} , since as we have already said the deformation involves more fissures.

Looking at the Figure 4.16 initially, in the non-cracked case, then we will have a linear elastic behavior on the part of the rod up to the point $C_{r,1}$ where the first crack is formed:

$$N_{cr,1} = f_{ct} \cdot A_0 \quad (10.1)$$

where

$$A_0 = A_c + nA_s \quad (10.2)$$

with n is the homogenization coefficient. The deformation will be equal to 0.01% and is obtainable from the ratio:

$$\varepsilon_{cr} = \frac{f_{ct}}{E_{cm}} \quad (10.3)$$

This stage just described is called *STAGE I* or *STAGE OF CONCRETE NOT CRACKED*.

According with aforementioned hypothesis the concrete deformation is equal to that of the steel in the area adjacent to the reinforcement as:

$$\varepsilon_s = \varepsilon_c \quad (10.4)$$

And knowing that the deformations are equal to:

$$\varepsilon_s = \frac{\sigma_s}{E_s} \quad (10.5)$$

$$\varepsilon_c = \frac{\sigma_c}{E_c} \quad (10.6)$$

And obtaining:

$$\frac{\sigma_s}{\sigma_c} = \frac{E_s}{E_c} = n \quad (10.7)$$

If the normal force increase , obviously exceeding $N_{cr,1}$ we have a variation in stiffness, or more precisely a decrease in stiffness occurs and there is an increase in the number of cracks. These cracks, observing experimentally, stop at almost constant distance and starting from $N_{cr,1}$ until the point $N_{cr,n}$, the number of cracks stops to increase (Figure 4.18):

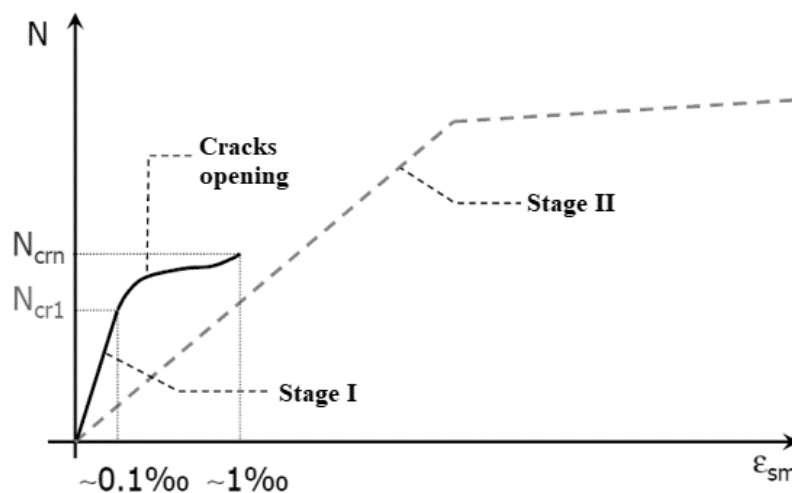


Figure 4.18: Description of the moment in which the cracks start to open, until when they stop (Giordano L.,2016).

So at the point $N_{cr,n}$, the number of cracks no longer increases and therefore we can ultimately say that the number of cracks is not infinite, but finite. The dotted line represents the trend of the steel behavior, or that elastic-perfectly plastic. Therefore, after cracking, there is no longer any formation of other cracks, but there is an elastic-linear behavior with a rigidity of the tie equal to that of the bar without concrete and:

$$\varepsilon_{sm,II} = \varepsilon_{sm} + \Delta\varepsilon_{sm} \quad (10.8)$$

The contribute of $\Delta\varepsilon_{sm}$ *tension stiffening* that describes the stiffening effect of the concrete that is between one bar and the other and increases the secant stiffness, while the tangent one always remains the same. This stiffening effect is important because the steel is in Stage II in the crack and in Stage I in the central area of the section between two cracks. The transition from one stage to another is ensured by the adhesion stresses that develop between steel and concrete. This behavior is described by the following figure (Figure 4.19):

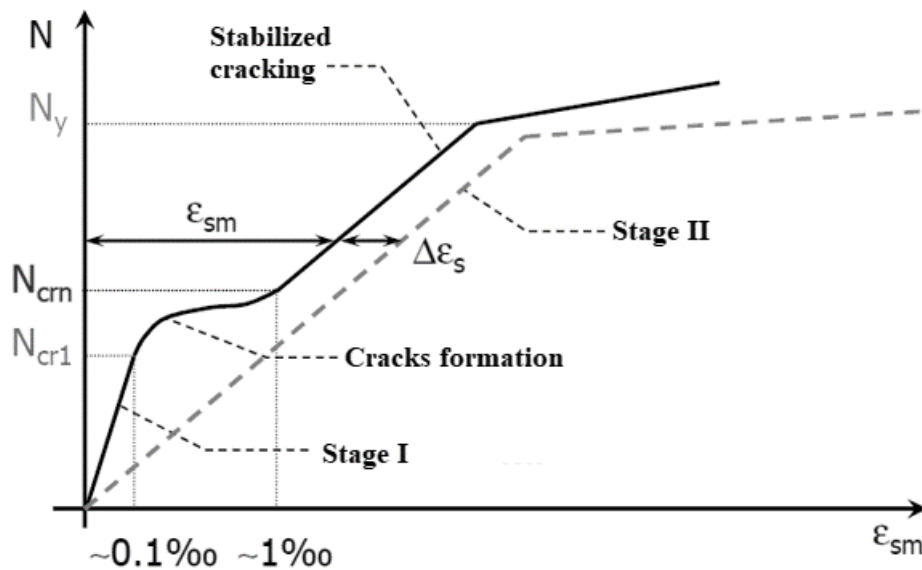


Figure 4.19: Description of the moment in which the cracking is stabilized (Giordano L.,2016).

Therefore, in stage I the cracks increase while in stage II the size of the crack increases.

According to Eurocodes the cracks opening has been calculated as:

$$w_k = S_{r,max}(\varepsilon_{sm} - \varepsilon_{cm}) \quad (10.9)$$

where:

- w_k is the design crack opening;

- $S_{r,max}$ is the distance between two cracks;
- ε_{sm} is the average deformation of the steel;
- ε_{cm} is the average deformation of the concrete.

$S_{r,max}$ has been calculated as:

$$S_{r,max} = k_3 c + k_1 k_2 k_4 \cdot \frac{\phi}{\rho_{eff}} \quad (11.1)$$

where:

- c is the cover;
- k_1 coefficient that take into account the adherence property of the steel. The recommended value is 0.8 for bars with improved adherence, or, 1.6 for smooth bars.
- k_2 coefficient that take into account the deformation distribution. The recommended value is 0.5 for bending and 1 for pure traction;
- k_3 recommended value is 3.4;
- k_4 recommended value is 0.425.

and

$$\varepsilon_{sm} - \varepsilon_{cm} = \frac{\sigma_s - k_t \frac{f_{ct,eff}}{\rho_{p,eff}} (1 + n \cdot \rho_{p,eff})}{E_s} \geq 0.6 \frac{\sigma_s}{E_s} \quad (11.2)$$

The allowed limits are summarized in the following table:

Group	Environmental conditions	Loads combination	Reinforcement			
			Sensitive		Less sensitive	
			Limit state	w_k	Limit state	w_k
A	Ordinary	frequent	Crack open.	$\leq w_2$	Crack open.	$\leq w_3$
		quasi-permanent	Crack open.	$\leq w_1$	Crack open.	$\leq w_2$
B	Aggressive	frequent	Crack open.	$\leq w_1$	Crack open.	$\leq w_2$
		quasi-permanent	decompression		Crack open.	$\leq w_1$
C	More aggressive	frequent	Cracks formation		Crack open.	$\leq w_1$
		quasi-permanent	decompression		Crack open.	$\leq w_1$

Table 4.15: Allowed limit according to Eurocodes for crack opening (Eurocode 2).

where:

- $w_1 = 0.2 \text{ mm}$;

- $w_2 = 0.3 \text{ mm}$;
- $w_3 = 0.4 \text{ mm}$.

4.4.4 Cracking Limit State for the real design case

The checks for the real design case (pile with length equal to 28 m) in case of *characteristic combination*, are summarized in the following tables:

<i>Serviceability check – Thermal load dominant combination - cooling</i>		
$w_{k,max}$ [mm]	w_k [mm]	check
0.3	2.49	✗

Table 4.16: Serviceability check for *characteristic combination* in case of heating cooling load.

In this case of quasi-permanent combination:

<i>Serviceability check – Thermal load dominant combination - cooling</i>		
$w_{k,max}$ [mm]	w_k [mm]	check
0.3	1.50	✗

Table 4.17: Serviceability check for *quasi-permanent combination* in case of heating cooling load.

In both cases, the crack opening check is not satisfied. Some points must be highlighted:

- The opening crack verification has been carried out only when the cooling thermal load has been applied. This because when a cooling thermal load is applied, within the pile generate a tensile stress that easily overcome the concrete tensile strength.
- Even in this type of check the most burdensome case is the single pile with a spring on its head.

4.4.5 Deformation Limit State

It is necessary to establish adequate deformation limit values, which take into account the nature of the structure, the finishes, the partitions and the accessories as well as the function of the structure itself. In this type of work the main point is verify that (Eurocode 7):

$$w^{m+tot} \leq w_{adm} = \frac{\text{min spacing}}{500} \quad (11.3)$$

In this chapter only single pile analysis have been performed and do not taking into account the group pile effect that increase the value of head displacement because take into account the interaction

among the piles. In fact, the deformation limit state verifications have been carried out in the chapter 5.

4.4.6 Tension Limit State for the proposed design case

In this chapter the SLS verification for the proposed design case (pile length equal to 19.2 m) have been carried out. Firstly, is important clarify some different details:

- In the proposed design case the pile length is lower than that of the real case and this involves that the values of total stresses are lower;
- In the proposed design the amount of reinforcement has been calculated with the equation (7.9) to ensure more ductility and this involves lower crack openings.

The checks in case of *characteristic combination* are summarized in the following tables:

<i>Serviceability check – Mechanical load dominant combination - Heating</i>					
$\sigma_{c,max,m+th}$ [kPa]	f_{ck} [Mpa]	f_{ck} [Kpa]	k_2	$k_2 \cdot f_{ck}$ [Kpa]	check
1890.85	25	25000	0.6	15000	✓
$\sigma_{s,max,m+th}$ [kPa]	f_{yk} [Mpa]	f_{yk} [KPa]	k_4	$k_4 \cdot f_{yk}$ [Kpa]	check
-12521.97	-500	-500000	1	-500000	✓

Table 4.18: Serviceability check for *characteristic combination* in case of mechanical load dominant during heating.

<i>Serviceability check – Thermal load dominant combination - Heating</i>					
$\sigma_{c,max,m+th}$ [kPa]	f_{ck} [Mpa]	f_{ck} [Kpa]	k_2	$k_2 \cdot f_{ck}$ [Kpa]	check
3046.63	25	25000	0.6	15000	✓
$\sigma_{s,max,m+th}$ [kPa]	f_{yk} [Mpa]	f_{yk} [KPa]	k_4	$k_4 \cdot f_{yk}$ [Kpa]	check
-19358.54	-500	-500000	1	-500000	✓

Table 4.19: Serviceability check for *characteristic combination* in case of thermal load dominant during heating.

<i>Serviceability check – Thermal load dominant combination - Cooling</i>					
$\sigma_{s,max,m+th}$ [kPa]	f_{yk} [Mpa]	f_{yk} [KPa]	k_4	$k_4 \cdot f_{yk}$ [Kpa]	check
-265716.70	-500	-500000	1	-500000	✓

Table 4.20: Serviceability check for *characteristic combination* in case of thermal load dominant during cooling.

The checks in case of *quasi-permanent combination* are summarized in the following tables:

<i>Serviceability check – Heating thermal load</i>					
$\sigma_{c,max,m+th}$ [kPa]	f_{ck} [Mpa]	f_{ck} [Kpa]	k_2	$k_2 \cdot f_{ck}$ [Kpa]	check
1585.55	25	25000	0.45	11250	✓
$\sigma_{s,max,m+th}$ [kPa]	f_{yk} [Mpa]	f_{yk} [KPa]	k_4	$k_4 \cdot f_{yk}$ [Kpa]	check
-10074.70	-500	-500000	1	-500000	✓

Table 4.20: Serviceability check for *quasi-permanent combination* in case of heating thermal load.

<i>Serviceability check – Cooling thermal load</i>					
$\sigma_{s,max,m+th}$ [kPa]	f_{yk} [Mpa]	f_{yk} [KPa]	k_4	$k_4 \cdot f_{yk}$ [Kpa]	check
-124929.20	-500	-500000	1	-500000	✓

Table 4.21: Serviceability check for *quasi-permanent combination* in case of cooling thermal load.

In both cases (*characteristic combination* and *quasi-permanent*) the tension limit state verifications have been satisfied.

4.4.7 Cracking Limit State for the proposed design case

The checks in case of *characteristic combination* are summarized in the following tables:

<i>Serviceability check – Thermal load dominant combination - cooling</i>		
$w_{k,max}$ [mm]	w_k [mm]	check
0.3	0.63	✗

Table 4.23: Serviceability check for *characteristic combination* in case of heating cooling load.

<i>Serviceability check – Thermal load dominant combination - cooling</i>		
$w_{k,max}$ [mm]	w_k [mm]	check
0.3	0.25	✓

Table 4.24: Serviceability check for *quasi-permanent combination* in case of heating cooling load.

4.5 Comparison between both design situations

In this chapter the comparison between the real design case and the proposed design case for characteristic and quasi-permanent combination have been carried out. In the Figure 4.21 – 4.24 comparisons have been reported in both heating and cooling cases.

In the Figure 4.21 the main difference regard the thermal stresses: in the case of proposed design as aforementioned in the previous chapter the values of stresses are lower than those of the real case.

This is very important because according to previous work (Rotta Loria et al.2017) designing a pile that is longer than it should not only involve higher displacement but also higher stresses. This could be a problem for serviceability limit state verifications, as seen in the previous chapter.

In the Figure 4.22 the displacement trends have been pictured and some point must be highlighted:

- The head displacement is higher in the pile with the higher length according to previous works (Rotta Loria et al. 2017);
- Using the characteristic combination provides higher values of displacements, but it is not directly related with the SLS verification.

The same points are also summarized in the Figures 4.23-4.24 for cooling thermal load.

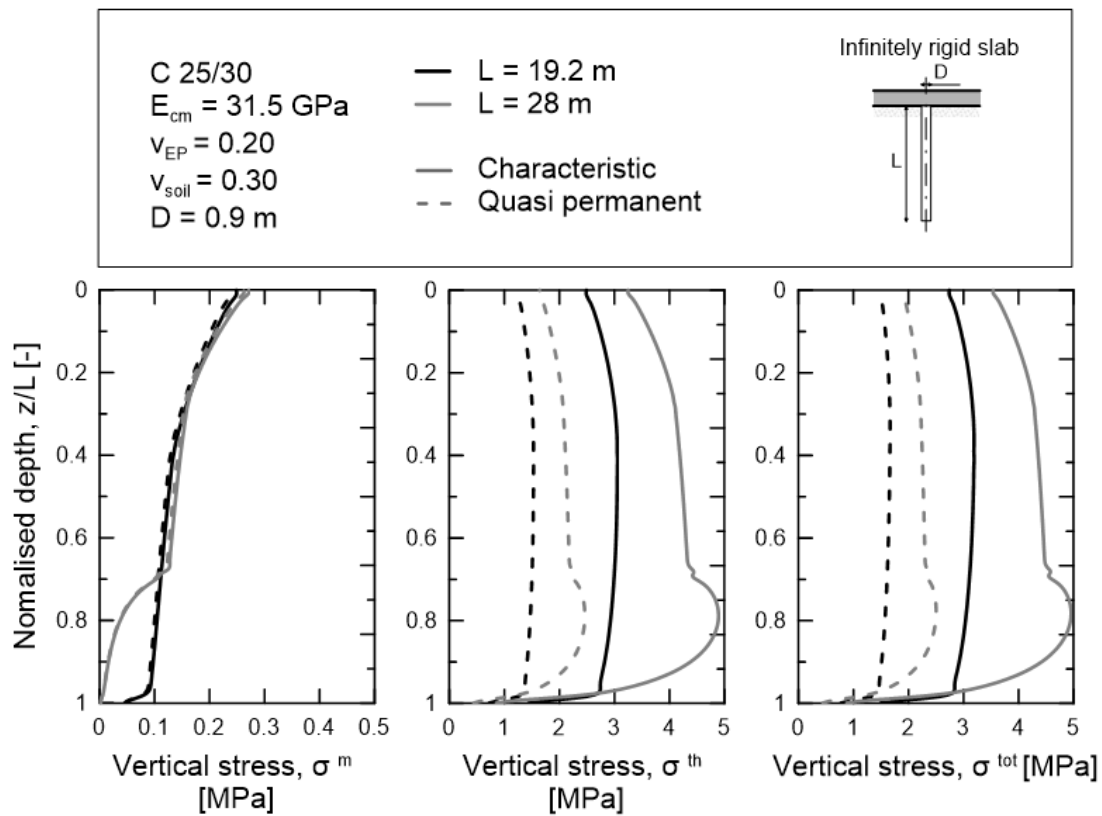


Figure 4.21: Comparative stress trends between two design cases for pile subjected upon thermal and mechanical loads.

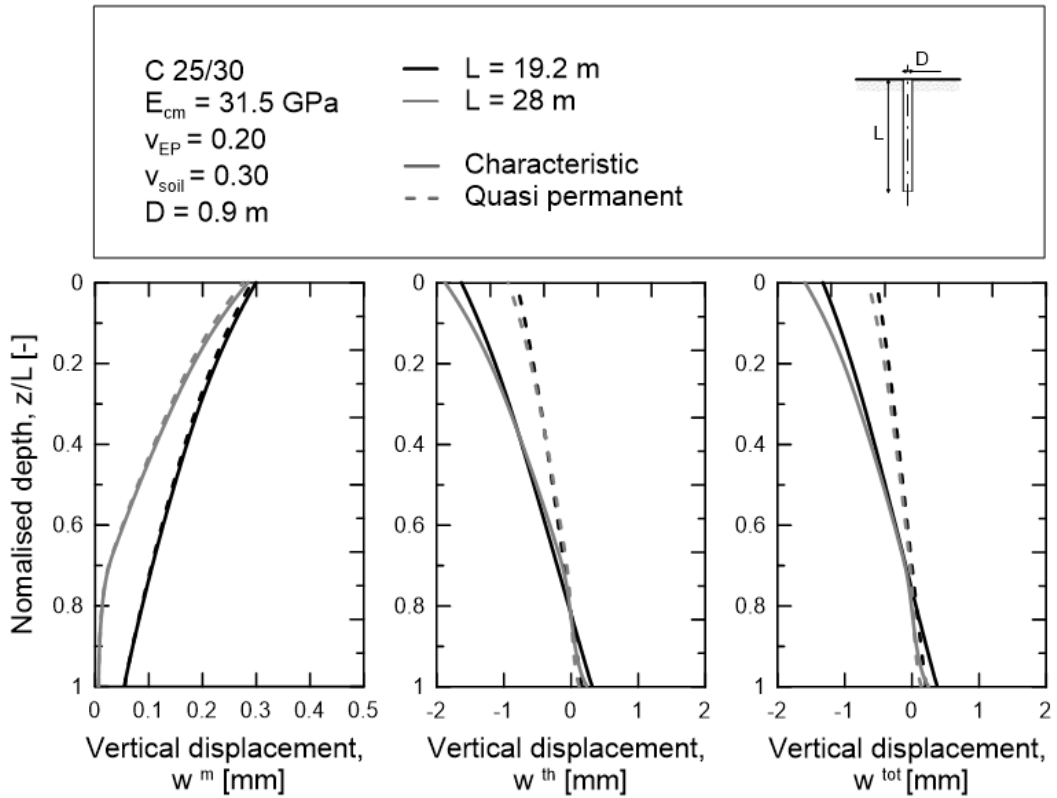


Figure 4.22: Comparative displacement trends between two design cases for pile subjected upon heating thermal and mechanical loads.

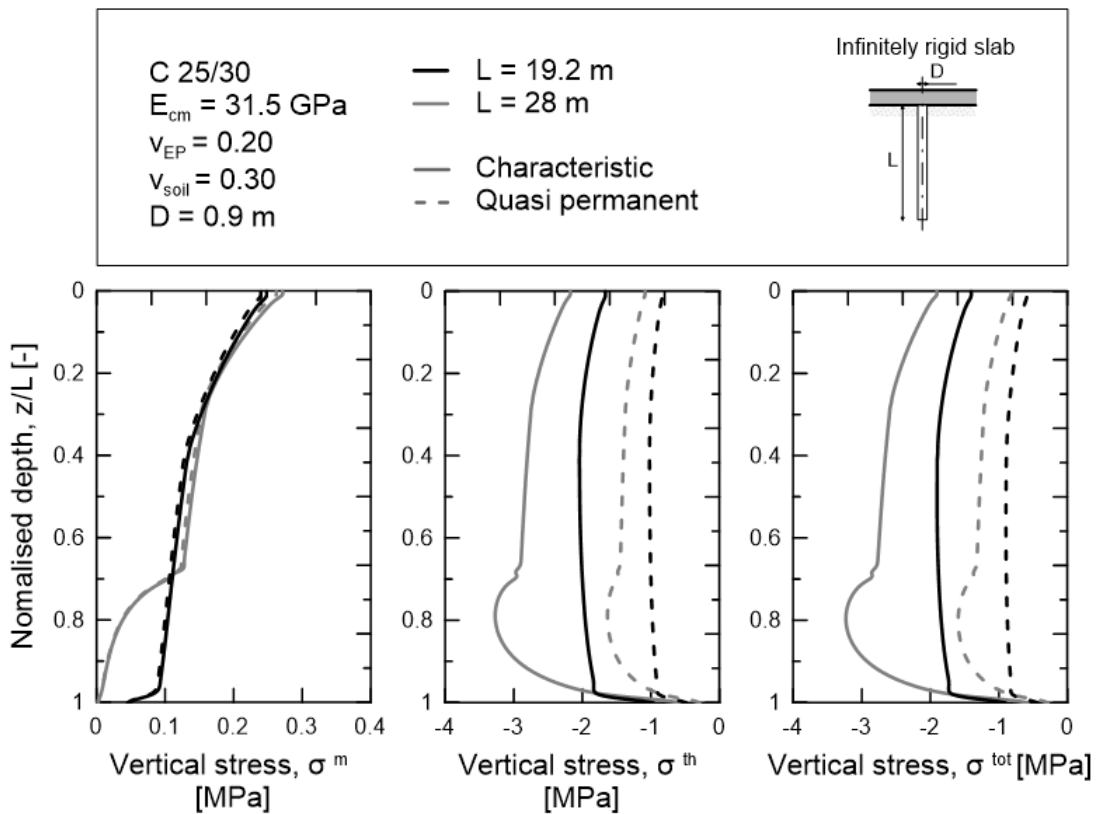


Figure 4.23: Comparative stress trends between two design cases for pile subjected upon cooling thermal and mechanical loads.

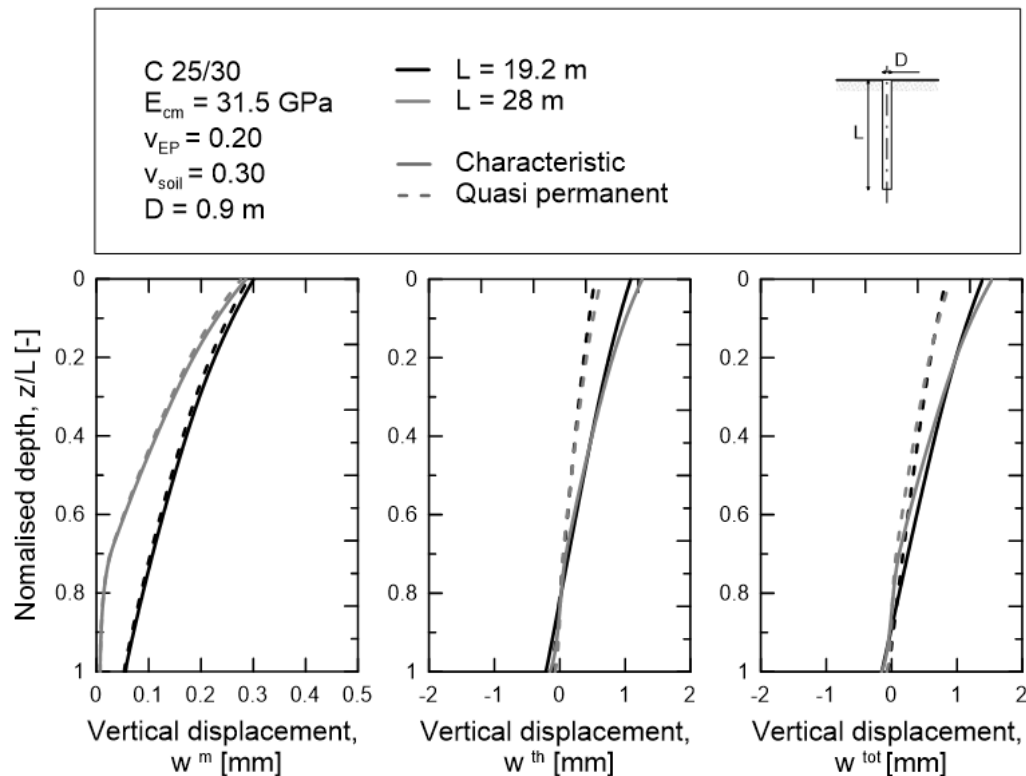


Figure 4.24: Comparative displacement trends between two design cases for pile subjected upon cooling thermal and mechanical loads.

4.6 Concluding remarks

In order to provide a complete design procedure for serviceability limit state verifications of energy piles subjected to mechanical and thermal loads, according with Eurocodes, the main conclusions have been pointed out:

- The Eurocodes dispositions for elastic analysis (nil Poisson ratio and Young's Modulus equal to that of the cracked section) underrate the thermal stresses and this represent a problem for the structure during its life.
- The effect of cracked Young's modulus is also visible in the thermal displacement: with a lower value of Young's Modulus the displacement decrease;
- The effect of the nil Poisson ratio is negligible;
- Even if the most burdensome load combination is the characteristic one, the verifications must be carried out with the quasi- permanent combination because is directly related with the equations provided by Eurocodes;
- When the verifications have been carried out with the characteristic combination there is the risk to increase the amount of the reinforcement, so overestimating it.
- The reinforcement design method that ensure more ductility ensure the lower cracks opening.

Chapter 5

Pile group effect

During the last fifty years, the interaction factor method has been widely used to address the vertical displacement and the increased deformation of conventional pile groups subjected to mechanical loads when group effects and interactions occur among the piles. In recent years, the interaction factor method has been extended to address energy pile groups subjected to thermal loads (Rotta Loria, 2018). Prior this work no application and no guideline were provided, in order to take into account the problems related with the analytical model and no application and no guideline were provided, in order to take into account the problems related with the analytical models and to quantify the approximation of them than 3D-FEM analysis.

5.1 Introduction

During the last decades the interaction factor method proposed by Poulos (1968) has been widely used to perform the analysis of the vertical displacement and increased deformation of pile groups caused by mechanical loads when group effects and interactions are present. This method assumes that the vertical displacement of any pile group, e.g., under serviceability conditions, may be estimated through elastic theory and superposition of effects by knowing:

- the displacement interaction relationship, quantified by an interaction factor, among two piles of the group considered in an isolated pair;
- the vertical displacement of one reference pile in the group that is the source of interaction for the receiver pile in the pair;
- the loads applied to the piles.

The expediency and capability of this method to model the problem previously described, which, although being an approximation of reality, is often considered for design purposes, have played a major role for its diffusion.

Originally, design charts for floating and end-bearing conventional piles have been proposed by Poulos (1968) and Poulos and Mattes (1974), respectively, to serve the aforementioned method in estimating the interaction factor. Afterward, analytical models have been proposed for floating and end-bearing conventional piles by Randolph and Wroth (1979b) and Randolph and Wroth (1979a), respectively. Another formulation of these models by Chow (1986) and an improvement related to the definition of the correct interaction factor by Mylonakis and Gazetas (1998) have been later presented.

The analytical models have been developed due to their capability of estimating the interaction factor in a broader range of conditions and performing more comprehensively and flexibly than the charts in the analysis of pile groups. In these models, differently from the original method proposed by Poulos (1968), the interaction factor has been defined with reference to the vertical displacement of a source pile assumed to be isolated. The main reason for this choice has been the possibility to estimate the vertical displacement caused by mechanical loads through closed form solutions.

In recent years, the interaction factor method has been extended and proven to be a suitable tool for estimating the vertical displacement of energy piles subjected to thermal loads alone or in conjunction with mechanical load. (Rotta Loria, 2018).

Design charts have been proposed for floating and end-bearing energy piles by Rotta Loria and Laloui (2016b) and Rotta Loria and Laloui (2017a). The design charts and interaction factor method for energy piles have been developed with reference to the vertical displacement of an isolated energy pile. The main reason for this choice has been that the vertical displacement of piles subjected to thermal loads cannot be determined through closed form solutions, i.e., running a numerical analysis is required. Therefore, considering the source pile as isolated allows for the use of a simpler analysis (e.g., axisymmetric) than that required for a pile in a pair (e.g., three-dimensional), and preserves the opportunity of a simplified procedure as the interaction factor method that would otherwise disappear. The previous study (Rotta Loria, 2018) addresses the development of two analytical performance models, i.e., a *layer model* and a *continuous model*, capable of the following:

- estimating the vertical displacement with depth of a thermally loaded source pile and receiver pile in a pair starting from the analysis of a single isolated pile;
- defining the interaction factor with depth between these piles regardless of the design situation;

- analyzing the vertical displacement with depth of any energy pile groups using the interaction factor method.

Prior this work, design charts and basic case study have been developed (pile embedded in a single soil layer), without identifying the limits of the various analytical models. In fact, one of the goals of this chapter is identify the best analytical model and quantify the approximation than a 3D-FEM.

5.2 Interaction factor concept

5.2.1 The problem: a group of two energy piles

The simplest situation to describe the interaction among energy piles group can be described by two energy piles in a deep soil deposit. In the considered problem, the energy piles are:

- subjected to a thermal load;
- free of superstructure mechanical loads;
- free to move vertically at their head.

The first point is a result of the geothermal operation of these elements. Cooling and/or thermal energy storage operations of energy piles can be associated to positive temperature variations applied to these elements. Heating operations of energy piles can be associated to negative temperature variations applied to these elements. Reference to a situation in which no superstructure mechanical load is applied to the energy piles (second point) allows focusing on the impact of the thermal load on the response of these elements. The third point (pile free to move at their head) has been generally accounted for in the analysis of conventional pile groups subjected to mechanical loads for estimates of the vertical displacement on the safety side, because as explained in the first chapter, the presence of the slab reduce the displacements. This approach appears to also be valuable for displacement analysis of energy pile groups and is considered in the following.

5.2.2 Idealization

The previously described scheme is idealized considering the following assumptions. The energy piles are two identical isotropic, homogeneous and uniform cylindrical solids. The soil is assumed to be a semi-infinite, isotropic, homogeneous and uniform mass. The soil is semi-infinite mass characterized by a layer surrounding the lateral area of the energy piles and a layer located below the toe of the energy piles where predominantly end-bearing energy piles are considered. The same uniform temperature variation is applied along the length of each of the energy piles. Initially, in order to understand the interaction among the piles under thermal load, no mechanical load is applied to the energy piles and no head restraint is present (i.e., perfectly flexible slab) in order to evaluate

the most burdensome situation. The energy piles are characterized by a linear thermo-elastic behavior, whereas the soil is characterized by a linear elastic behavior (i.e., the soil is an infinite heat reservoir that remains at a fixed constant temperature). No slip or yielding occurs between each of the energy piles and the adjacent soil (perfect contact between the pile and soil is assumed), and thus, reference is made to loading situations in which elastic (i.e., reversible) conditions prevail. The application of the temperature variation to the energy piles involves a thermally induced deformation of these elements. An expansion of the energy piles is observed for cooling and/or thermal energy storage operations of these elements (positive temperature variations applied to the energy piles) whereas a contraction of the energy piles is observed for heating operations of these elements (negative temperature variations applied). In the former case, the upper portion of each energy pile displaces upwards, whereas the lower portion displaces downwards around a setting characterized by zero thermally induced displacements. In the latter case, the upper portion of each energy pile displaces downwards, whereas the lower portion displaces upwards.

The considered elastic assumption involves that the null point does not move depending on whether positive or negative temperature variations are applied to the energy piles (Rotta Loria, 2018). Hence, the displacement variation along the length of these elements for the same temperature variation associated to their heating or cooling is the same in absolute value (Rotta Loria, 2018) due to the application of the elastic theory. The displacement field generated in each of the energy piles is transmitted in the adjacent soil. Interaction of the displacement fields generated by the thermally induced deformation of the energy piles thus occurs.

The total deformation field of a group of two energy piles subjected to a thermal variation can be representatively decomposed through the elastic principle of superposition of effects in two individual schemes.

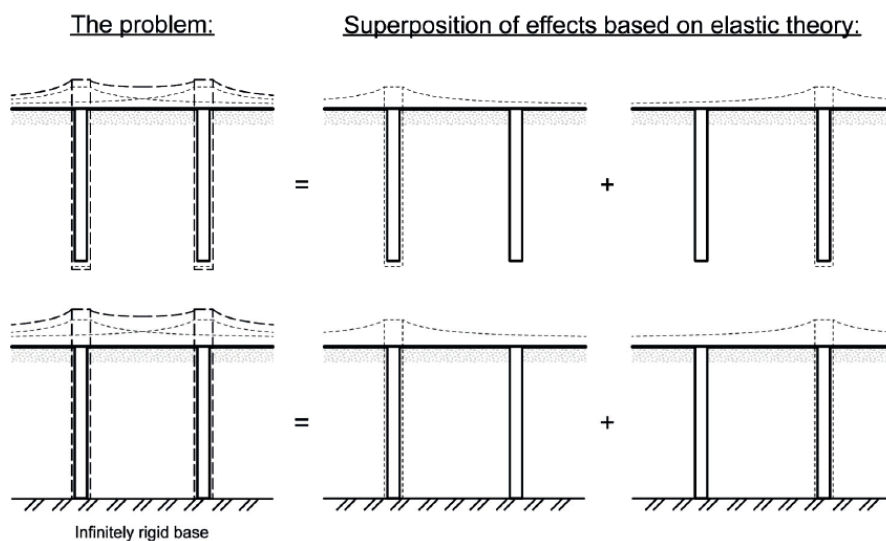


Figure 5.1: The modelling approach (Rotta Loria et al.2017).

Figure 5.1 provides an example of this decomposition for a situation in which a positive temperature variation is applied to predominantly floating and end-bearing energy piles. This decomposition approach has been proved to be suitable for describing the displacement interaction between conventional piles subjected to mechanical loads (Poulos and Davis, 1980; Fleming et al., 2008).

5.2.3 The interaction factor

The additional displacement of a pile due to the loading (e.g., thermal) of an adjacent pile or in other words given by the interaction among the piles is expressed in function of an interaction factor Ω , where:

$$\Omega = \frac{\text{additional displacement due to adjacent pile}}{\text{displacement of single isolated pile}} = \frac{w_j}{w_i} \quad (11.3)$$

where w_j is the vertical head displacement of a receiver pile in a pair, whereas w_i is the vertical head displacement of a single isolated pile subjected to the same load applied to the source pile in the elementary unit. This definition of the interaction factor relates the effect of loading a source pile on a receiver pile in a pair with the response of the source pile in an isolated case.

In the Rotta Loria's work (Rotta Loria, 2018) the typical trends of interaction factor both for mechanical load and thermal have been presented and pictured in the Figure 5.2 that presents the typical evolution of the interaction factor with a normalised centre-to-centre distance between two predominantly floating piles in the case of thermal and mechanical loading.

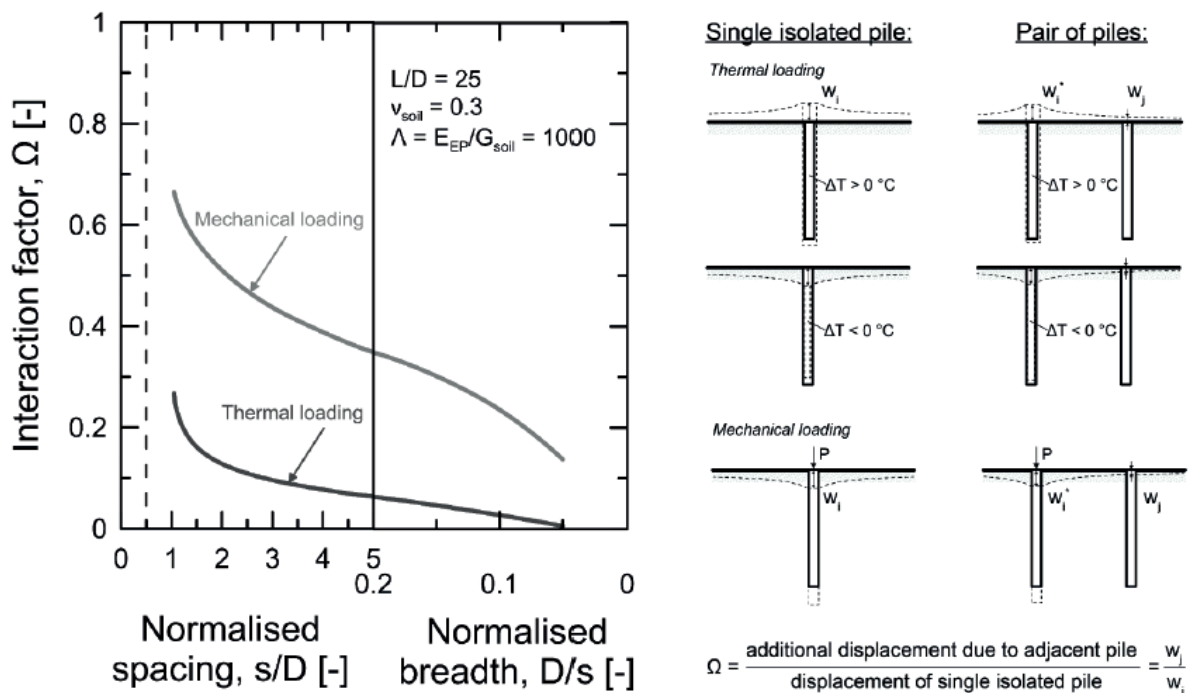


Figure 5.2: Displacement interaction between two piles in a deep soil layer (Rotta Loria, 2018).

The interaction decreases with increasing centre-to-centre distance between the piles. Mechanical loading causes a more pronounced displacement interaction between the piles compared to thermal loading.

Figure 5.3 presents the typical evolution of the interaction factor with a normalised centre-to-centre distance between the piles in the elementary units previously considered. *The interaction factor for predominantly end-bearing energy piles resting on infinitely rigid soil strata is greater than that for predominantly floating energy piles embedded in uniform soil deposits (on average 43% higher)* (Rotta Loria, 2018). This phenomenon is generally observed for any pile spacing and pile slenderness ratio.

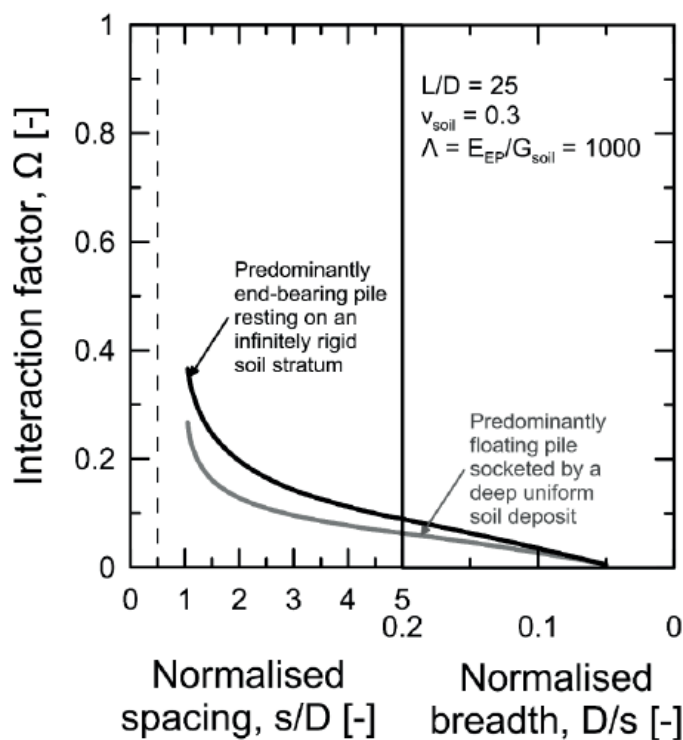


Figure 5.3: Interaction factor for predominantly floating and end-bearing energy piles resting on infinitely rigid soil strata and socketed in uniform soil deposits, respectively, under the application of a thermal load ((Rotta Loria, 2018)

The above figure show that the interaction factor for energy piles resting on finitely rigid soil strata generally lies between the interaction factor for energy piles resting on infinitely rigid soil strata and the interaction factor for energy piles surrounded by deep uniform soil deposits.

These schemes reported in Rotta Loria’s work (Rotta Loria, 2018) are referred to a generic situations, but are useful to understand the pile group effect and for approaching to the study cases analyzed in this work.

5.3 The interaction factor method for energy pile groups based on analytical models

5.3.1 Idealization, hypothesis and considerations

The schematization of the problem described above and the hypotheses and considerations that have been widely used in developments of the interaction factor method for conventional piles (Poulos and Davis, 1980; Fleming et al., 2008) have been extended to piles subjected to thermal loads by Rotta Loria (Rotta Loria, 2018).

The piles are identical, isotropic, homogeneous and uniform cylindrical solids. The soil is a semi-infinite isotropic mass assumed to be composed of a unique homogeneous layer or different horizontal layers. The aforementioned assumptions represent typical approximations of reality employed in engineering theory. Despite they are approximations, when applied with judgement, however, they can adequately represent real problems (Poulos and Davis, 1980).

A uniform temperature variation is applied to the source pile and a vertical mechanical load may be applied at the pile head as well. *The temperature variations observed within energy piles are not uniform, but can be considered uniform by choosing representative values of the temperature field within the cross-section and along the length of the pile* ((Rotta Loria, 2018). The consideration of a constant mechanical load applied at the pile head follows the widely used assumption of a negligible contribution of the uppermost slabs or other shallow foundations in the bearing capacity of piles for preliminary analyses and designs on the safety side (Poulos and Davis, 1980; Bowles, 1988; Fleming et al., 2008). No head restraint is present (i.e., infinitely flexible slab). This assumption conservatively analyses the vertical displacement of piles according to the widely used assumption of a negligible contribution of the uppermost slabs or other shallow foundations in the deformation of piles, at least for preliminary analyses and designs (Poulos and Davis, 1980; Bowles, 1988; Fleming et al., 2008). No slip or yielding occurs between the piles and the adjacent soil (i.e., perfect contact between the pile and soil is assumed).

The piles are characterized by a linear thermo-elastic behavior. The soil is characterized by a linear elastic behavior. Loading situations in which reversible conditions prevail are thus assumed, according to the previous hypothesis of no slip or yielding between the piles and the adjacent soil. Since the elastic theory has been used, the aforementioned hypothesis imply that the effect of thermal and mechanical loads can be superimposed at any time, based on the principle of superposition of effects, via separate analyses addressing thermal and mechanical loads, providing a simplified analysis tool. Considering the soil described by an elastic behavior involves assuming it is an infinite heat reservoir that remains at a constant fixed temperature. Hence, no influence caused by any

temperature sensitivity of the soil or thermal interaction between the source pile and the receiver pile is considered.

Only in situations where the thermal expansion coefficient of the soil is higher than that of the piles ($X > 1$) the thermally induced soil deformation have a marked effect on the pile interaction, especially at successive stages of geothermal operations of the piles (Rotta Loria, 2018).

In these situations, a simplified yet valuable approach for capturing the group displacement via the design charts has been proven to result from interaction factors still referring to pile pairs in isothermal soil (Rotta Loria, 2018). This situation happens in the case study analyzed in this work in the latter soil layer (Layer D); in fact, one of the goal of this chapter is quantify this effect on stress and displacement field.

The displacement field within the piles is assumed to be homogeneous. This hypothesis is justified in view of the notable stiffness that usually characterizes energy piles compared to that of the soil. The effect of bending moments on the displacement field of the piles and the soil is neglected. This consideration is justified in view of the small impact of bending moments on the vertical displacement of the piles in the considered problem (Rotta Loria, 2018).

5.3.2 The solution approach

To provide a simplified analysis method tool during the design situation to quantify the group pile effect, a semi-analytical analysis has been performed. This (semi-analytical) analysis may be similarly applied to pile groups subjected to vertical mechanical loads. It consists of five key steps:

1. The analysis of a single isolated source pile subjected to a thermal variation define the vertical displacement, $w_i(z)$, and the shear stress, $\tau_i(z)$, along the pile shaft. This analysis can be performed with any of the numerical methods currently available for this aim, although preferably with the finite element method (with an increasing of the computational time) (Figure 5.4.1 (a));
2. The calculation of the vertical displacement field of the soil, $w(r, z)$, at any given radial distance, s , from the axis of the previously analyzed single isolated pile subjected to a temperature variation, and along the vertical coordinate, z (Figure 5.4.1(b)). This step can be performed using the approximate pile-soil interaction factor as:

$$\tilde{\Omega}(r, z) = \frac{w(r, z)}{w_i(z)} \quad (11.7)$$

3. The analysis of the vertical displacement, $w_j(s, z)$, of a receiver pile located at a spacing $s = r + R$ (where $R = 0.5 D$ is the pile radius) from the source pile that was previously considered to be isolated. (Figure 5.4.1 (c));

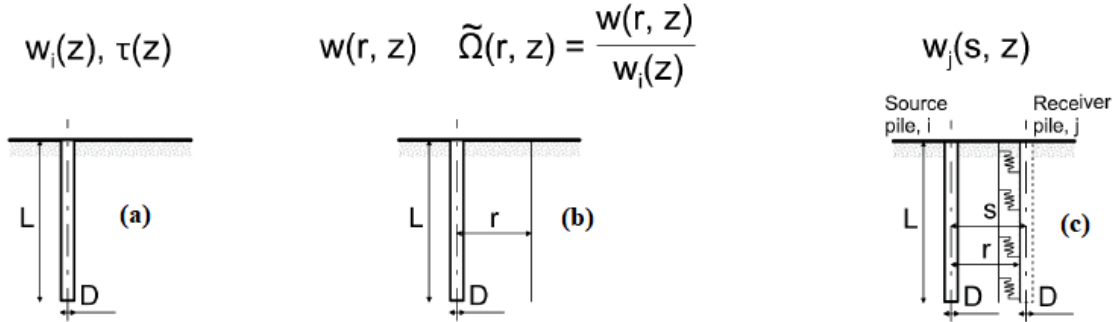


Figure 5.4.1: The approach for analyzing the vertical displacement of general energy pile groups (Rotta Loria 2018).

Figure 5.4.1(a): Analysis of single isolated pile; **Figure 5.4.1(b):** Calculation of vertical displacement of the soil and approximate interaction factor; **Figure 5.4.1(c):** Analysis of vertical displacement of receiver pile.

4. The determination of the corrected pile-soil-pile interaction factor as (Randolph and Wroth, 1979b; Mylonakis and Gazetas, 1998; Rotta Loria, 2018) (Figure 5.4.2 (a)):

$$\Omega(s, z) = \frac{w_j(s, z)}{w_i(z)} \quad (11.8)$$

5. The analysis of the vertical displacement of any pile, j , composing a general group with a total number of piles, n_{EP} , in which some or all of the piles may be subjected to a temperature variation (as in the case study analyzed in this work) as (Rotta Loria, 2018):

$$w_j(z) = w^1(z) \sum_{i=1}^{i=n_{EP}} \Delta T_i \Omega_{ij}(s, z) \quad (11.9)$$

where $w^1(z)$ is the vertical displacement along the length of a single isolated pile per unit temperature variation, ΔT_i is the applied temperature variation to pile i and Ω_{ij} is the interaction factor for two piles in a pair corresponding to the spacing between pile i and pile j (Figure 5.4.2 (b)).

This procedure described above will be valid for both analytical models that will be described in the following chapters. Therefore the formulation reported in equation (11.9) will be valid for both semi-analytical methods to estimate the total displacement for each pile due to the own displacement due to the applied loads and the interaction with other piles in turn subjected to their own reference loads.

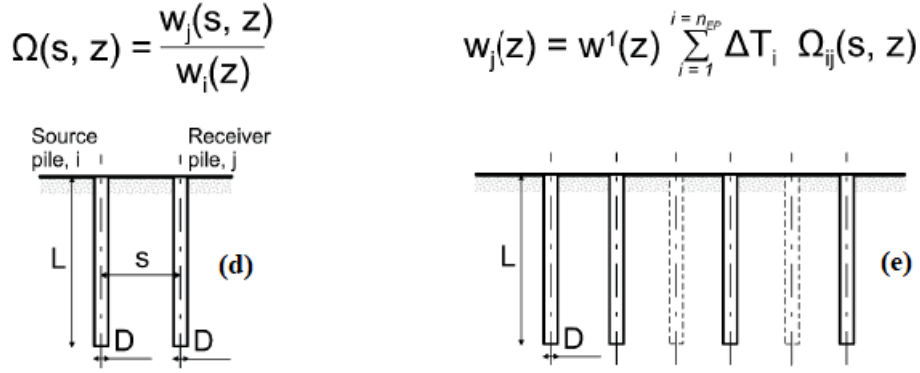


Figure 5.4.2: The approach for analyzing the vertical displacement of general energy pile groups (Rotta Loria, 2018). **Figure 5.4.2 (a):** Definition of corrected interaction factor; **Figure 5.4.2 (b):** Analytical process to define the pile group effect.

5.4 Layer model

5.4.1 Soil vertical displacement and approximate pile-soil interaction factor

The present analytical model is based on an important assumption, or that the soil around the lateral surface of the piles subjected to loads that induce vertical deformation may be idealized as consisting of concentric cylindrical elements, with shear stresses distributed on the surface of each element (cf., Figure 5.5 (a)). To satisfy the vertical equilibrium, the entity of the shear stress on each cylindrical element must decrease inversely with the vertical surface area of the element (Cooke et al., 1981). The equation (12.1) describe the equilibrium equation along z written for a single element using the cylindrical coordinate system (r, θ, z) , in which the effects of volume forces due to body loads are neglected:

$$\frac{\partial \tau_{rz}}{\partial r} + \frac{\tau_{rz}}{r} + \frac{\partial \sigma_{zz}}{\partial z} = 0 \quad (12.1)$$

where $\tau_{rz} = \tau$ is the shear stress increment and $\sigma_{zz} = \sigma_z$ is the vertical stress increment. The application of thermal loads in the context of energy piles assumes that $\partial \tau / \partial r \gg \partial \sigma / \partial z$. This means that the variation of τ along r is much greater than that of σ along z and verifying this situation through finite element analysis emerged that this phenomenon characterize those regions of soil in the vicinity of the pile shaft.

From this consideration, it follows that equation (12.1) has been simplified by Frank (1975) (Rotta Loria, 2018) and integrated in order to provide the general solution for the shear stress in the soil:

$$\tau(r, z) = \frac{\tau_i(z)R}{r} \quad (12.2)$$

The shear stress may be considered to be constant with depth in conventional applications of piles subjected to mechanical loads. This assumption may be valid because the vertical deformation of piles subjected to mechanical loads can be considered in a plane state of strain, $\varepsilon_z = 0$) or with simpler words, independent of the depth.

The application of a mechanical load at the head of piles involves an approximate constant distribution of the vertical displacement with depth. This consideration is particularly applicable to the analysis of rigid piles with a predominantly friction character but is also acceptable for most piles. The shear stress varies significantly with depth in innovative applications of piles subjected to thermal loads, i.e., energy piles. This means that the vertical deformation of piles subjected to thermal loads is crucially dependent on the depth and thus not associated with a plane state of strain.

The application of a thermal load along the length of piles involves an approximate linear distribution of the vertical displacement with depth and at worst a notably non-linear distribution of the vertical displacement. The latter condition occurs in the case of the energy piles with both great compressibility and slenderness. This consideration is applicable to the analysis of both rigid and deformable piles whether they have a predominantly frictional or end-bearing character.

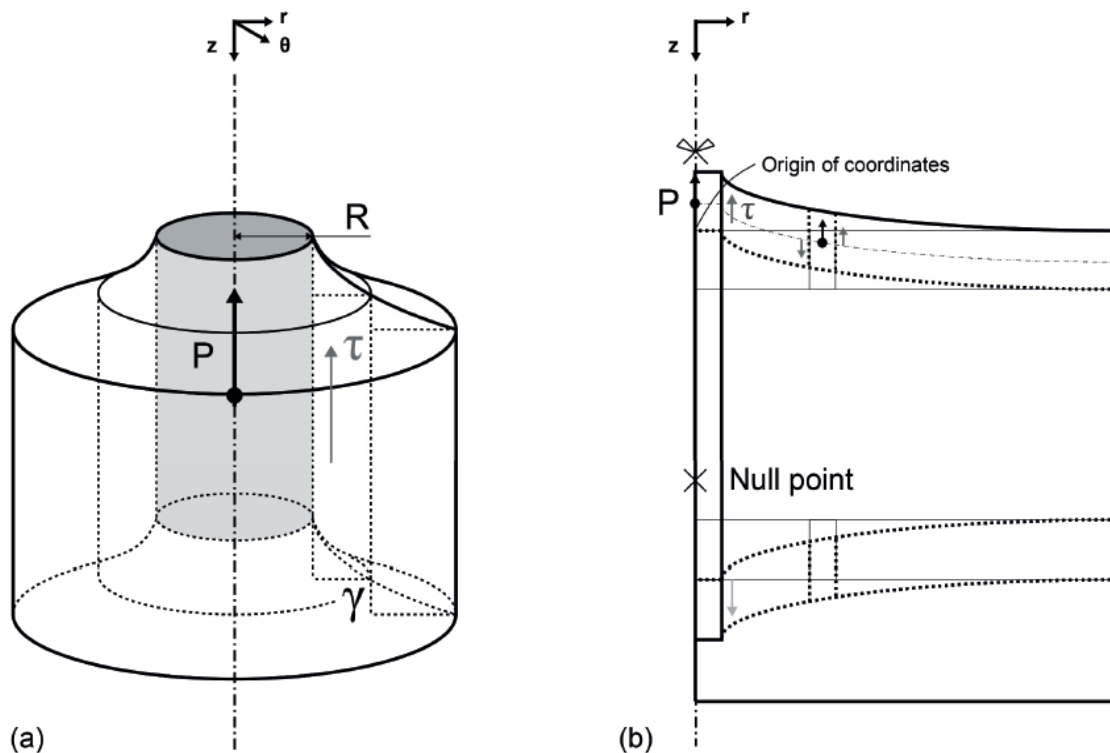


Figure 5.5: The layer model schematization: (a) the deformation mode of a layer of cylindrical elements characterizing any pile-soil system and (b) the effect due to deformation mode (Rotta Loria, 2018).

The shear strain associated with the aforementioned shear stress can be computed according to the elastic theory as

$$\gamma = \frac{\partial w}{\partial r} + \frac{\partial u}{\partial z} = -\frac{\tau}{G_{soil}} \quad (12.3)$$

where u is the radial displacement and G_{soil} is the shear modulus of the soil. In this model, both u and w depend only on r and z , respectively, and not on the angular coordinate, θ . This aspect arises because there is an invariance of the displacement field around the latter axis. Moreover, because no twist characterizes the pile, there is no orthoradial component, v , in the displacement field. The application of thermal loads in the context of energy piles is based on $\partial w/\partial r \gg \partial u/\partial z$. This means that the variation of w along r is much greater than that of u along z and verifying this situation through finite element analysis emerged that this phenomenon characterizes regions of soil in the vicinity of the pile shaft. Together with the previous assumption related to a negligible contribution of $\partial \sigma/\partial z$ represent, physically, a negligible interaction between different soil layers with depth (cf., Figure 5.5 (b)).

From the above consideration and the combination of equations (12.2) and (12.3), the first-order partial differential equation is found:

$$\frac{\partial w}{\partial r} = -\frac{\tau_i(z)R}{rG_{soil}} \quad (12.4)$$

Integration of equation (12.4) provides the general solution for the vertical displacement of the soil (Randolph and Wroth, 1978) as:

$$w(r, z) = w_i(z) - \frac{\tau_i(z)R}{G_{soil}} \ln\left(\frac{r}{R}\right) \quad (12.5)$$

5.4.2 Receiver pile vertical displacement and corrected pile-soil-pile interaction factor

The presence of a receiver pile usually decreases the displacement of the soil (Mylonakis and Gazetas, 1998) and this effect becomes more pronounced as the relative stiffness of the receiver pile increases than to that of the soil. Considering the equation that describe the vertical equilibrium of an element of a receiver pile whose axis is located at a spacing s from that of a corresponding element of the thermally loaded source pile gives the following equation (cf., Figure 5.6):

$$\left(\sigma_z \left(z - \frac{dz}{2} \right) - \sigma_z \left(z + \frac{dz}{2} \right) \right) A_{EP} + \iint K_s \left(w(\tilde{r}, \tilde{z}) - w_j(s, \tilde{z}) \right) dS = 0 \quad (12.6)$$

where K_s is the stiffness characteristic of the surrounding soil medium calculated as:

$$K_s \approx \frac{1.3G_{soil}}{\pi D} \left(\frac{E_{EP}}{E_{soil}} \right)^{-\frac{1}{40}} \left(1 + 7 \left(\frac{L}{D} \right)^{-0.6} \right) \quad (12.7)$$

From the mathematical point of view the rigorous solution of equation (12.6) would require integration of $(w(\tilde{r}, \tilde{z}) - w_j(s, \tilde{z}))$ over dS because of its non-homogeneity along the perimeter of the cross-section and the height of the element. In order to solve this equation an assumption has been done, considering a value of displacement $w(\tilde{r}, \tilde{z}) = w(r, z)$, where $r = s - R$. Three main advantages arise from this choice:

- the average shear stress that is mobilized over the vertical external surface of the elements of a receiver pile is greater compared to that mobilized in the soil at a distance s from a single isolated pile is implicitly considered for through a conservative approach;
- the non-homogeneity of the displacement that is mobilized over the vertical external surface of the elements of a receiver pile is implicitly considered;
- Integrating the displacement $w(\tilde{r}, \tilde{z}) - w_j(s, \tilde{z})$ over dS can be avoided with a simpler expedient resolution of equation (12.6). Based on these considerations, equation (12.6) becomes:

$$\frac{d\sigma_z}{dz} A_{EP} dz - \pi D K_s (w(r, z) - w_j(s, z)) dz = 0 \quad (12.8)$$

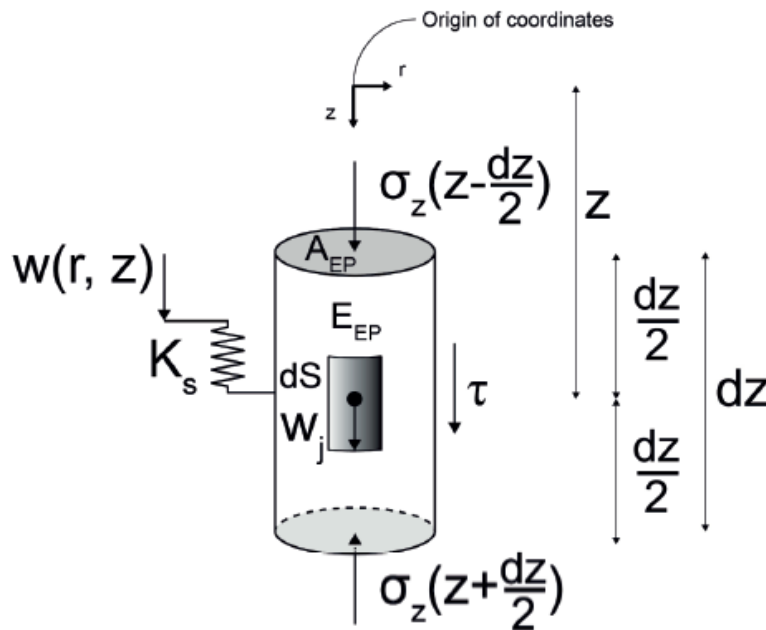


Figure 5.6: Schematization of the vertical equilibrium of a generic element of a receiver pile (Rotta Loria, 2018).

Using the constitutive equations, equation (12.8) can be rewritten in the form of the second-order differential equation governing the equilibrium of each element of the receiver pile (Mylonakis and Gazetas, 1998) as:

$$\frac{\partial^2 w_j}{\partial z^2} - \lambda_{lt}^2 (w(r, z) - w_j(s, z)) = 0 \quad (12.9)$$

Where λ_{lt} is the load-transfer coefficient given by the following equation:

$$\lambda_{lt} = \sqrt{\frac{\pi D K_s}{A_{EP} K_{EP}}} \quad (13.1)$$

In general the load-transfer coefficient for each soil layer is constant. When the piles are no embedded in a single soil layer, but in a layered soil the values of the load-transfer coefficient could be the mean only when the parameters are much close each other. The previous statement is not valid when a soil layer with a completely different parameters is present, as in the case study analyzed in this work, and in this case the equation (12.9) becomes:

$$\frac{\partial^2 w_j}{\partial z^2} - \lambda(z)_{lt}^2 (w(r, z) - w_j(s, z)) = 0$$

In principle, the presence of the relative displacement ($w(r, z) - w_j(s, z)$) in equation (12.9) is not in accordance with the no slip hypothesis presented in Section 5.2.2. However, in practice, it can be associated with the non-homogeneous distribution of the shear stress around a receiver pile in a pair and more generally around any piles in a group.

The equation (12.9) being a second order equation, needs two boundary conditions to be solved. The first boundary condition is chosen based on the consideration that because the pile is free to move vertically at its head no vertical stress will be present in this setting. This condition can be mathematically expressed through the constitutive equation as (Mylonakis and Gazetas, 1998)

$$\left. \frac{\partial w_j}{\partial z} \right|_{z=0} = 0 \quad (13.2)$$

The second boundary condition is chosen depending on where the shear stress is equal to zero along the soil profile adjacent to a receiver pile, the displacement of this pile is the same as that of the soil (i.e., $w(r, z) - w_j(s, z) = 0$). *Since the layer model accounts for no interaction between the different layers of elements, it may be considered that the location where zero thermally induced shear stress*

occurs coincides with the location where zero thermally induced vertical displacement occurs (Rotta Loria, 2018). This phenomenon arises because, for compatibility, upward, downward and zero vertical displacements will be caused if and only if upward, downward and zero shear stresses are applied at the corresponding element in the adjacent soil. The aim is know the location where the vertical displacement of the soil is $w(r, z) = w_j(s, z) = 0$ in order to define the second boundary condition. This location can be determined from the analysis of a single isolated pile according to equation (12.5). The discussed boundary condition can be mathematically expressed as

$$w_j(s, z = z|_{w=0}) = w(r, z = z|_{w=0}) = 0 \quad (13.3)$$

Equation (12.9), together with the boundary conditions expressed in equations (13.3) and (13.2), can calculate the values of $w_j(s, z)$. These values finally determine the values of the corrected pile-soil-pile interaction factor, $\Omega(s, z)$.

5.5 Continuous model

5.5.1 Soil vertical displacement and approximate pile-soil interaction factor

The assumption in this model is that the continuous distribution of the shear stresses at the pile shaft can be approximated as a distribution of point loads acting at the center of the elements constituting these piles as if they were linear entities generated by nodes (cf., Figure 5.7 (a)). At some distance, the effects of such stresses and point loads are indistinguishable (Chow, 1986).

The aforementioned assumption implies that the equations of Mindlin (1936) for a vertical point load acting in a semi-infinite, homogeneous and isotropic elastic half-space being exploited to determine through the elastic principle of superposition of effects the vertical displacement caused by a distribution of point loads acting on a single isolated source pile, thermally loaded. The vertical displacement of the soil can be defined as (Mindlin, 1936):

$$\begin{aligned} w(r, z) &= \sum_{l=1}^m w_{kl} \\ &= \sum_{l=1}^m \frac{P_l}{16\pi G_{soil}(1 - \nu_{soil})} \left(\frac{3 - 4\nu_{soil}}{R_1} + \frac{8(1 - \nu_{soil})^2 - (3 - 4\nu_{soil})}{R_2} \right. \\ &\quad \left. + \frac{(z_l - z_k)^2}{R_1^3} + \frac{(3 - 4\nu_{soil})(z_l + z_k)^2 - 2z_l z_k}{R_2^3} + \frac{6z_l z_k (z_l + z_k)^2}{R_2^5} \right) \end{aligned} \quad (13.4)$$

where w_{kl} is the vertical displacement of any soil node, k , caused by a point load, $P_l = 2\pi R L_{seg} \tau_l$, applied to the node, l , of a source pile (for which L_{seg} is the length of the element and τ_l is the shear

stress acting along it). The parameter m indicates the elements of the source pile from which the effects of the point loads are calculated; $R_1 = \sqrt{r_k^2 + (z_k - z_l)^2}$ (for which r_k is the horizontal distance between node l at which the load is applied and node k at which the influence is considered, z_k is the depth of node k , and z_l is the depth of node l); and $R_2 = \sqrt{r_k^2 + (z_k + z_l)^2}$.

Point loads acting on the nodes of a pile that is effectively considered to be a line avoids the need for integrating (analytically and numerically) the equations of Mindlin (1936) along and around the circumference of the elements that constitute the pile. This approximation has been verified through finite element analyses, results in a notable expediency and comparable accuracy of the analysis.

The equations of Mindlin (1936) involve that the continuous model allows the vertical displacement of stratified (non-homogeneous) soil deposits to be estimated only approximately. However, *an effective and accurate procedure has been shown in this context to consider a mean value of the shear modulus of the soil layer where the displacement is calculated at any soil node, k , and the shear modulus of the soil layer where the point load is applied at any pile node, l (Poulos and Davis, 1980) (Rotta Loria, 2018).*

Equation (13.4) highlights that the present continuous model considers the effects of the shear stress acting on any element of a source pile on all of the elements of the surrounding soil in a “continuous” way, regardless of the layer model. In fact in the former model the interaction between the studied layers (for each step) is taken into account (cf., Figure 5.7 (b)).

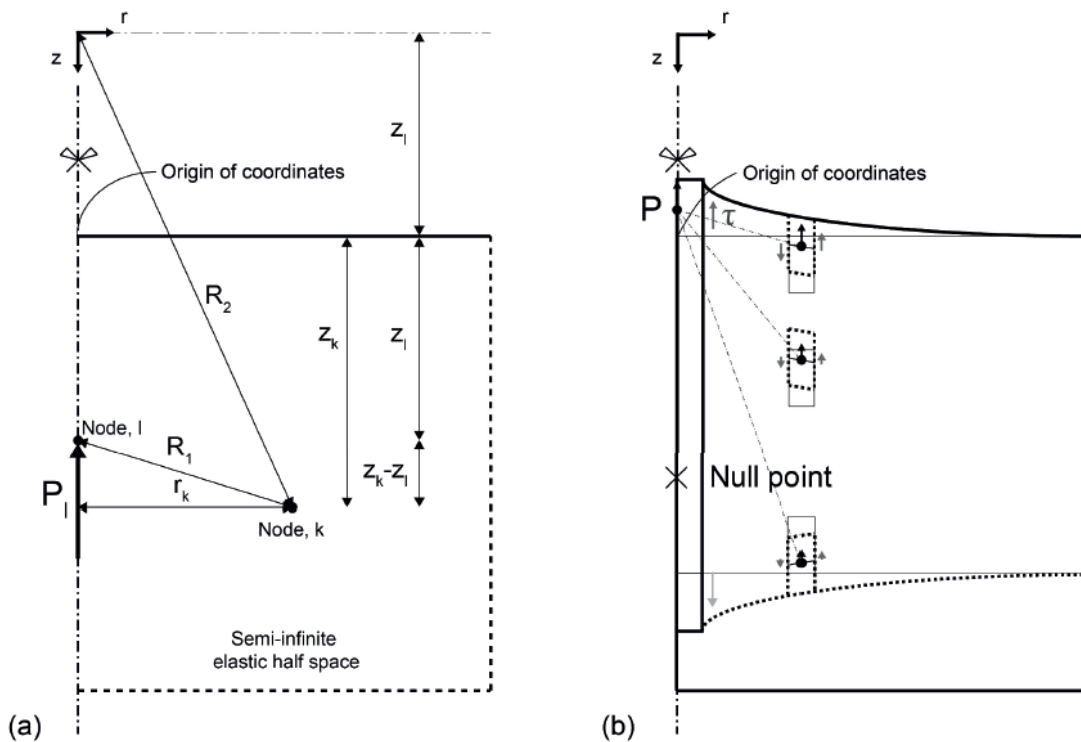


Figure 5.7: Schematization of continuous model: (a) Mindlin’s problem (Mindlin, 1936) and (b) the extension of this problem to that of a single isolated pile subjected to thermal loading (Rotta Loria, 2018).

5.5.2 Receiver pile vertical displacement and corrected pile-soil-pile interaction factor

Differently from layer model, in the present context, in order to address the hypotheses and considerations characterizing the continuous model another second boundary condition have been studied (Rotta Loria, 2018). As mentioned above, unlike the layer model, the continuous model accounts for interaction between the different layers of elements. According to this hypothesis and to continuum mechanics theory, it may be considered that the location where zero thermally induced shear stress occurs does not coincide with the location where zero thermally induced vertical displacement occurs. The location where the vertical displacement of the soil is $w(r, z) = w_j(s, z) \neq 0$ is the first step to define the second boundary condition. To overcome the issue that the specific value of $w(r, z) \neq 0$ and the associated location where $\tau(r, z) = 0$ is not known a priori, the equations of Mindlin (1936) can be exploited to determine through the elastic principle of superposition of effects the shear stress caused by a distribution of point loads acting on a single isolated source pile. This approach, which take into account the continuous character of the present model, allows for the direct determination of the location in the soil where $\tau(r, z) = 0$ and thus where $w(r, z) = w_j(s, z) \neq 0$ from the analysis of a single isolated pile. The shear stress in the soil can be defined as (Mindlin, 1936):

$$\begin{aligned} \tau(r, z) &= \sum_{l=1}^m \tau_{kl} \\ &= \sum_{l=1}^m \frac{P_l r_k}{8\pi(1 - \nu_{soil})} \left(-\frac{1 - 2\nu_{soil}}{R_1^3} + \frac{1 - 2\nu_{soil}}{R_2^3} - \frac{3(z_k - z_l)^2}{R_1^5} \right. \\ &\quad \left. - \frac{3(3 - 4\nu_{soil})z_k(z_k + z_l) - 3z_l(3z_k + z_l)}{R_2^5} - \frac{30z_k z_l (z_k + z_l)^2}{R_2^7} \right) \end{aligned} \quad (13.5)$$

where τ_{kl} is the shear stress acting on any soil node, k , caused by a point load, P_l , applied to the node, l , of a source pile. The discussed boundary condition can be mathematically expressed as:

$$w_j(s, z = z|_{\tau=0}) = w(r, z = z|_{\tau=0}) \quad (13.6)$$

Equation (12.9), together with equations (13.2) and (13.6), can calculate the values of $w_j(s, z)$. As before, these values can determine the values of $\Omega(s, z)$. The shear stress distribution that is found through equation (5.18) is an approximation of the actual shear stress distribution along the shaft of a receiver pile in a pair. The actual shear stress distribution caused by loading a source pile on a receiver pile in a pair may be determined rigorously as shown by Poulos and Davis (1980) or in a numerical analysis with a finite element model (2-D axisymmetric model). However, the null point

position of the shear stress distribution in the soil that is calculated through equation (13.4) has been verified through finite element analyses to be generally close to that along a receiver pile in a pair, e.g., within the distance of half a pile diameter. This fact, together with the consideration of the vertical displacement of the soil at the same distance r from the axis of the source pile, makes equation (13.4) suitable to solve equation (12.9) for estimating the vertical displacement of a receiver pile whose axis is located at a distance s . Furthermore, it is in accordance with the interaction factor analysis procedure based on the analysis of a single *isolated* pile.

5.6 Applications, validation and considerations for both design situations

In order to evaluate the total pile displacement due to the pile group effect with analytical model, before to calculate the real displacement for both design cases, the validations have been carried out.

In this chapter, the comparisons between layer model and continuous model have been performed with a MATLAB codes taking advantage of the aforementioned equation (equation (12.9)) with the respective boundary condition for layer and continuous model. In this way some point must be highlighted:

- for the proposed design case ($L_{EP} = 19.2 \text{ m}$) regarding the interaction factor for mechanical load (Ω^m) the values given by the numerical analysis both for layer and continuous model are not very far from those obtained from 3D-FEM analysis. As shown in the Figure 5.8 (a) the continuous model it is better able to capture the real trend, being almost overlapped on the one given by the 3D-FEM analysis;
- for the real case design ($L_{EP} = 28 \text{ m}$) regarding the interaction factor for mechanical load (Ω^m) the values given by the numerical analysis both for layer and continuous model are not very far from those obtained from 3D-FEM analysis, in fact the difference is negligible (Figure 5.8 (b)). It must specify that the 3D-FEM analysis has been performed modelling the soil layers with the linear thermal expansion coefficients equal to zero ($\alpha_{layer A,B,C,D} = 0$) because in the MATLAB code they have not been take into account;
- Regarding the interaction factor for the thermal load Ω^{th} for the proposed design case the values given by the numerical analysis both for layer and continuous model are not very far from those obtained from 3D-FEM analysis, in fact the difference is negligible (Figure 5.8 (c));
- In the real design case (Figure 5.8 (d)) the situation is completely different: the difference between the analytical model is negligible, but they do not coincide with that of 3D-FEM analysis. The only difference between the real and the proposed case is that the real case

design penetrates the layer D (molasses) for 8 meters while the other leans only on the molasses. Therefore, the role of the layer D is important when the pile is subjected upon thermal load: during the thermal action the molasses tends to pull down the piles group thus giving a higher interaction factor as show by the trend of 3D-FEM analysis in the Figure 5.7 (d).

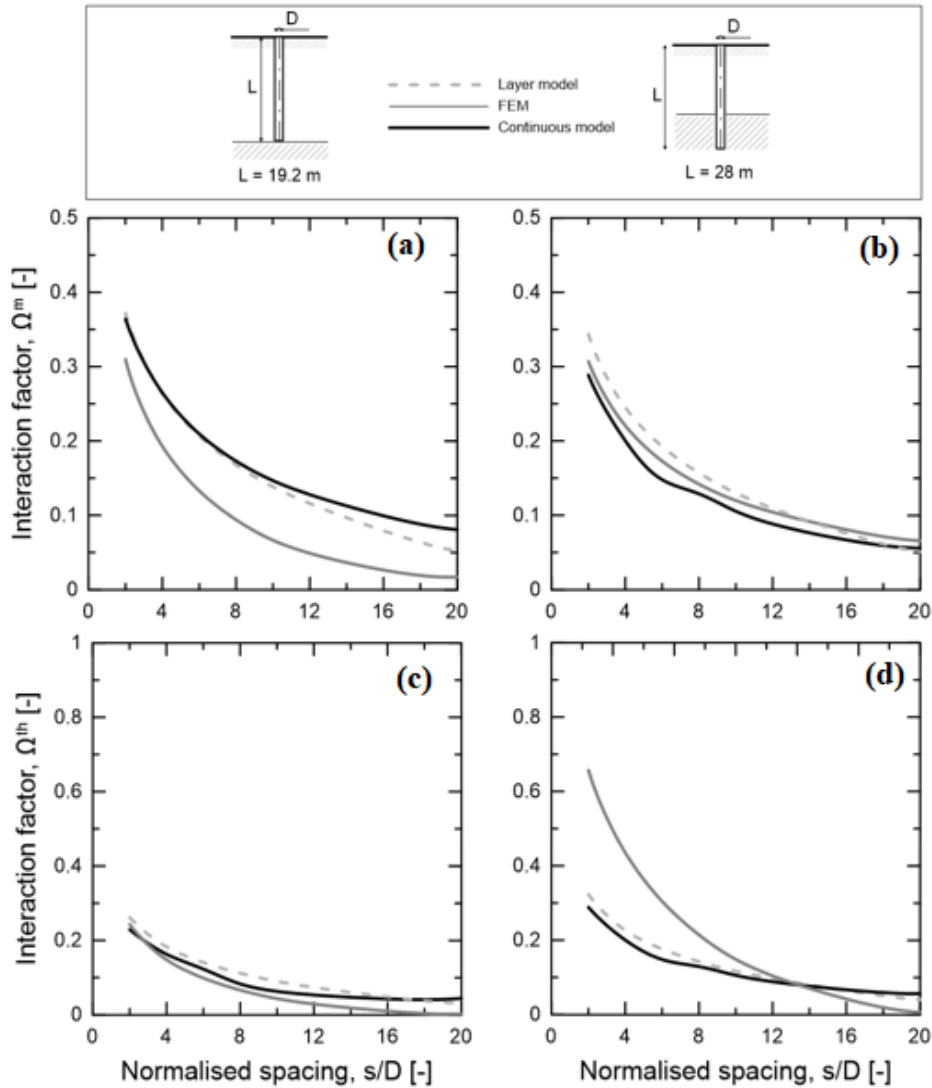


Figure 5.8: Analytical model validation with spacing for both design cases subjected upon both mechanical and thermal load. **Figure 5.8 (a):** interaction factor trend for proposed design case under mechanical load; **Figure 5.8 (b):** interaction factor trend for real design case under mechanical load; **Figure 5.8 (c):** interaction factor trend for proposed design case under thermal load; **Figure 5.8 (d):** interaction factor trend for real design case under thermal load;

In the Figure 5.9 the trends with the depth of analytical models and 3D-FEM analysis are pictured for the real design case and the proposed one. In this way some point must be highlighted:

- In the case of interaction factor for pile subjected upon mechanical load for both design situations (Figure 5.9 (a)-(b)) the trends of Ω^m given by the MATLAB code manage to capture the real behavior with a very low margin of error;

- In the case of proposed design subjected upon thermal load the best model that manage to capture the real behavior is the continuous model (according to Rotta Loria et al. 2017) because with this analytical model the interactions among the soil layers have been take into account (Figure 5.9 (c));

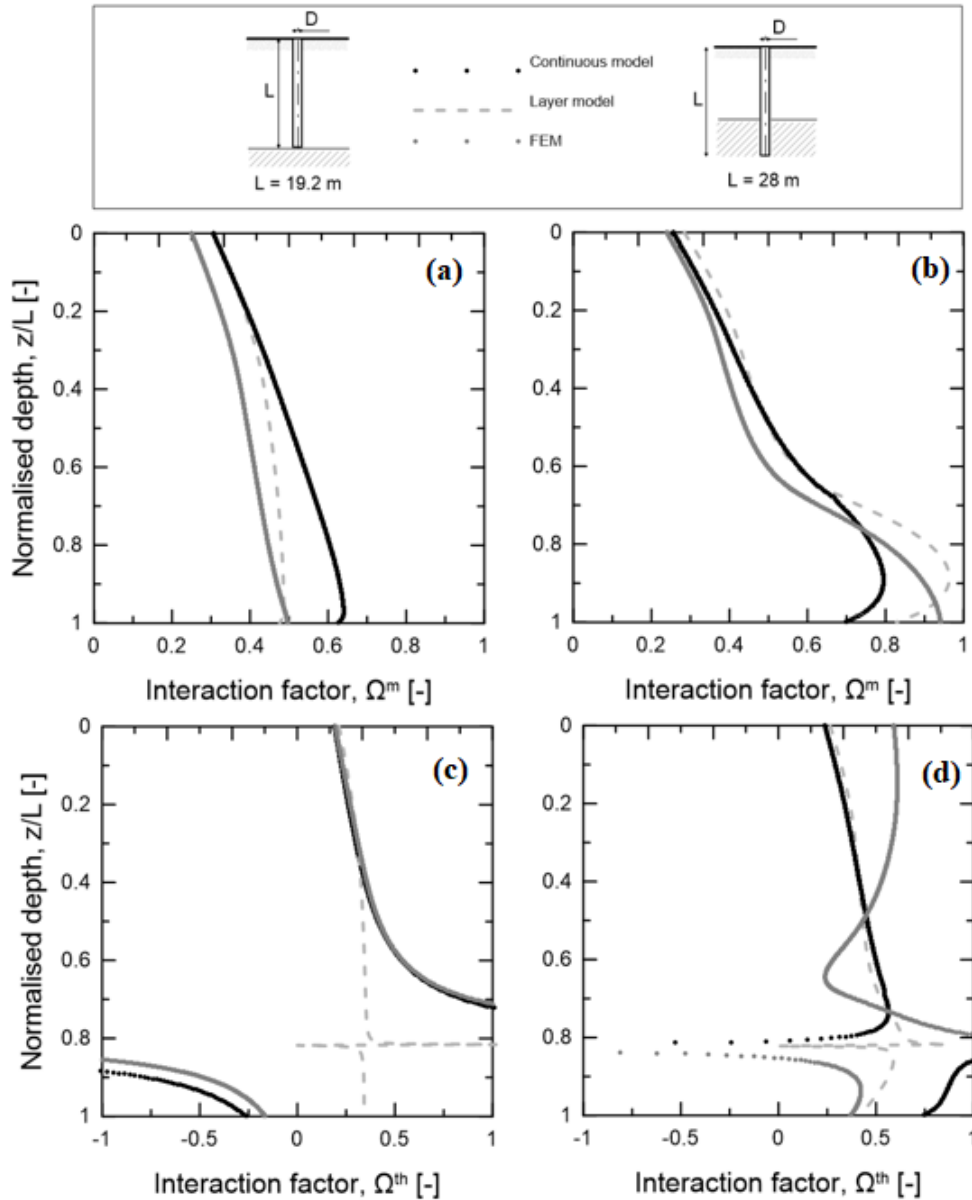


Figure 5.9: Analytical model validation with depth for both design cases subjected upon both mechanical and thermal load. **Figure 5.9 (a)**: interaction factor trend for proposed design case under mechanical load; **Figure 5.9 (b)**: interaction factor trend for real design case under mechanical load; **Figure 5.9 (c)**: interaction factor trend for proposed design case under thermal load; **Figure 5.9 (d)**: interaction factor trend for real design case under thermal load.

- The main point is pictured by the Figure 5.9 (d): in fact in average the best analytical model is the layer model, because the findings given by the continuous model are not truthful. So, the reason of that can be the presence of the layer D in the real design case: as mentioned

before the continuous model take into account of all interactions among the soil layers, but in this case the latter layer (layer D) is stiffer than the others and this it affects the reliability of the final results. In other words, since in the continuous model to evaluate the vertical soil displacement in a layered soil, must use the mean value of shear modulus of the soil layer where the displacement is calculated at any soil node, k the mean value when the Layer D is taken into account is very different form that of soil layers.

5.7 Equivalent pier method

This study presents a method to evaluate the average vertical displacement of energy pile groups subjected to thermal loads. The method consists of replacing any regular pile group with a single equivalent pier of the same length and an equivalent diameter. This method was widely used with a conventional piles group and after, extended for energy piles group by Rotta Loria (2018). This equivalent pier is described by material properties that are a homogenization of those of the piles and the surrounding soil and by a load-displacement relationship of a characteristic energy pile in the group. The load-displacement relationship of the equivalent pier differs from that of a single isolated energy pile because it is modified to take into account the group effects. These effects include a greater vertical displacement of the piles subjected to loading in the group compared to the case in which they are isolated, thus involving a more pronounced average group displacement. This method present advantages and disadvantages:

- This present analytical method is too easy to perform, paying attention during the calculation of the homogenization parameters;
- With the previous models the differential displacement could be calculated because for each pile, the value of displacement can be calculated; instead, the equivalent pier provide directly only the average pile group displacement.

5.7.1 Hypotheses and considerations

To perform the equivalent pier method some hypothesis have been formulated. In fact the equivalent pier is:

- free to move vertically at their heads (i.e., no head restraint);
- characterized by an infinitely flexible slab;
- free of superstructure mechanical loads.

The first point allows a safety side analysis against the effects of both monotonic and cyclic thermal loads (involving potentially irreversible effects at the pile-soil interface) to be made. The second and

the third allow focusing for the purpose of the present study on the effects of the thermal loads applied to the energy piles rather than on those of the mechanical loads. In those cases, an effective approach may consist in assuming the slab as infinitely rigid. *Poulos and Davis (1980) remark, however, that the average vertical displacement of a pile group characterized by an infinitely flexible slab is approximately equal to that of the same group with an infinitely rigid slab* (Rotta Loria, 2018).

The energy piles are approximated as solid cylindrical prisms and form a regular geometry in plain view (e.g., square groups of energy piles). The equivalent piers are also considered to be solid cylindrical prisms. The proposed approach can also consider other cross-sectional shapes of the energy piles and the equivalent piers as well as other energy piles arrangements.

The elastic theory is also used for this present model in fact, the materials constituting the energy pile, the consequent equivalent pier and the soil domains are assumed to be isotropic, homogeneous and uniform. The material properties are considered to be insensitive to the considered temperature variations. The pipes inside the energy piles and the equivalent piers are not modelled. This choice involves considering the temperature field in these domains as that of the heat carrier fluid circulating inside the pipes in the reality. The materials constituting the energy piles and the equivalent piers follow a linear thermo-elastic behavior. The soil follows an elasto-plastic behavior, although the impact of the temperature variations observed in reality in this material on the response of the pile group is implicitly considered in the analyses.

The energy piles are considered to be embedded in a deep soil layer at the same initial temperature T_0 and are subjected to a temperature variation, $\Delta T = T - T_0$, where T is an actual temperature value. This temperature variation is assumed to be

- applied instantaneously and uniformly along the length of all of the piles in the group;
- constant with time
- equal for all the piles.

The same temperature variation is assumed to be applied to the equivalent piers. Considering situations in which different temperature variations or (equal or different) thermal powers would be applied to the energy piles may indeed be feasible.

The dominant mode of heat transfer in the soil is considered to be conduction. The impact of ground water advection is considered to be negligible. Thermal contact resistance between the energy piles and the soil is discounted. The variation of the thermal field at the ground surface as a consequence of a potential variation in the environmental conditions is assumed to be negligible. The aforementioned assumptions allow an expedient although simplified analytical resolution of the thermal problem characterizing the single energy piles that may be needed when defining the homogenized material properties of the equivalent piers. The horizontal (top) boundary described by

the soil surface is treated as adiabatic. Differences in the thermal field around the energy piles are expected for scenarios where the soil surface may be assumed to be adiabatic or characterized by a fixed constant temperature, with a consequent impact on the mechanical behavior of these ground structures (Bodas Freitas et al., 2013). However, because the former condition appears to more closely characterize real energy pile applications than the latter (especially for piles located far from the external boundaries of large thermally insulated buildings), it has been considered in Rotta Loria (2018) providing reliable values. In the following, compressive stresses, contractive strains and downward displacements (i.e., settlements) are considered to be positive.

5.7.2 Geometry for equivalent pier

The main idea of the equivalent pier approach is that any regular pile group can be modelled as a single equivalent pier by considering the soil region in which the piles are embedded as a homogenized continuum (cf., Figure 5.10). Such an equivalent pier is characterized by an equivalent diameter that can be calculated as (Poulos, 1993)

$$D_{eq} \approx 1.27 \sqrt{A_g} \quad (13.7)$$

$$D_{eq} = \frac{2}{\sqrt{\pi}} \sqrt{A_g} \approx 1.13 \sqrt{A_g} \quad (13.8)$$

The equation (13.7) is referred for predominantly floating piles and (13.8) for predominantly end-bearing piles. In the previous equations, A_g is the plan area of the group. For any general configuration of piles, A_g can be determined as:

$$A_g = A_{t,EP} + A_{soil} \quad (13.9)$$

where $A_{t,EP}$ is the total cross-sectional area of the piles composing the group ($A_{t,EP} = n_{EP} A_{EP}$ where n_{EP} is the number of piles in the group and A_{EP} is the cross-sectional area of a single pile) and A_{soil} is the plan area of soil surrounding the piles delimited by the simplest polygon that better reproduces the shape of the pile group. In the general case, for a square piles group, A_g can be calculated as

$$A_g = [(\sqrt{n_{EP}} - 1)s + D]^2 \quad (14.1)$$

where s is the center-to-center distance (spacing) between the piles and D is the pile diameter.

Numerical analyses performed suggest that the choice of using equations (13.7) and (13.8) to determine D_{eq} leads to differences of up to 5% between the estimated values of average vertical

displacement. This result holds for both low and high magnitudes of thermal loads and mechanical loads imposed prior to the temperature variations to equivalent piers for common pile and soil strata stiffness and pile spacing.

Considering an equivalent pier of the same length of the piles in the group and of an equivalent diameter appears to be preferable to considering an equivalent pier of the same circumscribed plan area as the group and an equivalent length.

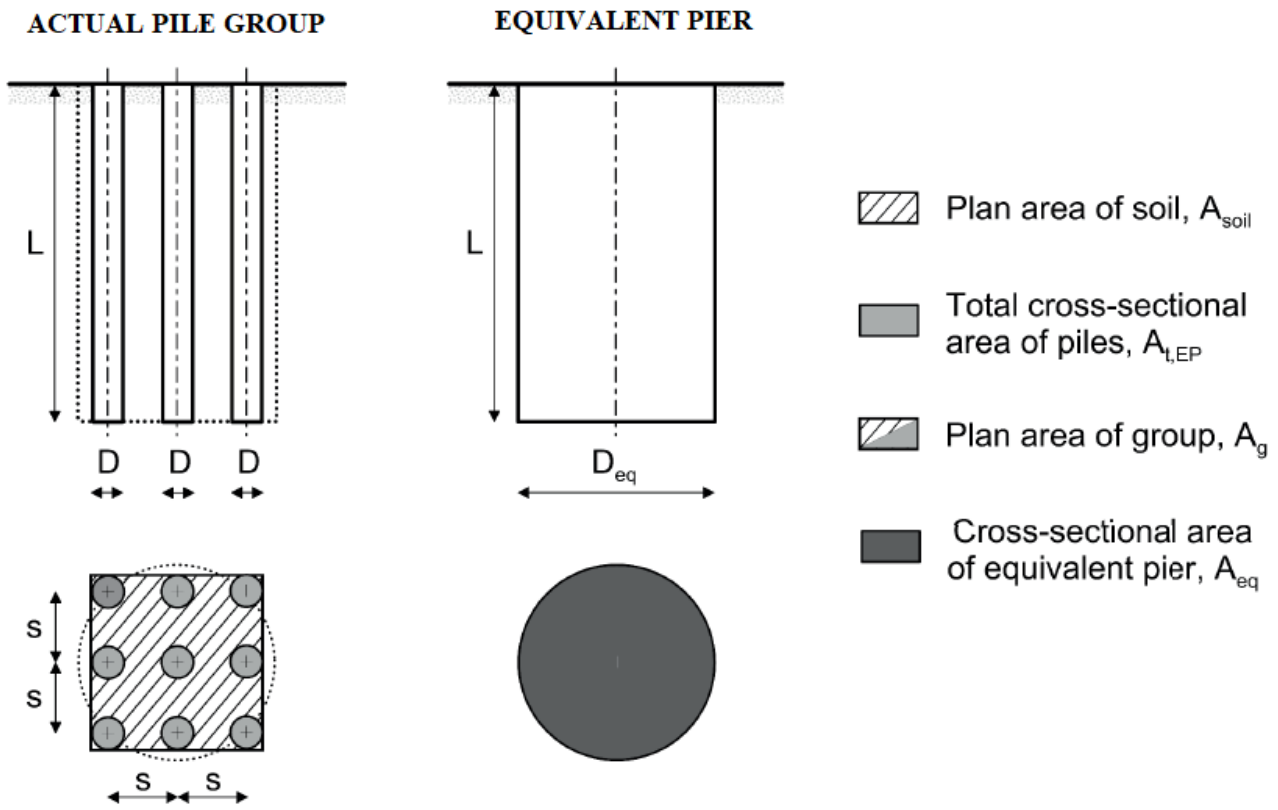


Figure 5.10: The equivalent pier schematization (Rotta Loria et al.2017).

5.7.3 Homogenized material properties of the equivalent pier

There are two important dimensionless parameters that characterize the response of energy pile groups subjected to thermal and mechanical loads:

- the pile-soil stiffness ratio, $\Lambda = E_{EP}/G_{soil}$, where E_{EP} is the Young's modulus of the piles composing the group and G_{soil} is the shear modulus of the soil ($G_{soil} = E_{soil}/(2(1 + \nu_{soil}))$), in which E_{soil} is the Young's modulus of the soil and ν_{soil} is the Poisson's ratio of the soil);
- the soil-pile thermal expansion coefficient ratio, $X = \alpha_{soil}/\alpha_{EP}$, where α_{soil} is the linear thermal expansion coefficient of the soil and α_{EP} is the linear thermal expansion coefficient of the piles.

The material parameters involved in defining these two dimensionless ratios are considered for determining two key material properties in the characterization of the response of the equivalent pier

to thermal (and mechanical) loads: the equivalent Young's modulus, E_{eq} , and the equivalent linear thermal expansion coefficient, α_{eq} . The equivalent pier can be characterized by an equivalent Young's modulus effectively homogenizing that of the piles and of the soil embedded between them that can be calculated as the weighted average of the Young's modulus of these bodies as (Poulos, 1993)

$$E_{eq} = \frac{A_{t,EP}E_{EP} + A_{soil}E_{soil}}{A_{t,EP} + A_{soil}} = E_{EP} \frac{A_{t,EP}}{A_g} + E_{soil} \left(1 - \frac{A_{t,EP}}{A_g} \right) \quad (14.2)$$

The equivalent pier can then be characterized by an equivalent linear thermal expansion coefficient that can be calculated as (Rotta Loria, 2018)

$$\alpha_{eq} = \alpha_{EP} \quad (14.3)$$

$$\alpha_{eq} = \frac{A_{t,EP}\alpha_{EP} + A_{exc}\alpha_{soil}\gamma}{A_{t,EP} + A_{exc}} = \alpha_{EP} \frac{A_{t,EP} + A_{exc}X\gamma}{A_{t,EP} + A_{exc}} \quad (14.4)$$

The equation (14.3) and (14.4) are respectively for values of $X \leq 1$ and > 1 , with $X = \alpha_{soil}/\alpha_{EP}$.

In the previous equations, γ is a coefficient that relates the average temperature variation in the soil to that in the energy piles within the plan area A_{exc} in which the thermal strain potential of the soil is in excess compared to the thermal strain potential of the energy piles (Rotta Loria, 2018).

The equation (14.4), together with the associated assumptions and governing parameters, is presented below. Equations (14.3) and (14.4) represent the key novelty that allows applying the classical equivalent pier concept originally proposed for the displacement analysis of conventional pile groups subjected to only mechanical loads to energy pile groups that are also subjected to thermal loads (Rotta Loria, 2018). The equation (14.3) expresses that when $X \leq 1$, the deformation of the energy pile group may be interpreted and described by considering only the thermal expansion coefficient of the piles and the related thermally induced deformation because it governs that of the group. The equation (14.4) highlights that when $X > 1$, the deformation of the energy pile group may be interpreted and described by considering also the thermal expansion coefficient of the soil surrounding the piles and the related thermally induced deformation because it profoundly characterizes that of the group. In particular, the equation (14.4) is based on a similar concept to that characterizing equation (14.2). The equation (14.4) accounts for the impact of a linear thermal expansion coefficient of the soil in excess compared to that of the piles on the deformability problem by considering superposition of the representative areas involved.

5.7.4 Modelling choice

In order to perform the analysis for equivalent pier method for energy piles and conventional piles group, a 2-D axisymmetric (Figure 5.13 (a) and (b)) analysis with COMSOL has been performed. The model used is the same used in the chapter 4.2 for single pile analysis for both case study ($L_{EP} = 19.2\text{ m}$ and $L_{EP} = 28\text{ m}$).

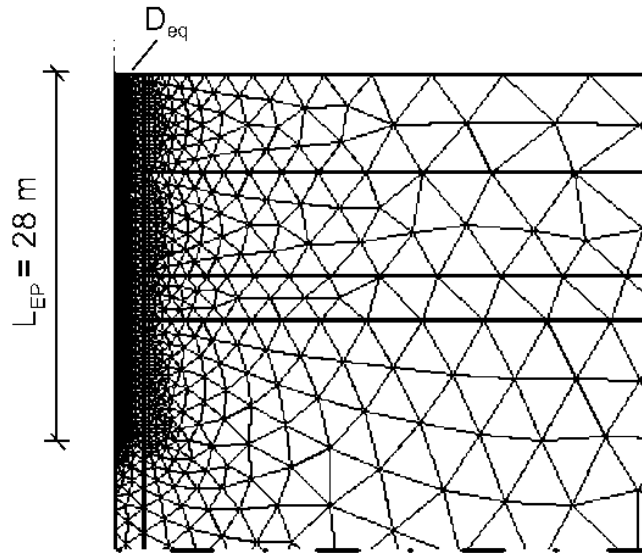


Figure 5.11 (a): Modelling choice for the real design case.

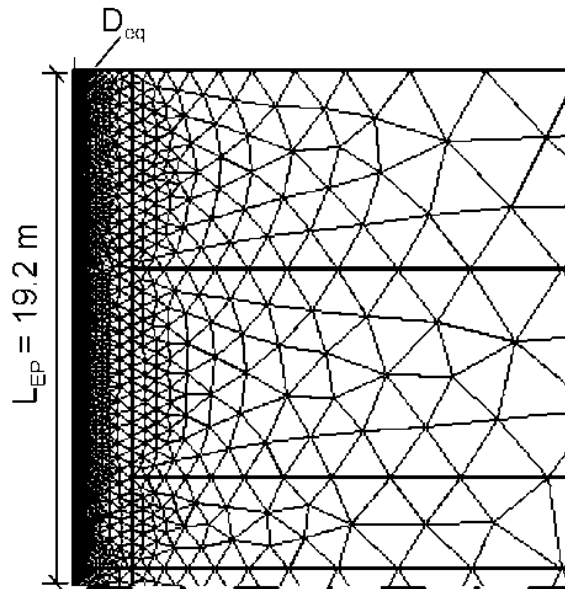


Figure 5.12 (b): Modelling choice for the proposed design case.

In the calculation of the equivalent parameters some simplifications have been done:

- in the calculation of equivalent Young's Modulus E_{eq} given by the equation (14.2), the value of E_{soil} is equal to \bar{E}_{soil} calculated as:

$$\bar{E}_{soil} = \frac{E_{Layer A} h_{Layer A} + E_{Layer B} h_{Layer B} + E_{Layer C} h_{Layer C} + E_{Layer D} h_{Layer D}}{h_{Layer A} + h_{Layer B} + h_{Layer C} + h_{Layer D}} \quad (14.5)$$

because in the present case study the piles are embedded in a layered soil. Obviously, for the proposed design case during the calculation of \bar{E}_{soil} the contribute of layer D has been neglected.

- the linear thermal expansion coefficients of the first three soil layers are lower than that of the piles or in other words, $X < 1$ and the situation is that described in the equation (14.3); for the latter soil layer (layer D) the situation is the opposite because $X > 1$. In order to perform a comparable analysis, with the results obtained from analytical models and 3-D FEM (where $\alpha_{soil} = 0$), the value of α_{eq} is equal to zero.

5.7.5 General framework of the influence of the slab in the Equivalent pier method

The equivalent pier method has been performed as free head model, but in both case study the presence of the slab play an important role. Even if Poulos and Davis (1980) remark that the average vertical displacement of a pile group characterized by an infinitely flexible slab is approximately equal to that of the same group with an infinitely rigid slab under mechanical load, the effect of the thermal load has been evaluated. More precisely in this chapter the role of K_{ss} for piles subjected upon thermal load has been evaluated in order to provide a complete procedure for any type of design situation.

First of all, must clarify the meaning of K_{ss} called slab-soil stiffness ratio calculated as:

$$K_{ss} = \frac{4E_{slab} B_{slab} t_{slab}^3 (1 - \nu_{soil}^2)}{3\pi E_{soil} L_{slab}^4 (1 - \nu_{slab}^2)} \quad (14.6)$$

Values of $K_{ss} \approx 0.001$ correspond to a flexible slab whereas values of $K_{ss} \approx 0.1$ correspond to an almost rigid slab (Brown, 1975). Practical ranges of K_{ss} are between 0.001 and 10 (Clancy and Randolph, 1996). The previous observation has been evaluated for pile-slab structure subjected upon mechanical load; the goal of this chapter is verify if this limit is also acceptable for pile-slab structure subjected upon thermal load.

Modifying the nature of the model and applying the slab on the equivalent pier head as “spring foundation” there is one important point that must be clarified. The equation (9.1) that provide the value of the slab stiffness may be used also in this analysis, but in the previous analysis was applied on the single pile and consequently the value of K_h is divided by A_{EP} ; now, in this model the situation is completely different because an equivalent single pile analysis has been performed due to the

equivalent pier has been calculated also taking into account the soil parameters, following the equations (13.7), (13.8) and (14.2).

The main point is understand if the slab stiffness calculated with equation (9.1) must be divided by the total pile area ($A_{t,EP}$) or by the equivalent pier area (A_{eq}). As mentioned before if:

- $K_{SS} < 0.1$ the slab is flexible;
- $K_{SS} > 0.1$ the slab is rigid.

Therefore, the value of slab stiffness for the equivalent pier method become:

- $\overline{K}_h = K_h/A_{eq}$ when the slab is rigid;
- $\overline{K}_h = K_h/A_{t,EP}$ when the slab is flexible.

For equivalent pier subjected upon mechanical load the concept is clear. The main point is understand if this limit value ($K_{SS} = 0.1$) is also valid for equivalent pier subjected upon thermal load.

In order to solve this problem a general sensitive analysis with a pile-slab structure made by four piles (Figure 5.14) and nine piles (Figure 5.15) respectively in the first and in the second case has been performed. The fundamental points of this sensitive analysis are:

- The effect of the slab is negligible when the displacement is transferred entirely to the equivalent pier, or in other words when $w_{slab}/w_{pile} = 1$ and this situation occurs when the slab is rigid (when $K_{SS} = 0.1$ is exceeded);
- the influence of the spacing is negligible when the difference among the curves is less than 5%;

In the Figure 5.14 (a) the case of square slab with four piles subjected upon mechanical load has been pictured: in this case the aforementioned limit is valid, in fact when $K_{SS} = 0.1$ the ratio between the slab displacement and the pile displacement is more or less equal to 1.

In the Figure 5.14 (b) the case of rectangular slab with four piles subjected upon mechanical load has been pictured: in this case the aforementioned limit is valid, in fact when $K_{SS} = 0.1$ the ratio between the slab displacement and the pile displacement is more or less equal to 1.

In the Figure 5.14(c) the case of square slab with four piles subjected upon thermal load has been pictured: in this case the limit is lower than that of the same structure subjected upon mechanical load ($K_{SS} = 0.064$). For more flexible slab cases the displacement of the slab is much higher than that of the equivalent pier, reaching values of $w_{slab}/w_{pile} \approx 2.75$.

In the Figure 5.14 (d) the case of rectangular slab with four piles subjected upon thermal load has been pictured: in this case the limit is lower than that of the square slab with four piles subjected upon thermal load ($K_{SS} = 0.05$).

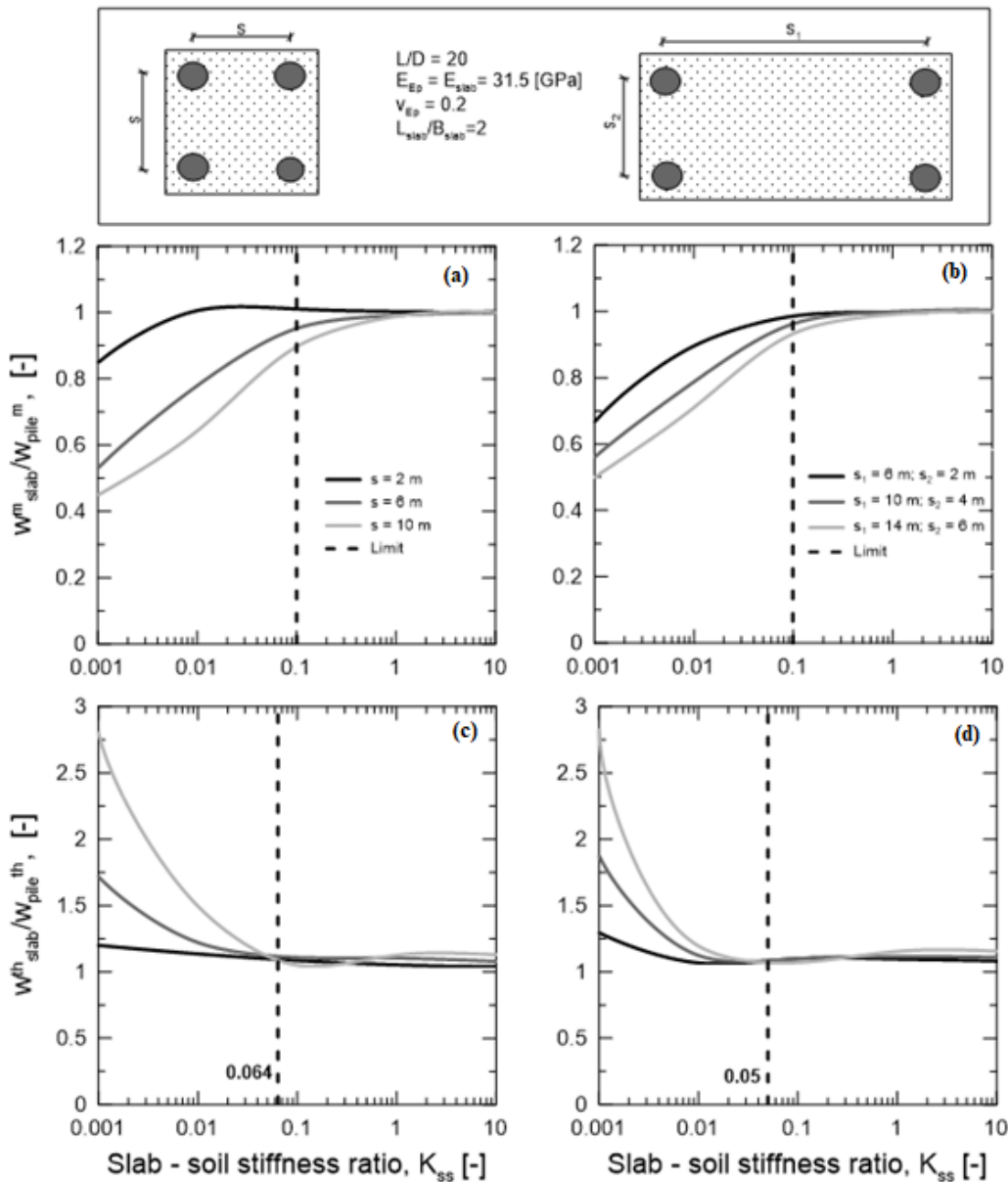


Figure 5.13: w_{slab}/w_{pile} trends varying the spacing and the shape of the slab with four piles. **Figure 5.13 (a)** square slab with four piles subjected upon mechanical load; **Figure 5.13 (b)** rectangular slab with four piles subjected upon mechanical load; **Figure 5.13 (c)** square slab with four piles subjected upon thermal load; **Figure 5.13 (d)** rectangular slab with four piles subjected upon thermal load

Therefore for this cases with a little approximation the limit $K_{SS} = 0.1$ is also valid for pile-slab structures subjected upon thermal loads.

In the Figure 5.15 a square and rectangular slab with nine piles subjected upon mechanical and thermal load has been represented. In the Figures 5.15 (a) and (b) the aforementioned limit $K_{SS} = 0.1$

valid, even if the curves tend to 1 for values less than 0.1 because a higher number of piles stiffen the structure in both cases (square and rectangular slab). In the Figures 5.15 (c) and (d) the limit is higher than 0.1: in other words, the slab transfer the total displacement to the pile for higher value of K_{SS} .

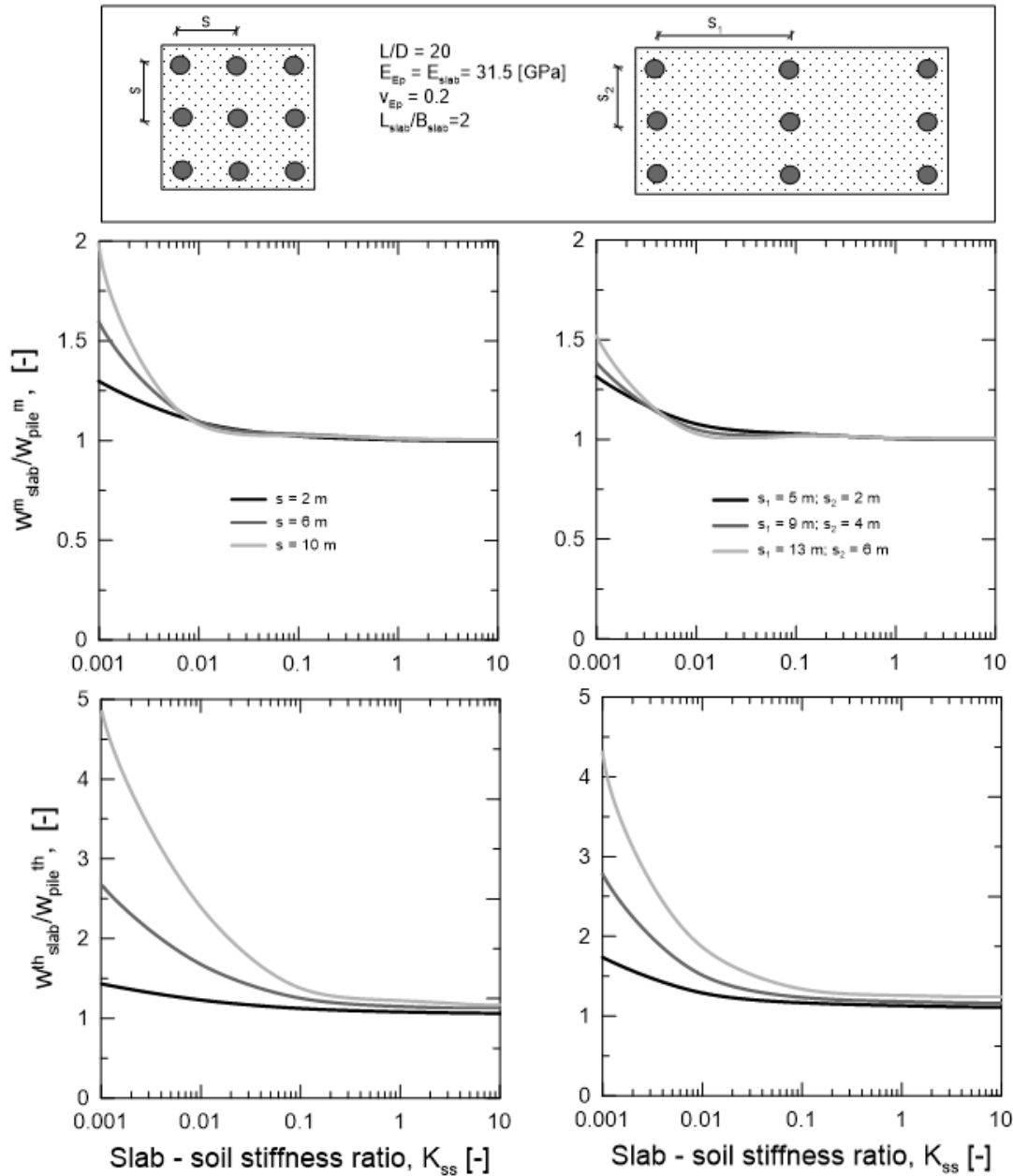


Figure 5.14: w_{slab}/w_{pile} trends varying the spacing and the shape of the slab with nine piles. **Figure 5.14 (a)** square slab with nine piles subjected upon mechanical load; **Figure 5.14 (b)** rectangular slab with nine piles subjected upon mechanical load; **Figure 5.14 (c)** square slab with nine piles subjected upon thermal load; **Figure 5.14 (d)** rectangular slab with nine piles subjected upon thermal load

Concluding:

- the limit $K_{SS} = 0.1$ is also valid for slab-piles structures subjected upon thermal load;

- according to the first point, when the slab is flexible the value of K_h given by the equation (9.1) is divided by the area of the equivalent pier; when the slab is flexible the value of K_h is divided by the total area of the piles;
- the value of K_h given by the equation (9.1) is a lower bound: less values are not acceptable because equation (9.1) is performed taking into account only the slab and the soil layers, not taking into account the piles stiffness.

Linking up to the two case study, the value of K_{ss} is much less than 0.1 and this mean that the slab in both cases is more flexible and therefore the 2-D FEM analysis have been performed with a free head equivalent pier.

5.8 3-D FEM solution

5.8.1 Modelling solution

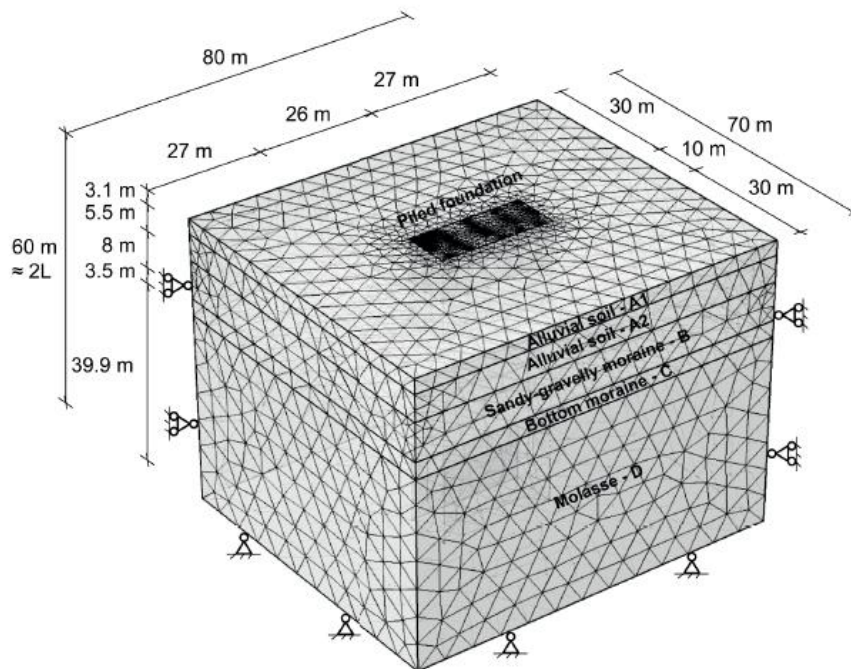
A 3-D finite element model of the site was developed using the software COMSOL Multiphysics (COMSOL, 2014). The $80 \times 70 \times 60$ m³ model is composed of 438,443 tetrahedral, prismatic, triangular, quadrilateral, linear and vertex elements (Figures 5.15 – 5.16 - 5.17). The model reproduces the entire foundation supporting the water retention tank. It does not take into account the presence of the tubes in the energy stacks because to compare the results provided by the analytical models and the equivalent method of the pillar. Another important consideration must be made for the coefficients of linear thermal expansion of the soil layers: in this type of analysis, the linear thermal expansion coefficient for each layer of soil is equal to zero. This finite element model was used by Rotta Loria (2018) to run thermo-mechanical finite element predictions of Test 20EP1.

5.8.2 Hypotheses and considerations

As in the chapter 4.2, in this numerical analysis of the response of the reinforced concrete foundation in the soil under mechanical and thermal loads is based on the following assumptions:

- the displacements and deformations of all of the materials can be representatively described through a linear kinematic approach under quasi-static conditions (i.e., negligible inertial effects);
- the materials that constitute the pile foundation are considered to be isotropic with pores that are fully filled by air and are assumed to be purely conductive domains with equivalent thermo-physical properties that are given by the fluid and the solid phases;

- the materials that make up the soil layers are assumed to be isotropic, fully saturated by water and purely conductive domains with equivalent thermo-physical properties that are given by the fluid and the solid phases;
- the loads that are associated with this problem have a negligible impact on the variation of the hydraulic field in the soil;
- all the materials are considered to be representatively described by linear thermo-elastic behaviors. Under these conditions, a thermo-mechanical mathematical formulation is employed.



-  Pinned support (i.e., fixed displacement in the two horizontal directions). Boundary condition applied to the bottom horizontal surface of the model (the uppermost surface of the model is free of any restraint)
 -  Roller support (i.e., fixed displacement in the horizontal direction perpendicular to the surface upon which the boundary condition is applied). Boundary condition applied to the four vertical external surfaces of the model
 -  The initial stress state due to gravity in the foundation and the soil is considered to be geostatic and assumes a coefficient of earth pressure at rest of $K_0 = 1$. Initial condition applied to the entire domain
- No residual stress from the installation of the piles are considered. Perfect contact between the bodies is assumed. Conditions accounted for the entire model

Figure 5.15: Geometry, initial and boundary conditions of the 3-D finite element model (Rotta Loria, 2018).

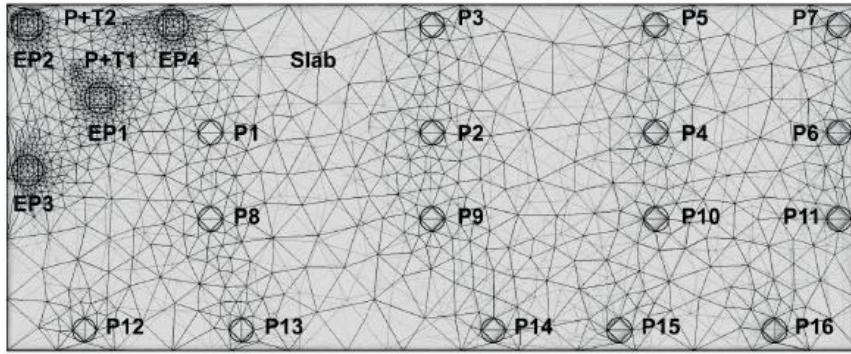


Figure 5.16: plan view of the foundation listing the piles and other relevant features (Rotta Loria, 2018).

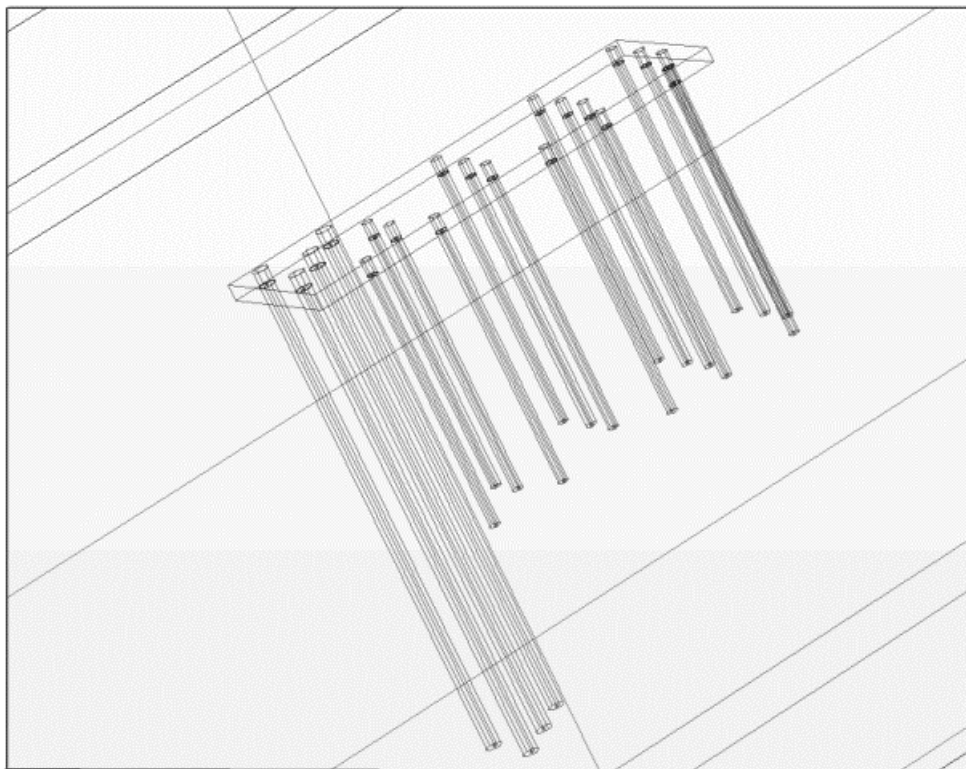


Figure 5.17: 3-D view of the pile-slab structure in case of real design case ($L_{EP} = 28\text{ m}$).

5.9 Findings and discussion

5.9.1 Energy piles

In this chapter the comparisons, in terms of average and differential displacement for both thermal (heating and cooling) and mechanical case, between the three analytical models and the 3-D FEM analysis have been carried out. In these comparisons the value of the average displacement correspondent to continuous model is not reported because as previously shown this model does not provide reliable results when a rigid stratum is present. So, in the comparisons and in the displacement

checks the value correspondent to continuous model, for energy piles, has not been calculated. In the following figures the normalized average displacement comparison for mechanical load, heating and cooling thermal load has been shown..

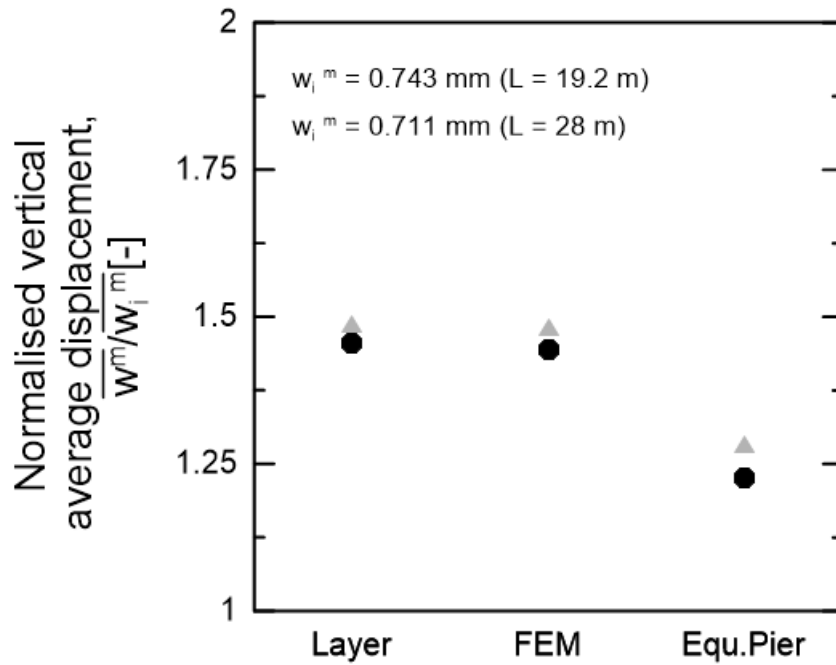


Figure 5.18: comparisons of normalized average displacement due to mechanical load.

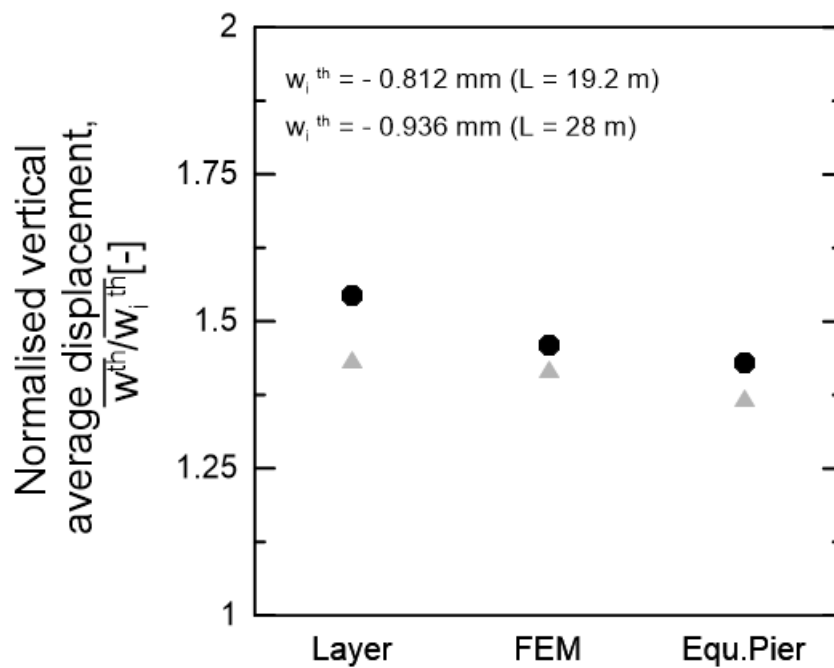


Figure 5.19: comparisons of normalized average displacement due to heating thermal load.

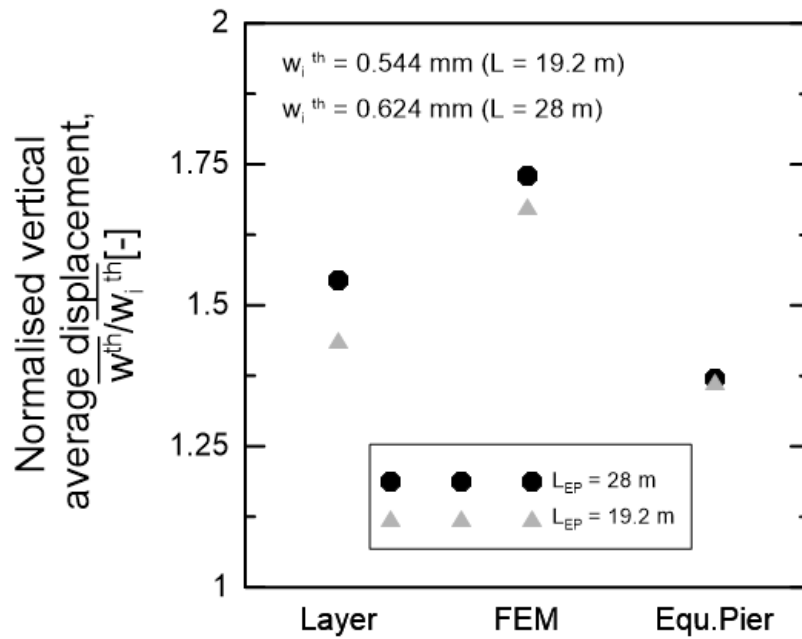


Figure 5.20: comparisons of normalized average displacement due to cooling thermal load.

In the following figures the normalized differential displacement comparison for mechanical load, heating and cooling thermal load has been shown. In all three figures the value of the differential displacement given by the layer model is overestimated than that given by 3-D FEM analysis. The value of differential displacement given by the equivalent pier is equal to zero, because this model provide only the average head displacement of the piles group.

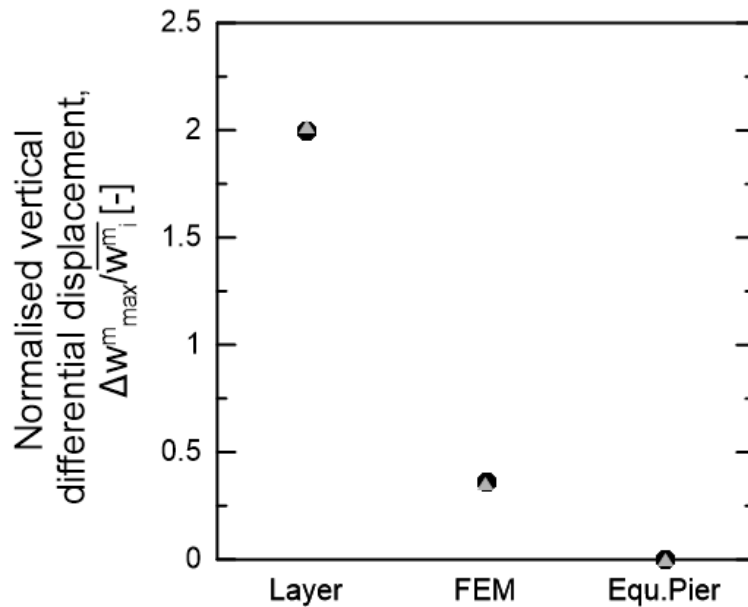


Figure 5.21: comparisons of normalized differential displacement due to mechanical load.

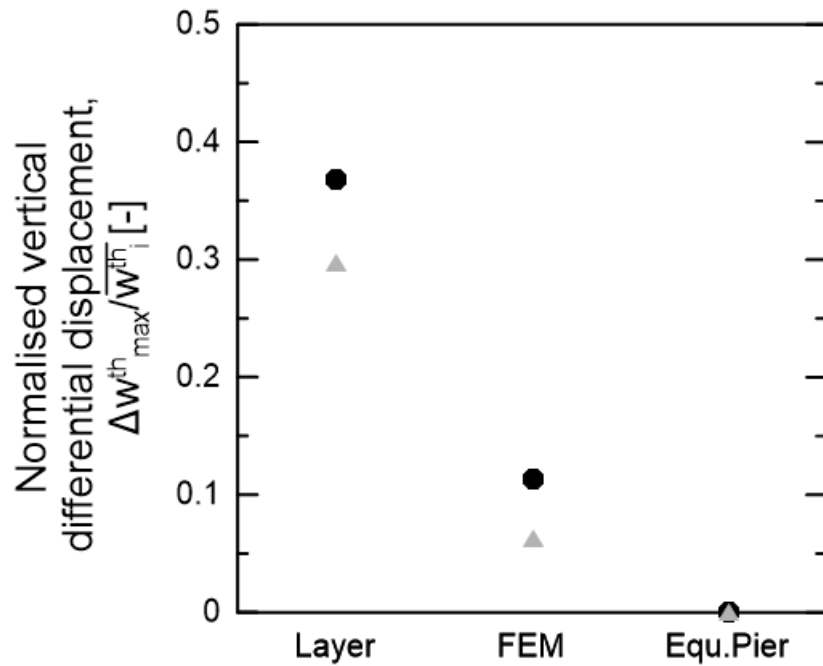


Figure 5.22: comparisons of normalized differential displacement due to heating thermal load.

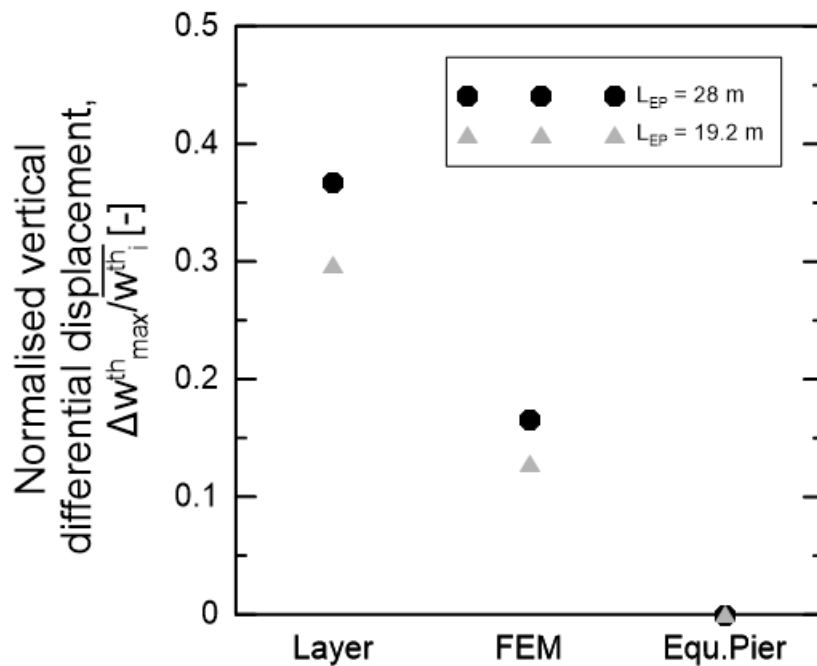


Figure 5.23: comparisons of normalized differential displacement due to cooling thermal load.

The value of differential displacement provided by the layer model is overestimated, because the layer model has been conceived as a free head model and it does not take into account the presence of the slab and the effect due to it; in the 3-D FEM analysis, instead, the slab has been modelled as infinitely rigid slab in order to transfer the load to the piles. Since the EP1 is unloaded, in the layer model its displacement is due only to interaction among the other piles. In the 3-D FEM analysis the

slab equally redistributes the loads and therefore the displacement of the EP1 is due both to the interaction and to the action of the redistribution of the slab loads and is higher than that given by the layer model as shown in the following tables:

<i>LAYER MODEL</i>			
	w^m	w^{th+}	w^{th-}
EP1	0.12	-1.17	0.78
EP2	0.98	-1.56	1.04
EP3	1.49	-1.52	1.01
EP4	1.54	-1.52	1.01

Table 5.1: Displacement values for each pile given by the layer model for the real design case.

<i>FEM</i>			
	w^m	w^{th+}	w^{th-}
EP1	0.95	-1.42	1.07
EP2	0.88	-1.37	1.16
EP3	1.07	-1.31	1.03
EP4	1.21	-1.36	1.06

Table 5.2: Displacement values for each pile given by the 3-D FEM analysis for the real design case.

In fact the maximum differential displacement in both analysis has been calculated between EP1 and EP4:

- in case of layer model: $\Delta w_{max} = 1.42 \text{ mm}$;
- in case of 3-D FEM analysis: $\Delta w_{max} = 0.26 \text{ mm}$

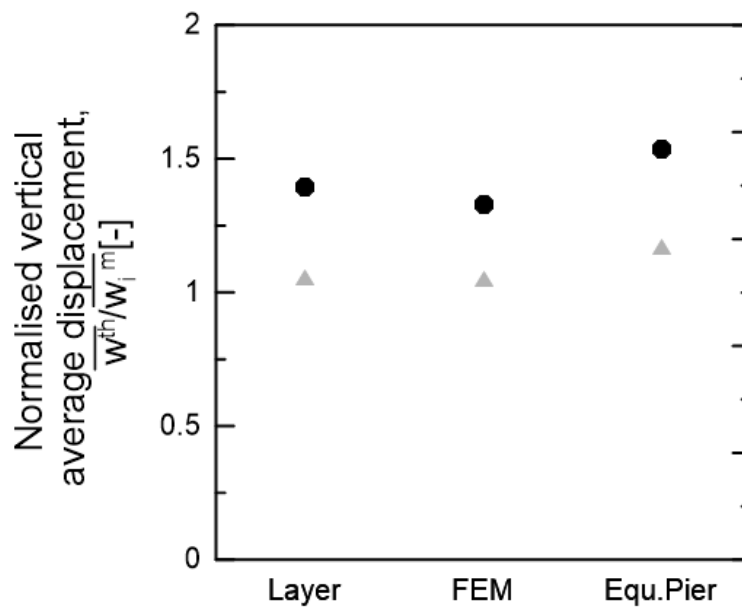


Figure 5.24: comparisons of average displacement normalized with the mechanical displacement in case of heating.

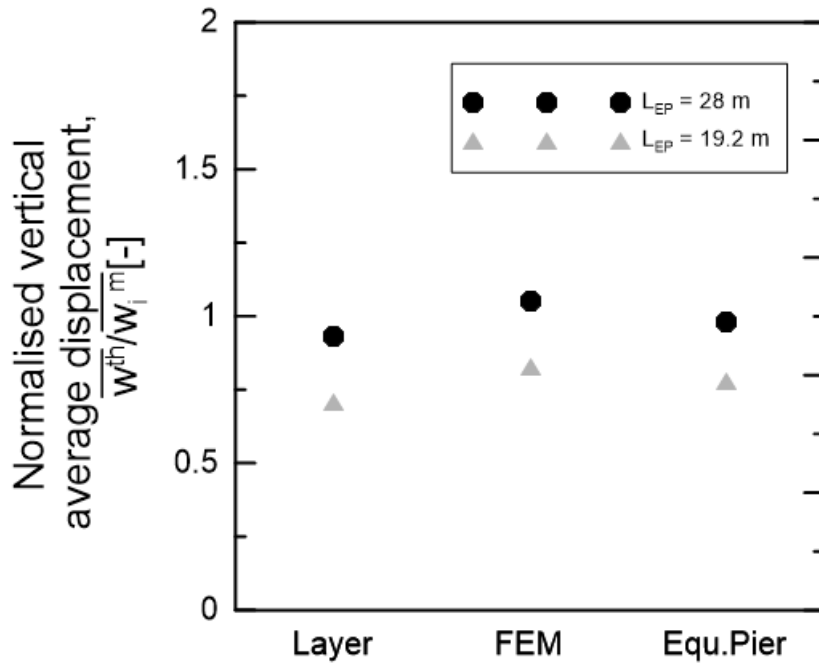


Figure 5.25: comparisons of average displacement normalized with the mechanical displacement in case of cooling.

In figures 5.24 and 5.25 a comparison was made between the values of average vertical normalized displacement with the respective values of mechanical displacement, obtained with the various methods. In both figures the displacement values in case of the real design case ($L_{EP} = 28 \text{ m}$) than those in case of the proposed design ($L_{EP} = 19.2 \text{ m}$). In the Figure 5.25 in case of real design case the value of the thermal displacement is more or less 40-50 % higher than that of mechanical one, while in the case of cooling the thermal displacement is more or less the same of the mechanical one.

5.9.2 Conventional piles

Conventional piles group is made by 16 piles subjected only under mechanical load and in this chapter the results given by the analytical models, equivalent pier and 3-D FEM analysis will be discussed. In this case the results given by the continuous have also been reported because the shear modulus of the soil layers were similar among them. In the Figure 5.26 the average vertical displacement comparisons have been pictured, while in the Figure 5.27 the differential vertical displacement.

In the Figures 5.26 and 5.27 the values given by all the analysis have been normalized respect the average vertical displacement calculated in the case of single pile analysis that does not take into account the interaction among the conventional piles.

In the Figure 5.26 the values of average conventional piles group given by the analytical models and equivalent pier method are higher than that given by the 3-D FEM analysis because the latter analysis

take into account the presence of the slab and provide lower displacement values. To evaluate the average displacement in 3-D FEM analysis for the conventional piles group, only the effect due to mechanical load was taken into account, thus avoiding the potential effects due to thermal load on the conventional piles.

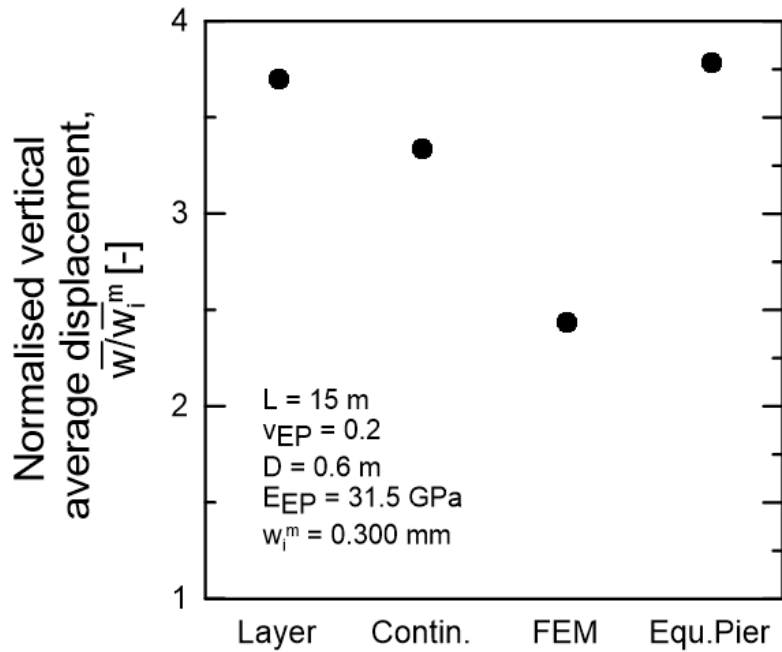


Figure 5.26: Comparisons of the average displacement obtained between the various methods for conventional piles group.

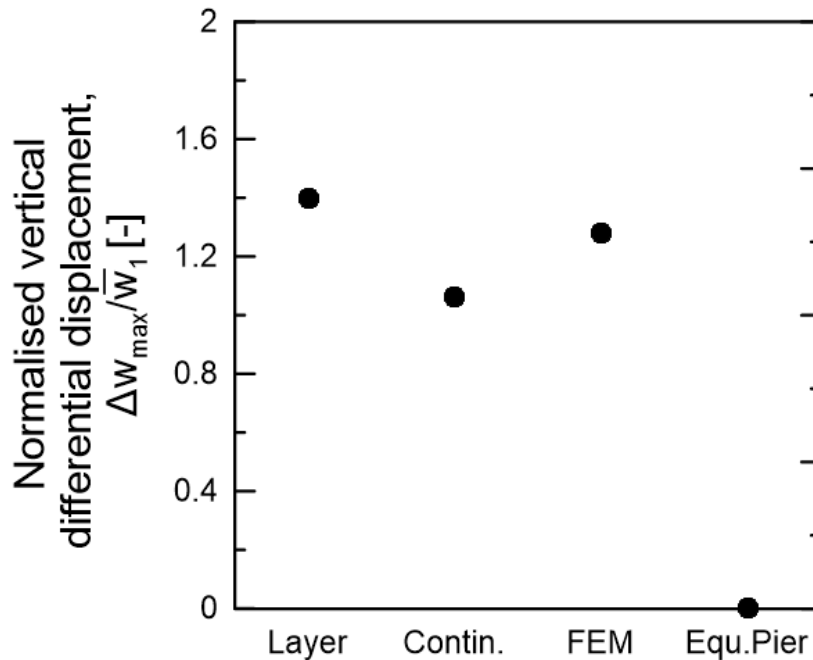


Figure 5.27: Comparisons of the differential displacement obtained between the various methods for conventional piles group.

In the Figure 5.27 the differential displacement obtained from different methods is more or less the same, except for the equivalent pier method because this method provide only the mean head displacement of the group.

Another important point to highlight is the influence of the thermal load applied within the energy piles on the conventional piles group. This effect it is only perceptible when a 3-D FEM analysis is performed because it can not be studied with the analytical models or with the equivalent pier because in all the aforementioned method the piles must have the same length and is not to possible to study energy and conventional piles in the same analysis with this tools. In the Figure 5.28 and 5.29 the comparisons between the average and differential displacement have been pictured.

In the Figure 5.28 the value $FEM\ m$ is obtained from a 3-D analysis of the entire structure subjected only under mechanical load, while $FEM\ m+h$ and $FEM\ m+c$ are obtained from a 3-D analysis of the entire structure subjected under mechanical load coupled with respectevly with heating and cooling thermal load. Obviously the value given by $FEM\ m+h$ analysis is lower than that given by $FEM\ m$ because the effect of the thermal load applied within the energy piles is very strong for the closest piles and during heating, since the displacement is negative, the head average displacement is lower. The opposite applies in the case of the value given by $FEM\ m+c$ analysis.

In the Figure 5.29 the evaluation of the effect on the differential displacement of the thermal load applied within the energy piles has been done.

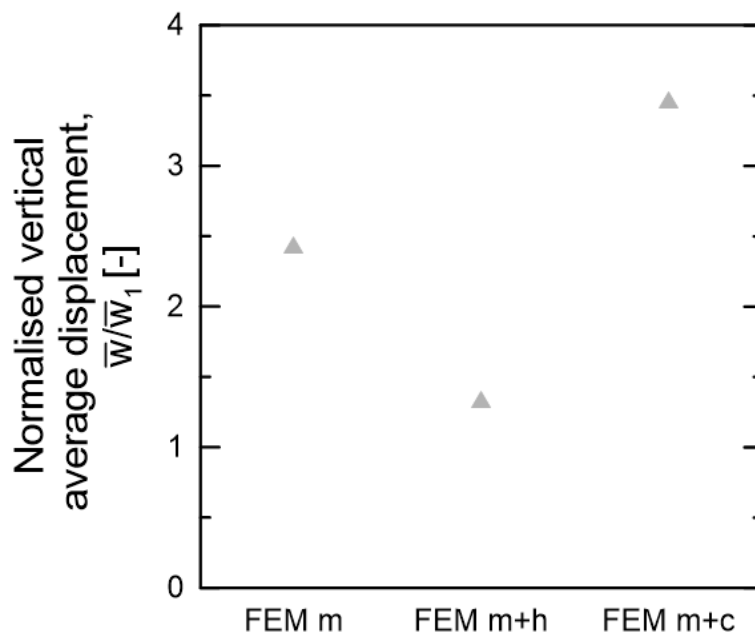


Figure 5.28: Comparisons of the average displacement obtained between the various methods for conventional piles group taking into account the effect of the energy piles.

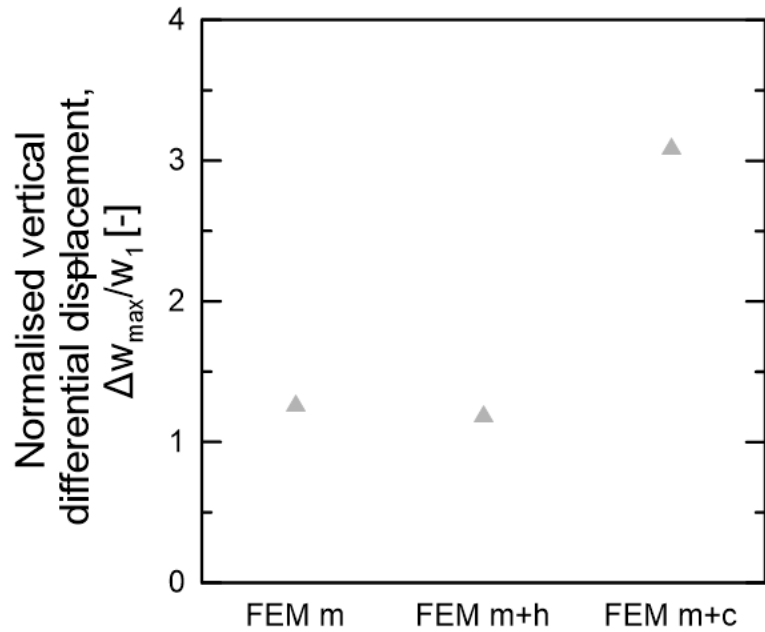


Figure 5.29: Comparisons of the differential displacement obtained between the various methods for conventional piles group taking into account the effect of the energy piles.

5.9.3 Deformation limit state verification for energy piles group

Resuming the deformation limit state verification described in the chapter 4.4.5, the checks is satisfied when the equation (11.3) is verified. In the following tables the verifications done for the energy piles group have been summarized:

<i>Average displacement obtained with Layer model for real design case ($L_{EP} = 28 \text{ m}$)</i>		
	$ w^{m+h} $	w^{m+c}
Design	0.408	1.996
Limit	5.954	5.954
<i>Check</i>	✓	✓

Table 5.3: Deformation limit state checks for the average displacement for the real design case when all energy piles are active.

<i>Average displacement obtained with Layer model for proposed design case ($L_{EP} = 19.2 \text{ m}$)</i>		
	$ w^{m+h} $	w^{m+c}
Design	0.060	1.885
Limit	5.954	5.954
<i>Check</i>	✓	✓

Table 5.4: Deformation limit state checks for the average displacement for the proposed design case when all energy piles are active.

For the differential displacement verifications for both design cases the highest differential displacement is calculated between EP1 and EP4 when EP1 is thermally active (for heating thermal load). In the following tables the checks are summarized:

<i>Differential displacement obtained with Layer model for real design case ($L_{EP} = 28 \text{ m}$)</i>	
	$ w^{m+h} $
Design	2.141
Limit	5.954
<i>Check</i>	✓

Table 5.5: Deformation limit state checks for the differential displacement for the real design case when EP1 is active.

<i>Differential displacement obtained with Layer model for real design case ($L_{EP} = 19.2 \text{ m}$)</i>	
	$ w^{m+h} $
Design	2.189
Limit	5.954
<i>Check</i>	✓

Table 5.6: Deformation limit state checks for the differential displacement for the proposed design case when EP1 is active.

When a cooling thermal load is applied the highest differential displacement is valued between EP4 and EP1 when EP4 is thermally active. The checks are summarized in the following tables:

<i>Differential displacement obtained with Layer model for real design case ($L_{EP} = 28 \text{ m}$)</i>	
	w^{m+c}
Design	1.985
Limit	5.954
<i>Check</i>	✓

Table 5.5: Deformation limit state checks for the differential displacement for the real design case when EP1 is active.

<i>Differential displacement obtained with Layer model for real design case ($L_{EP} = 19.2 \text{ m}$)</i>	
	w^{m+c}
Design	1.884
Limit	5.954
<i>Check</i>	✓

Table 5.6: Deformation limit state checks for the differential displacement for the proposed design case when EP1 is active.

All checks have been done for the displacement given by the layer model because this model gives higher values both for thermal and mechanical displacement.

5.10 Concluding Remarks

In order to take into account the pile group effect because the displacement for each pile is higher than the case in which the single pile is analyzed, the following point must be highlighted:

- in average the best analytical model is the layer model because provide acceptable values also when a rigid stratum is present, instead of the continuous model. This happens because the continuous model take into account the interaction between the soil layers and if there is a rigid soil layer the Young's Modulus of it is much higher than that of others soil layers and when the mean value of shear modulus between two layers is very far from the real values of shear modulus of each soil layers;
- when the soil layers parameters are similar among them the best model to use is the continuous model (as seen in the case of proposed design case subjected upon thermal and mechanical load);
- equivalent pier method has been modelled as free head model but in case in which needs to add the slab because its effect is very important, the value calculated with the equation (9.1) must be divided by the total piles area (when the slab is rigid or when $K_{SS} > 0.1$) or by the equivalent pier area (when the slab is flexible or when $K_{SS} < 0.1$) both for thermal and mechanical load;
- in order to perform a comparison with analytical models and the equivalent pier method, the 3-D FEM analysis must be performed with the linear thermal expansion coefficient of each soil layers equal to zero.

Chapter 6

Cyclic Analysis

6.1 Introduction

In the previous chapters all the analyzes to evaluate the stress and displacement field were carried out in stationary conditions (not time dependent) since the objective was to evaluate the effect of the thermal load acting alone or in combination with the load mechanical on stress and displacement of fields. Prior to this work, no time-dependent analysis have been performed on this case study with a complete 3-D FEM analysis with pipes running water inside them. In this chapter, time-dependent analysis has been performed to evaluate the long-term effect only of the thermal load on the pile-slab structure because the effect due to mechanical load is constant with time.

6.2 Modelling choice

In order to evaluate the long-term effect on the energy piles the modelling choice is the same described in the chapters 5.8.1 and 5.8.2 with two important differences:

- in the previous model the pipes have not been modelled because the thermal variation were applied on all the pile domain, instead in this model the pipes have been modelled and the fluid that circulates inside the pipes is water. The inner diameter of the pipes is $d_{p,in} = 26.2 \text{ mm}$ (the outer diameter is 32 mm and the wall thickness is 2.9 mm). A thermal

conductivity of $\lambda_p = 0 \text{ W/(m } ^\circ\text{C)}$ is imposed in the shallowest 4 meters of the inlet and outlet of the pipes to simulate the thermal insulation near the ground surface (Figure 6.1);

- in the previous model the linear thermal expansion coefficient of each soil layers was equal to zero, while in this model they are different from zero. They are summarized in the following table:

<i>Soil layer</i>	α_{soil}
A	$3.3 \cdot 10^{-6}$
B	$3.3 \cdot 10^{-6}$
C	$3.3 \cdot 10^{-6}$
D	$0.23 \cdot 10^{-4}$

Table 6.1: Linear thermal expansion coefficients of each soil layer.

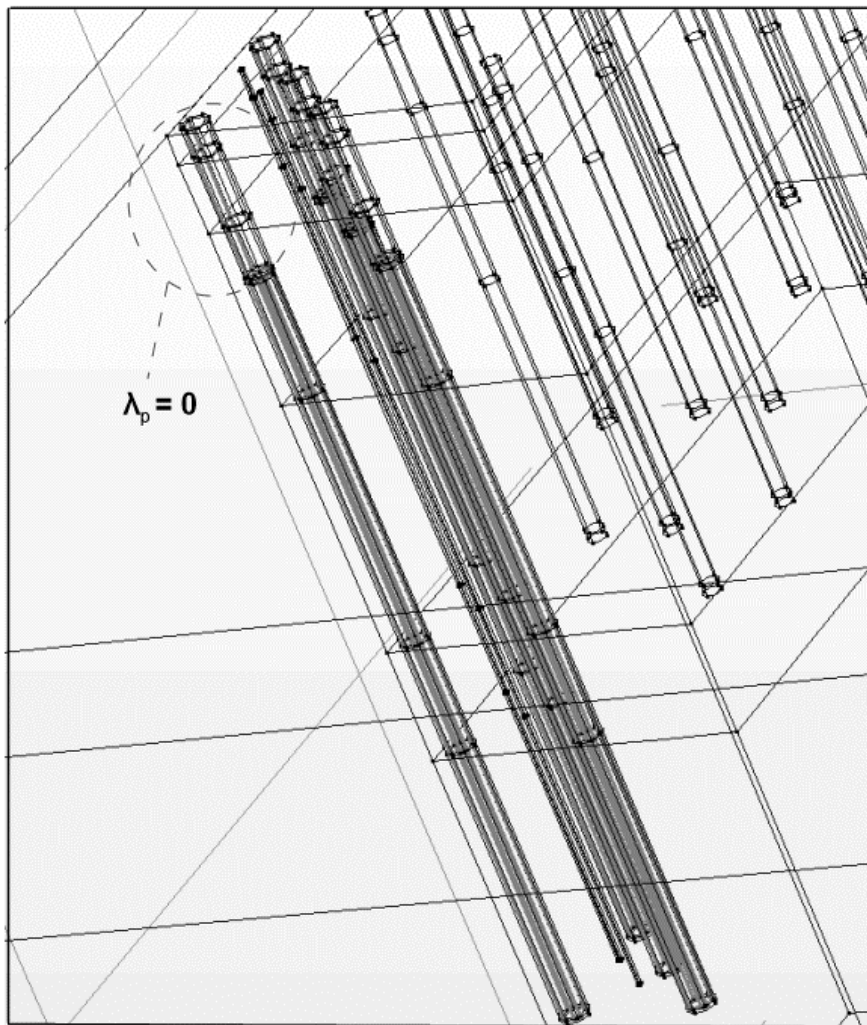
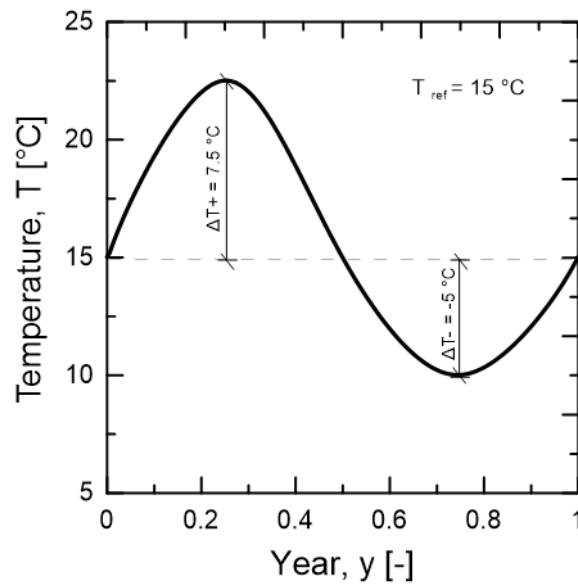


Figure 6.1: 3-D view of the pile-slab structure with pipes in case of real design case ($L_{EP} = 28 \text{ m}$).

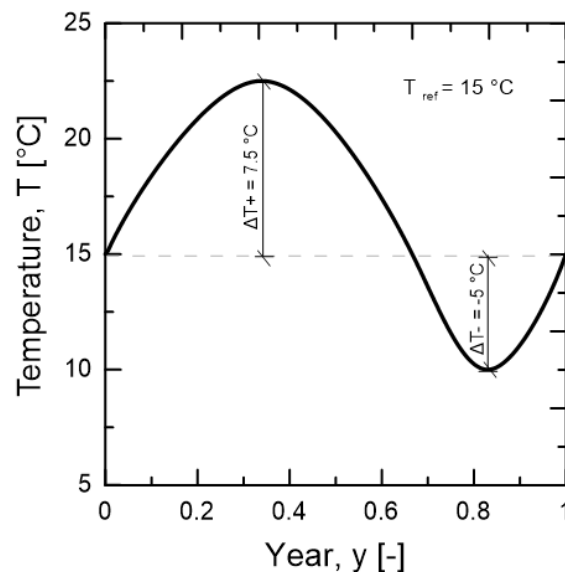
6.3 Idealization of cyclic design load

The first step to do to perform the most realistic possible analysis was to identify the most suitable type of solicitation to get as close as possible to reality. We know that in reality there are seasonal peaks in which the highest or lowest temperatures are reached and therefore, depending on the case, we need to heat or cool the structure supported by the energy piles. During the seasons then the temperature rises to a peak and then decreases as the season ends (imagine that in summer the peak occurs in August, but the season has started since June). So from here came the idea of soliciting the group of poles with a sinusoidal action in such a way as to perceive reality as closely as possible. In order to evaluate more possible case, the following configurations have been built:

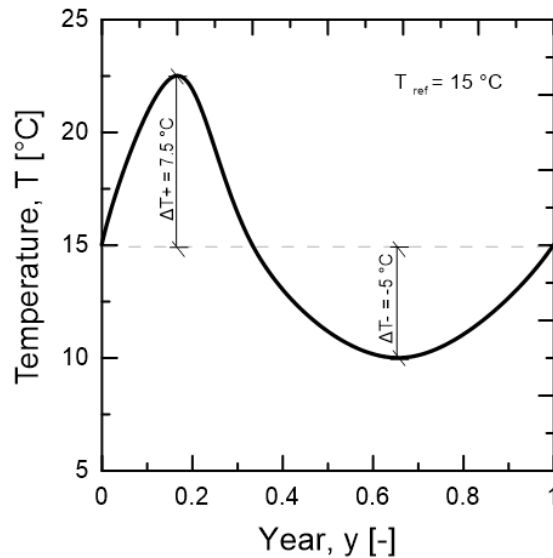
- 6 months heating + 6 months cooling



- 8 months heating + 4 months cooling



- 4 months heating + 8 months cooling



6.4 Findings and discussion

6.4.1 Displacement trends obtained in the real design case

In this chapter the comparison between the displacement trends obtained with the three aforementioned configurations have been carried out in the case of the real design case with the pile length equal to 28 m (Figure 6.2 – Figure 6.4).

In the figure 6.2 the comparison between all models have been done: in fact the time trends of the analytical models, equivalent pier, of the 3-D FEM analysis with linear thermal expansion coefficient equal to zero and with the first cyclic loading configuration, or the 6 months of heating plus 6 months of cooling, have been reported. For this type of configuration there was no increase in the pile head displacement because the sinusoidal is balanced and also because the heating and cooling thermal variations are very close to each other ($\Delta T_{heating} = +7.5$ and $\Delta T_{cooling} = -5$). Another important particular is the entity of the cyclic displacement: the displacement given by the cyclic analysis over 10 % that given by the single pile analysis, but in general view is not burdensome neglect this contribute. In the Figure 6.3 the comparison between the stationary models and the second configuration (8 months of heating plus 4 months of cooling) has been pictured. For this type of configuration, the head displacement increase with the time reaching the value given by the equivalent pier method. In the Figure 6.4 the comparison between the stationary models and the second configuration (4 months of heating plus 8 months of cooling) has been represented. In this case an increasing of cooling displacement has been registered reaching the value given by the 3-D FEM analysis with linear thermal expansion coefficient equal to zero. Obviously the contribute given by

the cooling displacement during 4 months of heating plus 8 months of cooling is lower than that given by the 8 months of heating plus 4 months of cooling because the thermal variations are not the same.

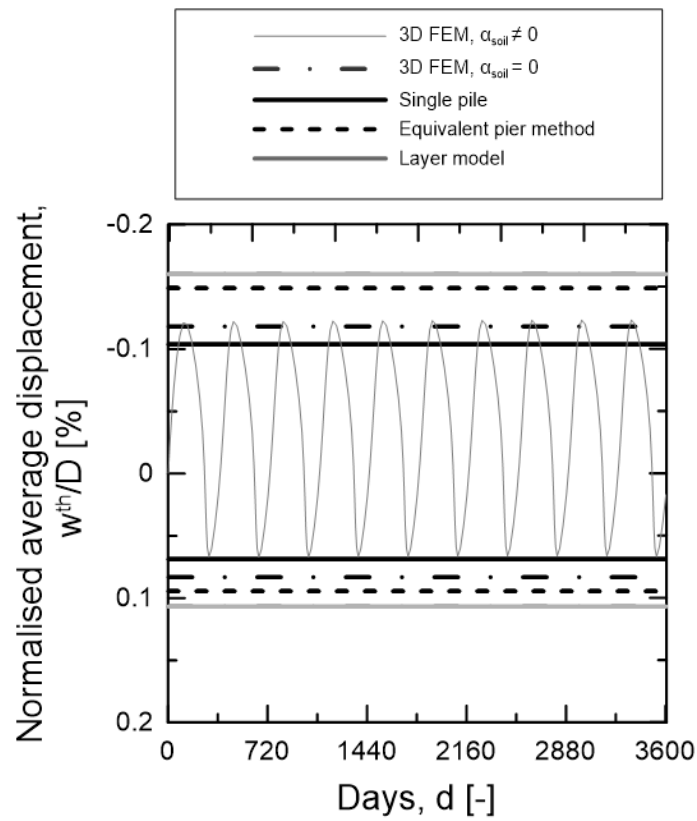


Figure 6.2: Displacement trend obtained with 6 months heating + 6 months cooling configuration in case of the real design case.

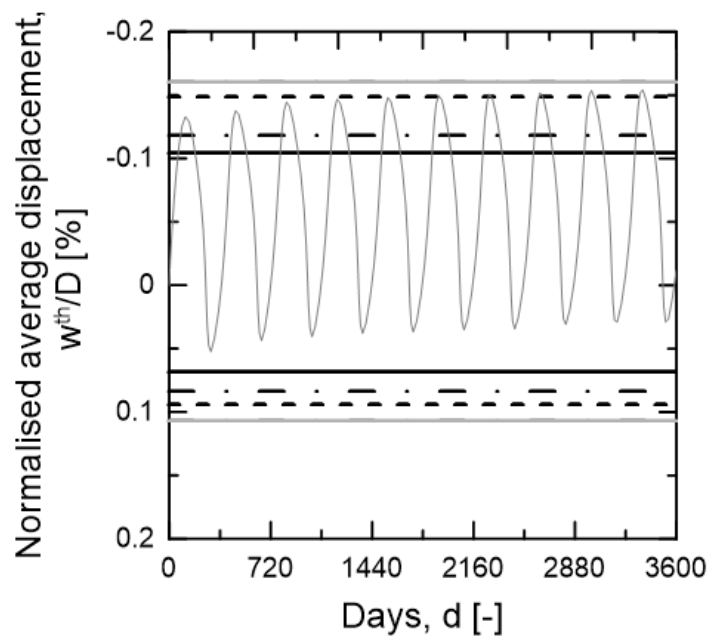


Figure 6.3: Displacement trend obtained with 8 months heating + 4 months cooling configuration in case of the real design case.

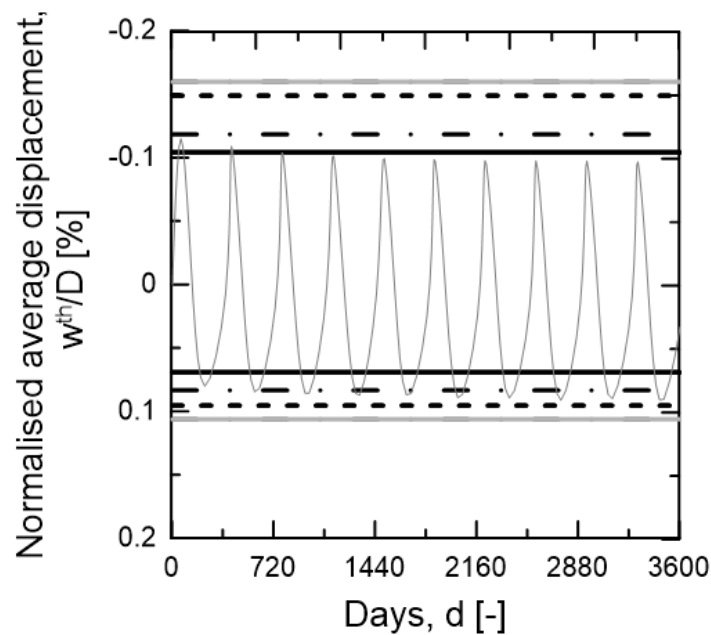


Figure 6.4: Displacement trend obtained with 4 months heating + 8 months cooling configuration in case of the real design case.

6.4.2 Displacement trends obtained in the proposed design case

In this chapter the comparison between the displacement trends obtained with the three aforementioned configurations have been carried out in the case of the proposed design case with the pile length equal to 19.2 m (Figure 6.5 – Figure 6.7).

In the figure 6.5 the comparison between the stationary models and the second configuration (6 months of heating plus 6 months of cooling) has been pictured. For this type of configuration there was no increase in the pile head displacement because the sinusoidal is balanced and also because of for the same reasons stated for figure 6.2. The displacement given by the cyclic analysis does not exceed that given by the single pile analysis. In the Figure 6.6 the comparison between the stationary models and the second configuration (8 months of heating plus 4 months of cooling) has been pictured. For this type of configuration, the head displacement increase with the time 5% exceeding the value given by the single pile analysis. In the Figure 6.7 the comparison between the stationary models and the second configuration (4 months of heating plus 8 months of cooling) has been represented. In this case an increasing of cooling displacement not exceed the value given by the 3-D FEM analysis with linear thermal expansion coefficient equal to zero.

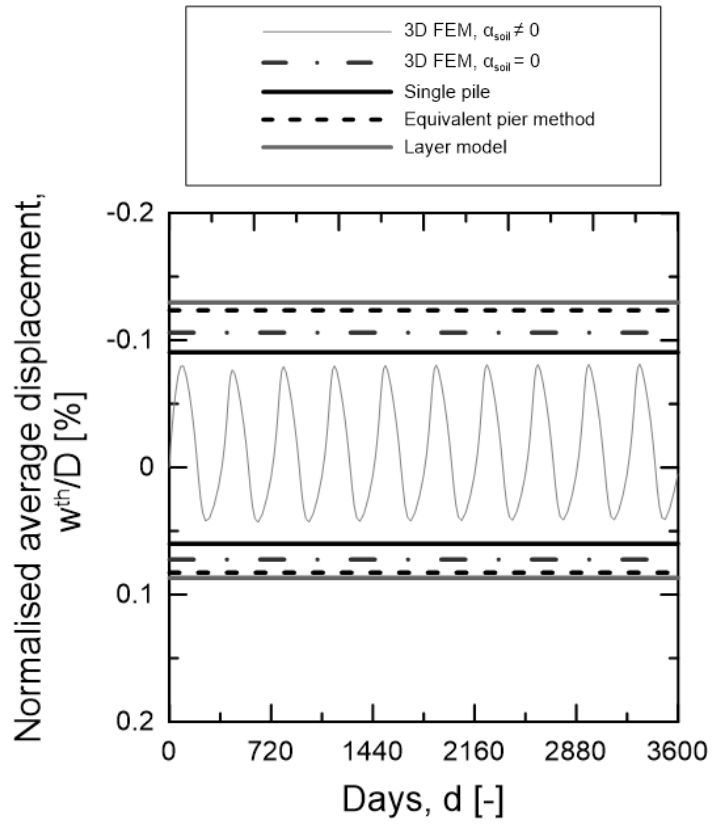


Figure 6.5: Displacement trend obtained with 6 months heating + 6 months cooling configuration in case of the proposed design case.

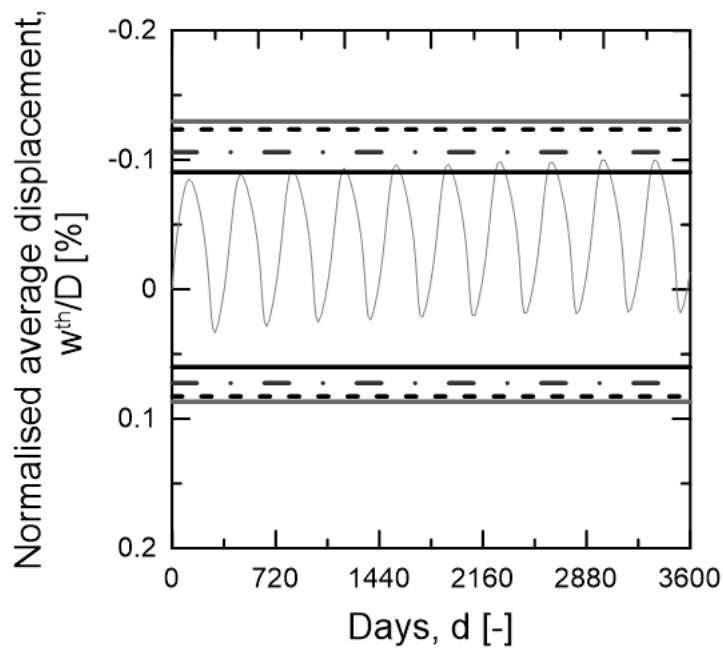


Figure 6.6: Displacement trend obtained with 8 months heating + 4 months cooling configuration in case of the proposed design case.

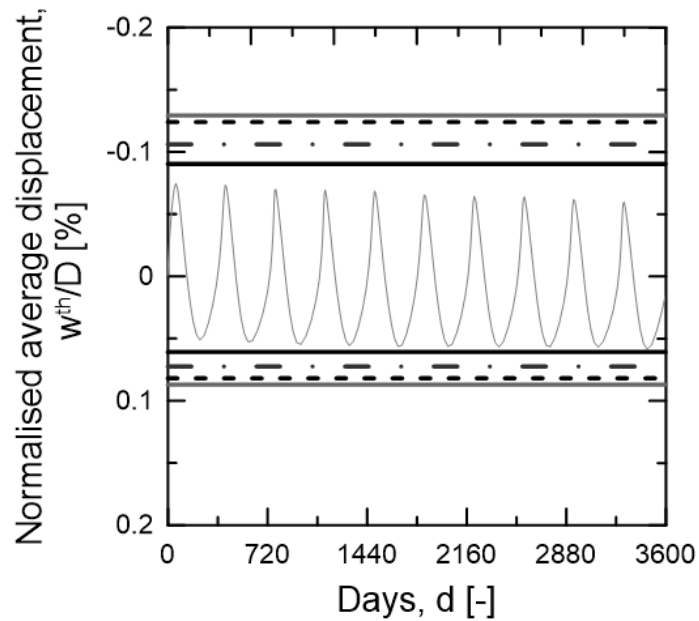


Figure 6.7: Displacement trend obtained with 4 months heating + 8 months cooling configuration in case of the proposed design case.

Concluding:

- In both design cases the most burdensome situation is the configuration 2 (8 months of heating plus 4 months of cooling);
- In this configuration, the value of displacement value provided by the real design case is higher than that in the proposed design case, even reaching the value provided by the equivalent pier method.
- In the proposed design case the single pile analysis is a benefit of safety;
- In the general case the value of layer model has never been exceeded and during a simplified design may use the values of displacement provided by it.

In the following chapters will be called:

- Configuration I: 6 months heating + 6 months cooling;
- Configuration II: 8 months heating + 4 months cooling;
- Configuration III: 4 months heating + 8 months cooling.

6.4.3 Stress field comparisons between the study cases for Configuration I

In the Figure 6.8 the comparison between the stress trends obtained with single pile analysis (2-D axisymmetric model), 3-D FEM analysis with linear thermal expansion coefficient equal to zero and

3-D FEM analysis with linear thermal expansion coefficient different from zero in case of the real design case for the Configuration I, have been pictured:

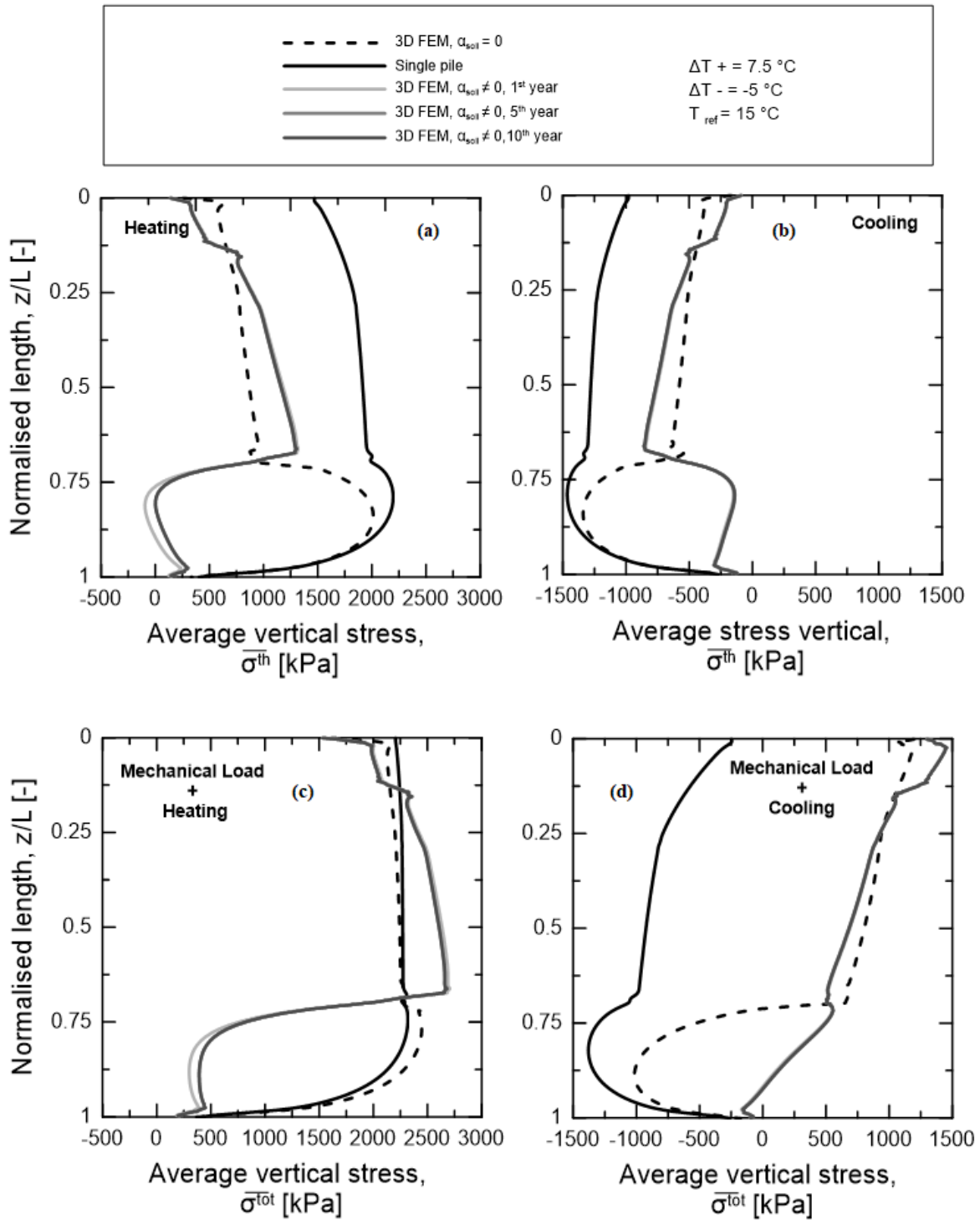


Figure 6.8: Comparison of stress trends with depth in case of the real design case for Configuration I.

Figure 6.8 (a): comparison between thermal stress trends due to heating thermal load; **Figure 6.8 (b):** comparison between thermal stress trends due to cooling thermal load; **Figure 6.8 (c):** comparison between total stress trends due to heating thermal load in conjunction with mechanical load; **Figure 6.8 (d):** comparison between total stress trends due to cooling thermal load in conjunction with mechanical load.

In the Figure 6.8 (a) the comparison between the stress trends in case of heating thermal load have been reported: the single pile analysis (with $\alpha_{soil} = 0$ for each soil layer) tend to overrate the value of stress within the pile, but the maximum stress is almost similar to that given by 3-D FEM analysis with linear thermal expansion coefficient equal to zero. In case of cyclic analysis, as explained in the previous chapters, the value of stresses do not change drastically because the sinusoidal is balanced and the thermal variation are very close each other. An important point to explain is the value of the tension in the bottom part of the pile depth: during the cyclic analysis in the layer D (molasse) there is a return in traction and in fact almost all the compression is lost because the $\alpha_{Layer D}$ is greater than that of the pile (α_{EP}) and tends to pull down the pile. The reverse situation occurs for cooling thermal load (Figure 6.8 (b)). In the Figure 6.8 (c) and (d) the total stress trends have been pictured. In the Figure 6.8 (c) the maximum stress obtained from each analysis is almost the same. In the Figure 6.8 (d) the values of the maximum stress are different each other because in the models where the linear thermal expansion coefficients are equal to zero and the maximum occurs in the bottom part of the pile (layer D) where in the cyclic analysis the behavior is completely different. Another important note is about the value of head pile stress in the single pile analysis: that value is negative because is the average value of the stress within each pile and in this analysis EP1 is mechanically unloaded and the values of stresses are all negative.

In the Figure 6.9 the comparison between the stress trends obtained with single pile analysis (2-D axisymmetric model), 3-D FEM analysis with linear thermal expansion coefficient equal to zero and 3-D FEM analysis with linear thermal expansion coefficient different from zero, in case of the proposed design case for the Configuration I, have been represented.

In the Figure 6.9 (a) the comparison between the stress trends in case of heating thermal load have been reported. The single pile analysis (with $\alpha_{soil} = 0$ for each soil layer) tend to overrate the value of stress within the pile, in fact the maximum stress is almost two times to that given by 3-D FEM analysis with linear thermal expansion coefficient equal to zero. The same situation occurs in the case of cooling thermal load (Figure 6.9 (b)). In the Figure 6.9 (c) and (d) the total stress trends have been pictured. The difference highlighted in the Figure 6.9 (d) occurs for the same aforementioned reason.

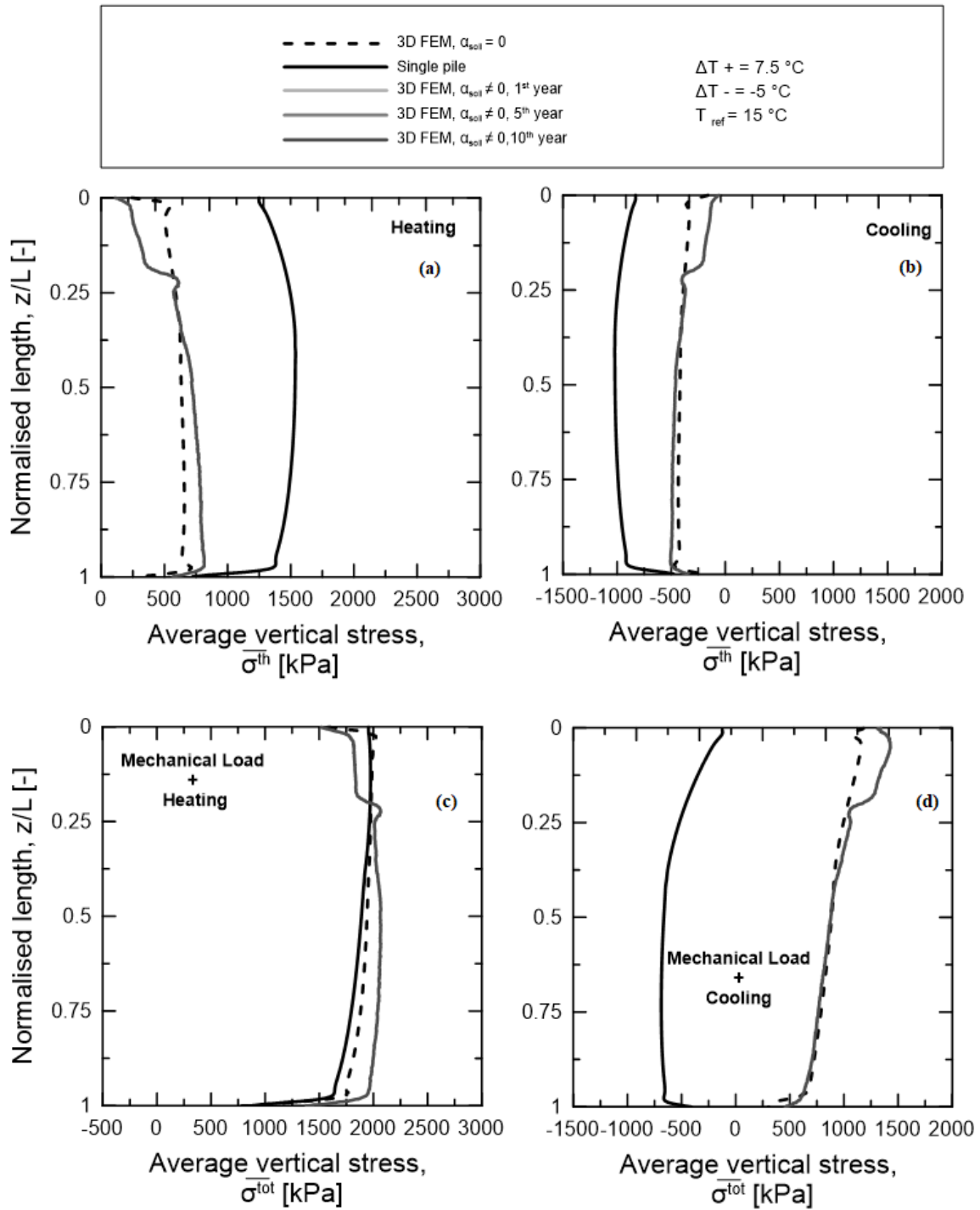


Figure 6.9: Comparison of stress trends with depth in case of the proposed design case for Configuration I.

Figure 6.9 (a): comparison between thermal stress trends due to heating thermal load; **Figure 6.9 (b):** comparison between thermal stress trends due to cooling thermal load; **Figure 6.9 (c):** comparison between total stress trends due to heating thermal load in conjunction with mechanical load; **Figure 6.9 (d):** comparison between total stress trends due to cooling thermal load in conjunction with mechanical load.

6.4.4 Stress field comparisons between the study cases for Configuration II

In the Figure 6.10 the comparison between the stress trends obtained with single pile analysis (2-D axisymmetric model), 3-D FEM analysis with linear thermal expansion coefficient equal to zero and

3-D FEM analysis with linear thermal expansion coefficient different from zero in case of the real design case for the Configuration II, have been pictured:

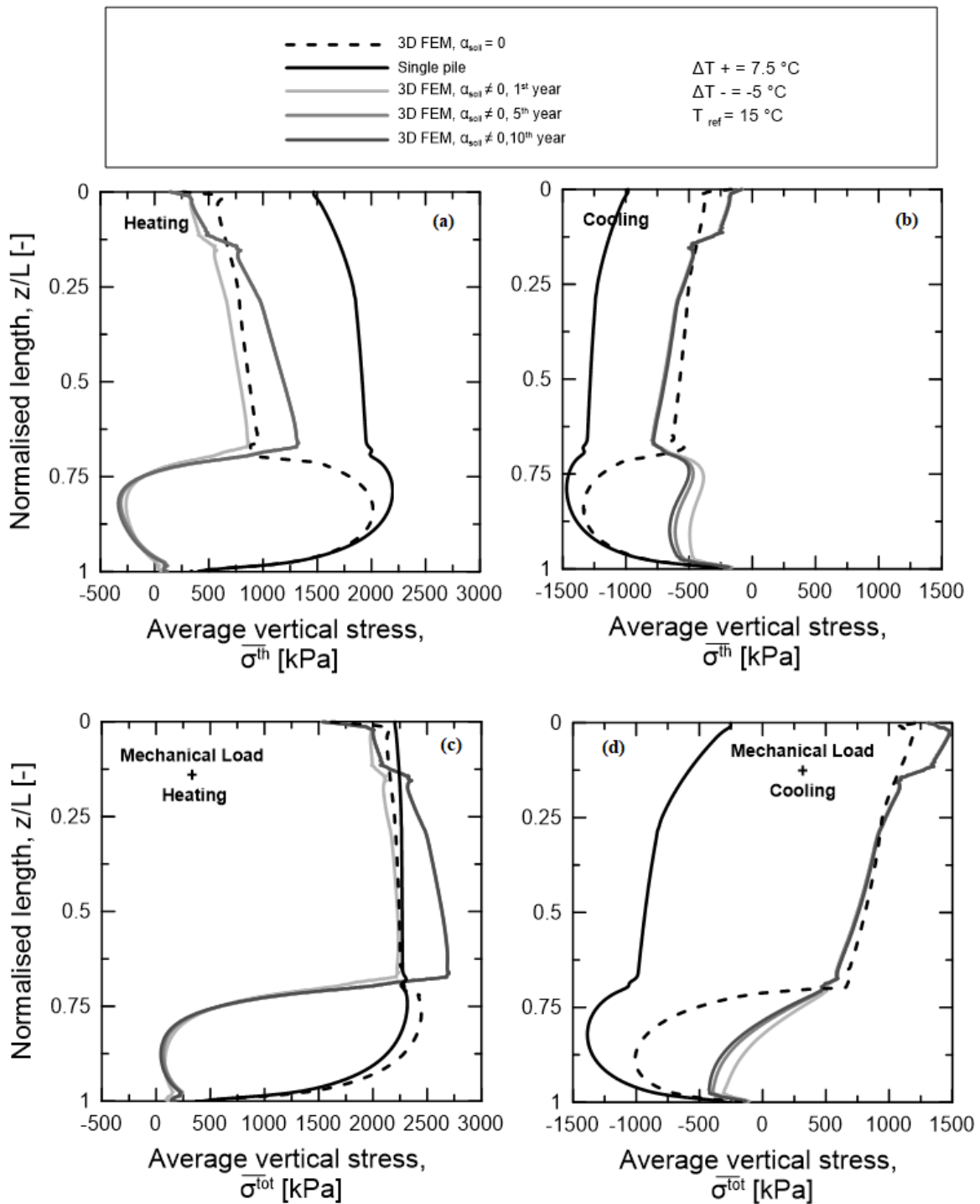


Figure 6.10: Comparison of stress trends with depth in case of the real design case for Configuration II.

Figure 6.10 (a): comparison between thermal stress trends due to heating thermal load; **Figure 6.10 (b):** comparison between thermal stress trends due to cooling thermal load; **Figure 6.10 (c):** comparison between total stress trends due to heating thermal load in conjunction with mechanical load; **Figure 6.10 (d):** comparison between total stress trends due to cooling thermal load in conjunction with mechanical load.

In the Figure 6.10 (a) since the sinusoidal action is unbalanced and as the number of cycles increases and therefore the structure tends to store as much heat as possible, the values of the stresses increase. In fact, in the last cycle the values of the stresses are greater than those given by the first. But in general they never exceed those given by the models with linear thermal expansion coefficient equal to zero. The inverse situation occurs under the action of the cooling thermal load, because it tends to cool down less and the traction stresses decrease (Figure 6.10 (b)).

In the Figure 6.11 the comparison between the stress trends obtained with single pile analysis (2-D axisymmetric model), 3-D FEM analysis with linear thermal expansion coefficient equal to zero and 3-D FEM analysis with linear thermal expansion coefficient different from zero, in case of the proposed design case for the Configuration II, have been represented.

In the Figure 6.11 (a) and (b) the values of thermal stresses change, but this variation is negligible even if the sinusoidal action is unbalanced.

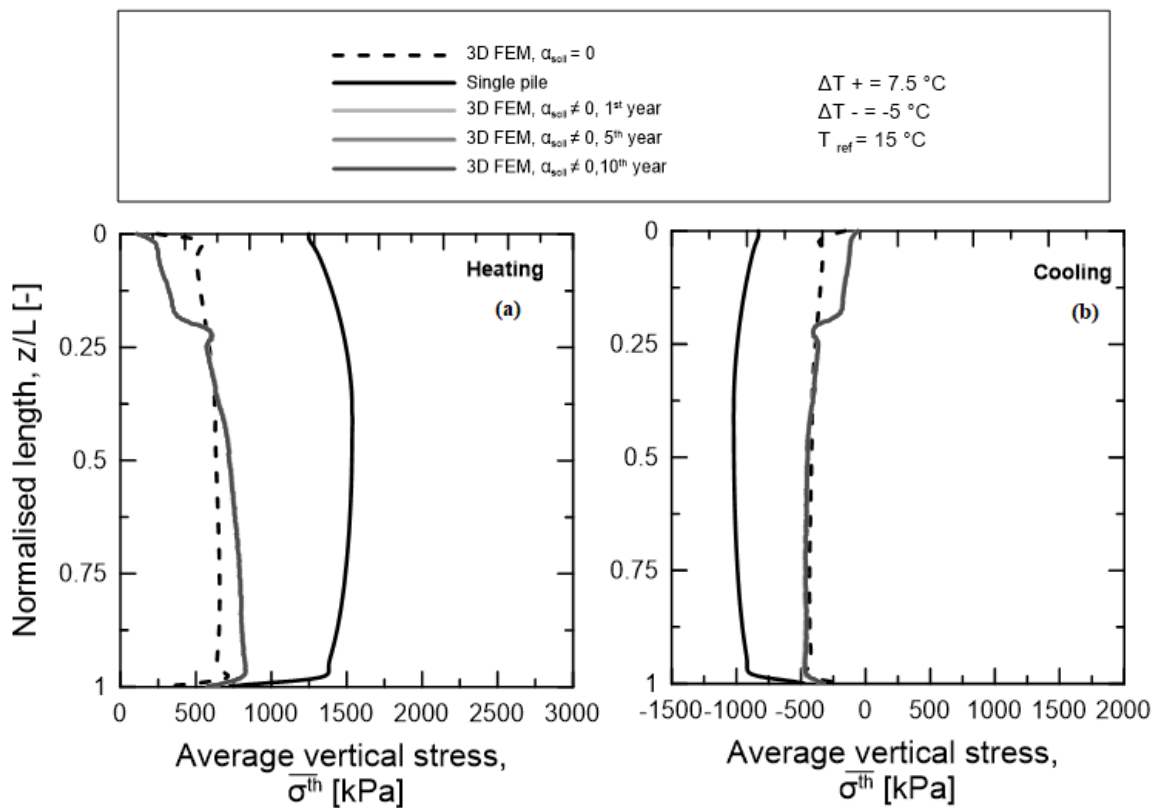


Figure 6.11: Comparison of stress trends with depth in case of the proposed design case for Configuration II.

Figure 6.11 (a): comparison between thermal stress trends due to heating thermal load; **Figure 6.11 (b):** comparison between thermal stress trends due to cooling thermal load;

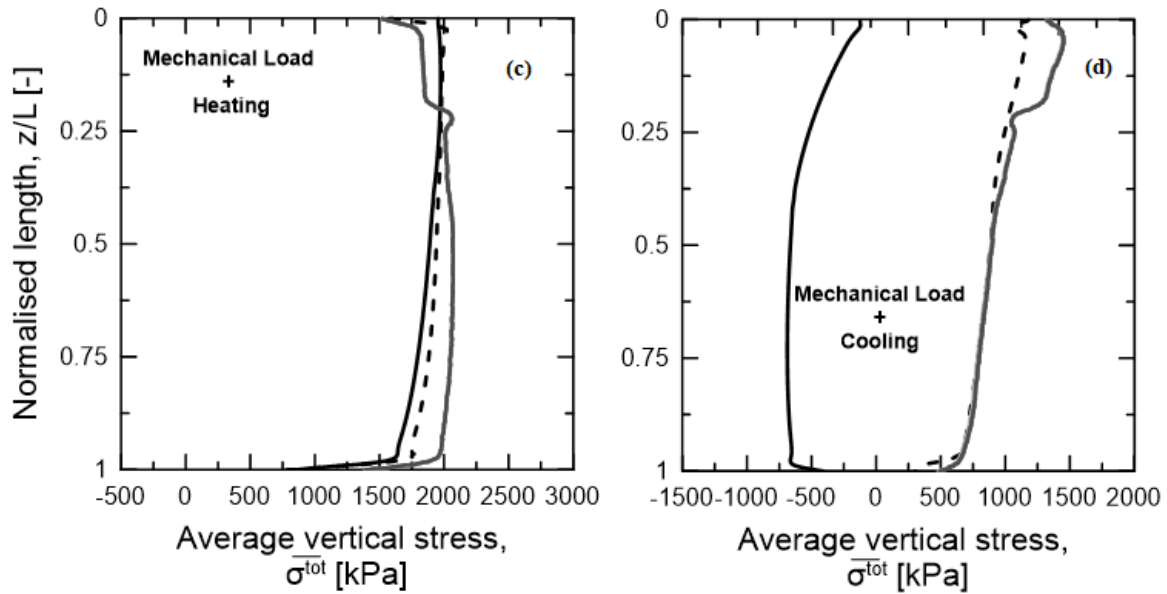


Figure 6.11 (c): comparison between total stress trends due to heating thermal load in conjunction with mechanical load; **Figure 6.11 (d):** comparison between total stress trends due to cooling thermal load in conjunction with mechanical load.

6.4.5 Stress field comparisons between the study cases for Configuration III

In the Figure 6.12 the comparison between the stress trends obtained with single pile analysis (2-D axisymmetric model), 3-D FEM analysis with linear thermal expansion coefficient equal to zero and 3-D FEM analysis with linear thermal expansion coefficient different from zero in case of the real design case for the Configuration III, have been pictured.

In the Figure 6.12 (a) since the sinusoidal action is unbalanced and as the number of cycles increases and therefore the structure tends to cool more and more, the values of the compressive stresses decrease. In fact, in the last cycle the values of the stresses are lower than those given by the first. But in general they never exceed those given by the models with linear thermal expansion coefficient equal to zero. The inverse situation occurs under the action of the cooling thermal load, because as the soil tends to cool more and more the tensile stresses increase (Figure 6.12 (b)). In the Figure 6.12 (c) and (d) the total stress trends have been pictured.

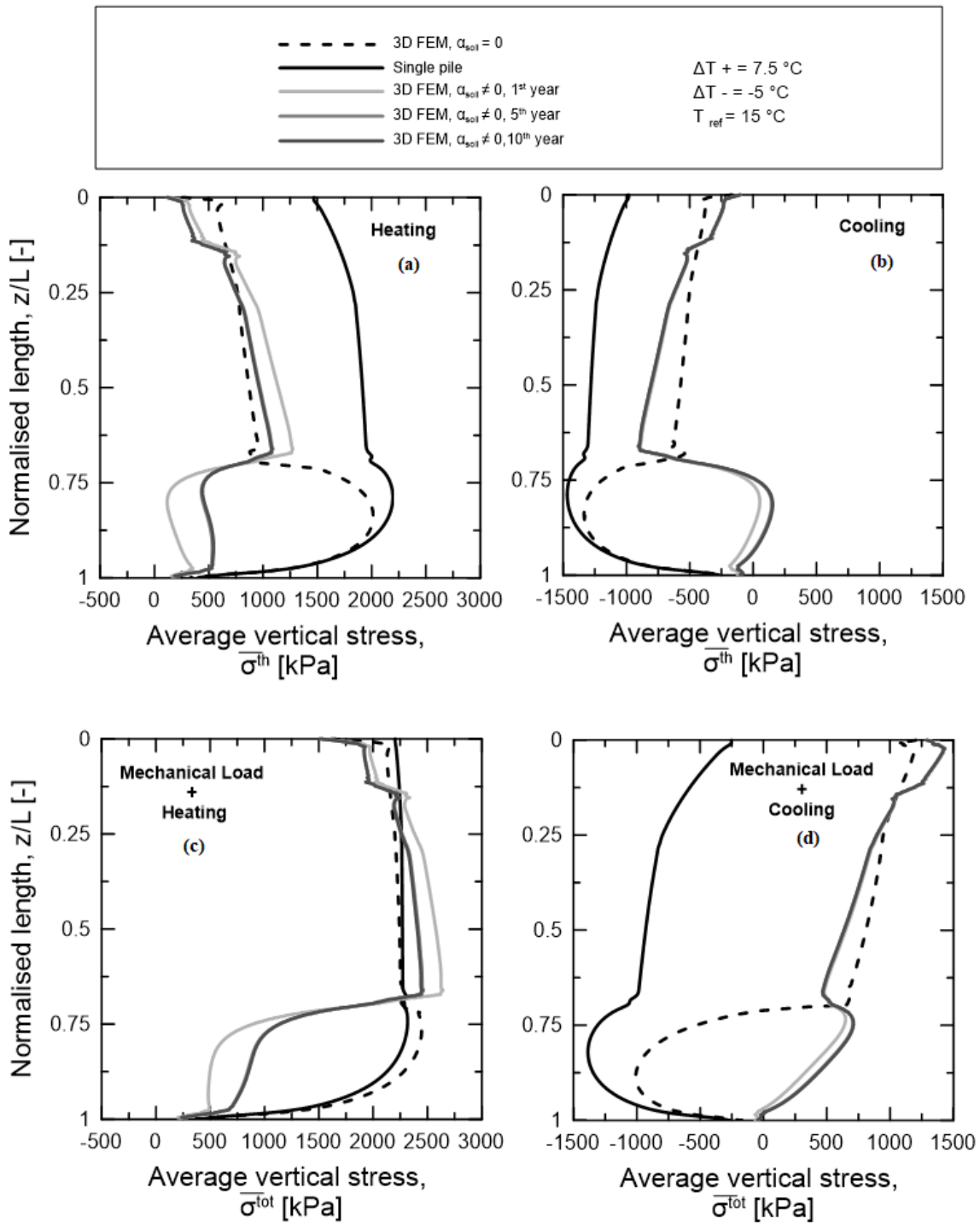


Figure 6.12: Comparison of stress trends with depth in case of the real design case for Configuration III.

Figure 6.12 (a): comparison between thermal stress trends due to heating thermal load; **Figure 6.12 (b):** comparison between thermal stress trends due to cooling thermal load; **Figure 6.12 (c):** comparison between total stress trends due to heating thermal load in conjunction with mechanical load; **Figure 6.12 (d):** comparison between total stress trends due to cooling thermal load in conjunction with mechanical load.

In the Figure 6.13 the comparison between the stress trends obtained with single pile analysis (2-D axisymmetric model), 3-D FEM analysis with linear thermal expansion coefficient equal to zero and 3-D FEM analysis with linear thermal expansion coefficient different from zero in case of the proposed design case for the Configuration III, have been pictured.

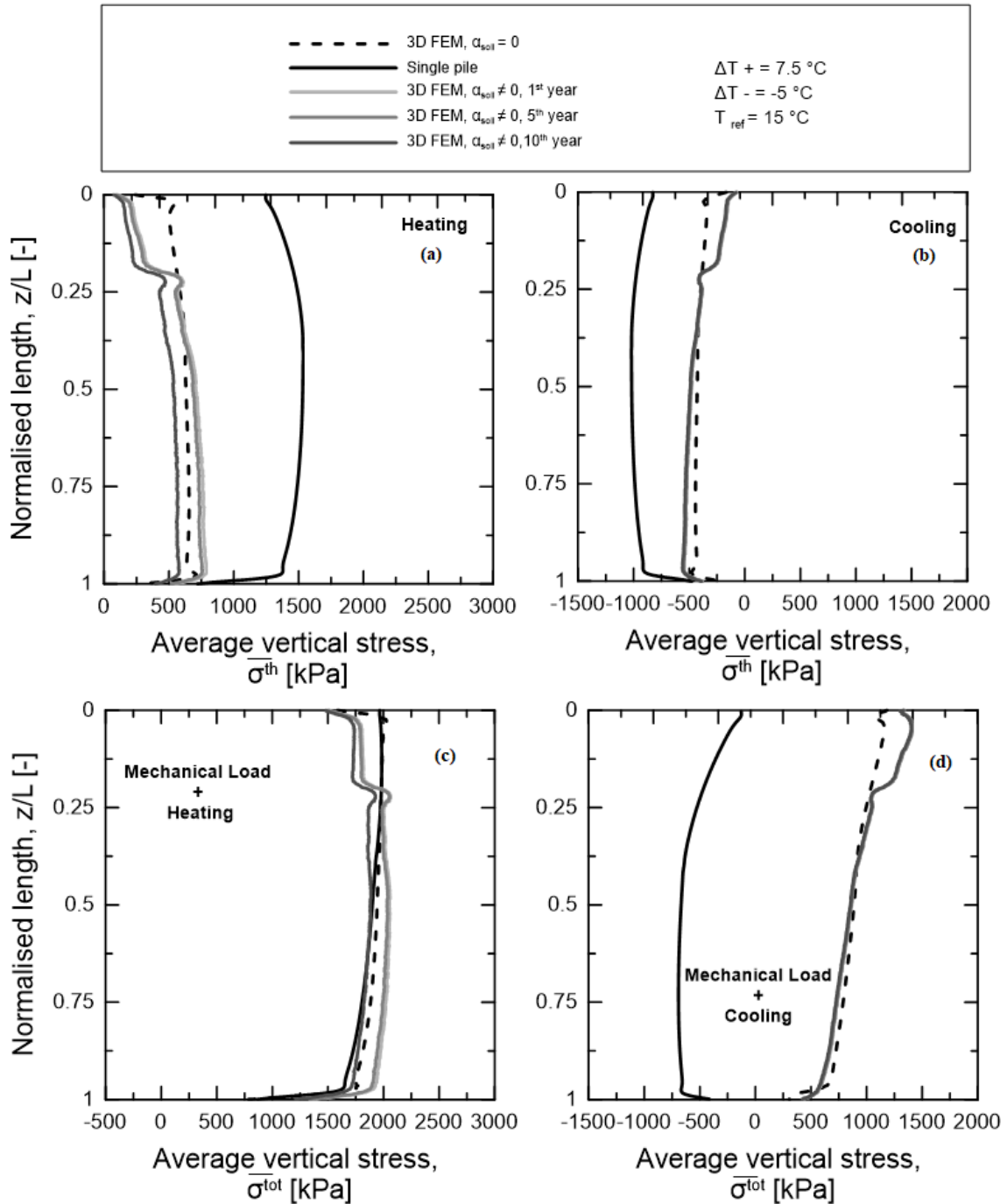


Figure 6.13: Comparison of stress trends with depth in case of the proposed design case for Configuration III.

Figure 6.13 (a): comparison between thermal stress trends due to heating thermal load; **Figure 6.13 (b):** comparison between thermal stress trends due to cooling thermal load; **Figure 6.13 (c):** comparison between total stress trends due to heating thermal load in conjunction with mechanical load; **Figure 6.13 (d):** comparison between total stress trends due to cooling thermal load in conjunction with mechanical load.

In the Figure 6.13 (a) as the cycles increase the compressive stresses, due to the thermal load, decrease. In the Figure 6.13 (b) the tensile stress variation is different from zero, but is negligible.

6.4.6 Concluding Remarks

In order to perform a complete design procedure for energy piles, taking into account the long-term effects due to the action of the thermal load, some concluding points must be highlighted:

- the most burdensome situation in both study cases is the Configuration II when the compressive stresses are evaluated; instead for the traction ones the most dangerous is the third;
- when the situation $\alpha_{soil}/\alpha_{EP} > 1$ or $X > 1$ occurs in one of the soil layers, the stress trend could be completely different than that of given by the analysis with linear thermal expansion coefficient equal to zero;
- as regards stresses, the analysis of the single pile (2-D axisymmetric analysis) is conservative in any case. Therefore, besides saving computational time, it also provides acceptable values, but sometimes it tends to overestimate the tensile stresses especially when the condition explained in the previous point occurs.

Chapter 7

Concluding remarks

7.1 Summary

This master thesis focused on the thermo-mechanical behavior and performance of an innovative, multifunctional technology that can be used for energy transfer applications as well as for providing structural support to any type of built environment, i.e., energy piles. Energy piles are geostructures generally applied in groups that operate as structural supports and geothermal heat exchangers. As a consequence of their twofold operation, these geostructures are subjected to the unprecedented coupled action of mechanical and thermal loads. This action involves innovative challenges for engineers, particularly from analysis and design viewpoints. The reason is that it causes variations in the temperature, stress, deformation and displacement field in the subsurface. These phenomena profoundly influence the energy, geotechnical and structural behavior and performance of the energy piles, with a consequential impact on the behavior and performance of the superstructures they support and supply with energy.

Exactly the main goal of this work has been provide a complete procedure in order to perform the Ultimate Limit State (ULS) and Serviceability Limit State (SLS) verifications, extending the procedure widely used for conventional piles. Analyzing all features of the entire problem (single pile and group piles) a complete guideline has been provided, in order to avoid some problems related to some design choices and approximations to do during the design phase.

Prior to this work, a substantial amount of research had been made available to address the thermomechanical performance of single energy piles (Rotta Loria, 2018), providing a complete framework about the effects due to thermal load applied on the single pile and taking into account the pile group effect. However, in contrast to the currently available knowledge for energy piles subjected to mechanical loads and thermal load,

- I. Limited knowledge, if available, was present to quantify the effects due to thermal load during the life of the structure;
- II. Even if simplified models have been developed in order to take into account the pile group effect, firstly, a real application was never performed. Moreover, with this lack, the possible problems that can be addressed during the design phase was never evaluated;
- III. No complete comparisons between all possible methods (in a real case application) was never done, in order to identify the best model to use during the design related to energy piles group;
- IV. No long-term analysis was never carried out in order to quantify the effect of the thermal load over time.

To address the aforementioned challenges, this master thesis took the following steps:

- Investigated the thermo-mechanical behavior and performance of energy pile considered isolated (single pile analysis) in order to quantify the thermal effects;
- Perform all serviceability verifications for energy piles;
- Extend the analytical models performed in the previous work (Rotta Loria, 2018) for the real case, in order to quantify the values given by all models to take into account the pile group effect;
- Perform a complete time-dependent analysis in order to take into account the long-term effect.

The methods employed in this master thesis comprised numerical modelling and analytical modelling.

In these contexts:

- I. The coupling numerical and analytical modelling has been useful, above all, for the comparisons and the validations of the analytical models;
- II. Analytical modelling has been used to provide a simplified and quick tool to estimate the interaction among the piles;
- III. Numerical modelling has been used to provide a sophisticated and precise analysis tool to avoid any type of mistakes.

7.2 General conclusion

The results presented in this master thesis project allow summarizing the following conclusions:

- The effect of the thermal load is not significant at Ultimate Limit State, but during the life of the structure (Serviceability Limit State) because the stress and displacement fields change considerably;
- During the geotechnical ultimate limit state design it is advisable not to pierce layers of rock to ensure a greater shaft capacity, but try to place the base of the pile on it. Not piercing it, the problem of estimating the lateral flow rate is excluded, which can be calculated with certain relationships according to certain conditions;
- During the structural ultimate limit state design calculate the minimum reinforcement with the new relation, according to Eurocodes, avoids the risk of not verifying the SLS checks;
- The Eurocodes dispositions for elastic analysis (nil Poisson ratio and Young's Modulus equal to that of the cracked section) underrate the thermal stresses and this represent a problem for the structure during its life;
- The effect of cracked Young's modulus is also visible in the thermal displacement: with a lower value of Young's Modulus the displacement decrease;
- The effect of the nil Poisson ratio is negligible;
- Even if the most burdensome load combination is the characteristic one, the verifications must be carried out with the quasi- permanent combination because is directly related with the equations provided by Eurocodes;
- When the verifications have been carried out with the characteristic combination there is the risk to increase the amount of the reinforcement, so overestimating it;
- the best analytical model (in average) is the layer model because provide acceptable values also when a rigid stratum is present, instead of the continuous model. This happens because the continuous model take into account the interaction between the soil layers and if there is a rigid soil layer the Young's Modulus of it is much higher than that of others soil layers and when the mean value of shear modulus between two layers is very far from the real values of shear modulus of each soil layers;
- when the soil layers parameters are similar among them the best model to use is the continuous model;
- equivalent pier method has been modelled as free head model but in case in which needs to add the slab because its effect is very important, the value calculated with the equation (9.1)

must be divided by the total piles area (when the slab is rigid or when $K_{SS} > 0.1$) or by the equivalent pier area (when the slab is flexible or when $K_{SS} < 0.1$) both for thermal and mechanical load;

- when both numerical and analytical analysis are performed with a linear thermal expansion coefficient of each soil layer equal to zero, the difference with the those performed with α_{Layer} in terms of displacement is not great;
- during the cyclic analysis, the most burdensome situation for both type of stresses (compressive and tensile) is that when an unbalanced sinusoidal is applied;
- when the situation $\alpha_{soil}/\alpha_{EP} > 1$ or $X > 1$ occurs in one of the soil layers, the stress trend could be completely different than that of given by the analysis with linear thermal expansion coefficient equal to zero;
- as regards stresses, the analysis of the single pile (2-D axisymmetric analysis) is conservative in any case. Therefore, besides saving computational time, it also provides acceptable values, but sometimes it tends to overestimate the tensile stresses especially when the previous point occurs;
- Linear thermo-elasticity theory appears to be an expedient and sufficiently accurate tool for describing the geotechnical and structural behavior of a wide number of energy pile groups for both research and engineering purposes. In fact the displacement never exceed the 2% of diameter (chapter 6, Figure 6.2-6.7): below this threshold value we can consider an elastic behavior;
- Thermo-mechanical numerical analyses appear to be suitable tools for modelling the geotechnical, structural and energy behavior of most energy pile groups surrounded by saturated soil deposits without intrinsic groundwater flow.

Page intently left white

Bibliography

- [I] Bowles, J. E. (1988). *Foundation analysis and design*. McGraw-Hill.
- [II] Burland, J. & Twine, D. (1988). The shaft friction of bored piles in terms of effective strength. *Proceeding of 1st International Conference on Deep Foundations, Bored and Augered Piles*, pp. 411-420.
- [III] COMSOL (2014) COMSOL Multiphysics version 4.3: User's Guide. Burlington, Massachusetts, United States of America.
- [IV] Cooke, R., Sillett, D., Smith, D. & Gooch, M. (1981). Some observations of the foundation loading and settlement of a multi-storey building on a piled raft foundation in London clay. In *ICE Proceedings*. Thomas Telford, vol. 70: 433-460.
- [V] Chow, Y. (1986). Analysis of vertically loaded pile groups. *International Journal for Numerical and Analytical Methods in Geomechanics* 10(1): 59-72.
- [VI] Ente Nazionale Italiano di Unificazione (UNI) (1992). *Eurocode 2 - Design of concrete structures* or *UNI EN 1992*.
- [VII] Ente Nazionale Italiano di Unificazione (UNI) (1992). *Eurocode 7: Geotechnical Design*.
- [VIII] Ente Nazionale Italiano di Unificazione (UNI) (1992). *Eurocode 0: Basis of structural design* or *UNI EN 1990*.
- [IX] Ente Nazionale Italiano di Unificazione (UNI) (2016). UNI 11104 - Prospetto 5 "Valori limite per la composizione e le proprietà del calcestruzzo".
- [X] Fleming, K., Weltman, A., Randolph, M. & Elson, K. (2008) *Piling engineering*. CRC press.
- [XI] Frank, R. (1975) Etude théorique du comportement des pieux sous charge verticale: Introduction de la dilatance. Laboratoires des Ponts et Chaussées, Ph.D. Thesis, pp. 243.
- [XII] Giordano L. (2016). Construction of Interaction domain. *Slides of R.C. and P.R.C. course*. Politecnico di Torino (2015/2016).

- [XIII] Gorbunov-Posadov, M. I. & Serebrjanyi, R. V. (1961) Design of structures on elastic foundation. In *5th International conference on Soil Mechanics and Foundation Engineering.*, vol. 1, pp. **643-648**.
- [XIV] Horvath, R., Kenney, T. & Trow, W. (1980) Results of tests to determine shaft resistance of rock-socketed drilled piers. In *International Conference on Structural Foundations on Rock, 1980, Sydney, Australia.*, vol. 1.
- [XV] Knellwolf C., Peron H. and Laloui L. (2011), *Geotechnical Analysis of Heat Exchanger Piles*.
- [XVI] Lancellotta, R. (1995) *Geotechnical engineering*. Balkema, Rotterdam.
- [XVII] Laloui L. and Rotta Loria A.F. (2019), Analytical modelling of capacity and deformation of single energy piles (Ch. XVIII). *Analysis and Design of Energy Geostructures*, pp. **5-26**.
- [XVIII] Marti P. (2013), Strip method, *Theory of structures*, pp. **563-567**.
- [XIX] Mindlin, R. D. (1936) Force at a point in the interior of a semi-infinite solid. *Journal of Applied Physics* **7(5)**, pp. **195-202**.
- [XX] Mylonakis G. (1996), *Settlement and load transfer mechanism of pile and pile groups in layered soil*. Contributions to Static and Seismic Analysis of Piles and Pile-Supported Bridge Piers, State University of New York at Buffalo, Ph.D. thesis, pp. **1-26**.
- [XXI] Mylonakis, G. & Gazetas, G. (1998). *Settlement and additional internal forces of grouped piles in layered soil*. *Geotechnique* 48, No. 1: 55-72, pp. **62-69**.
- [XXII] Mylonakis G. (2001), Non-linear regression analyses. *Winkler modulus for axially loaded piles*. *Geotechnique* 51, No. 5: 455-461, p. **460**.
- [XXIII] Muttoni and M. Fernández Ruiz (2015), Dalles: Méthode des bandes. *Slide of "Structures en béton"*. EPFL.
- [XXIV] Poulos, H. G. (1968) Analysis of the settlement of pile groups. *Géotechnique* 18(4): **449-471**.
- [XXV] Poulos, H. G. & Mattes, N. S. (1974) Settlement of pile groups bearing on stiffer strata. *Journal of Geotechnical and Geoenvironmental Engineering* 100(GT2): **185-190**.
- [XXVI] Poulos H.G. and Davies E.H. (1980), Settlement of pile groups. *Pile foundations analysis and design*.

- [XXVII] Poulos, H. G. (1993) Settlement prediction for bored pile groups In Proceedings of Deep Foundations on Bored and Auger Piles. Balkema, Rotterdam, pp. 103-117.
- [XXVIII] Randolph, M. F. & Wroth, C. P. (1978) Analysis of deformation of vertically loaded piles. *Journal of the Geotechnical Engineering Division* 104(12): **1465-1488**.
- [XXIX] Randolph, M. & Wroth, C. (1979a) A simple approach to pile design and the evaluation of pile tests. In Behavior of Deep Foundations. ASTM International.
- [XXX] Randolph, M. F. & Wroth, C. (1979b) An analysis of the vertical deformation of pile groups. *Géotechnique* 29(4): **423-439**.
- [XXXI] Rammal D., Mroueh H and Burlon S. (2018), *Impact of thermal solicitations on the design of energy piles*.
- [XXXII] Rotta Loria A.F. (2018), The role of thermal loads in the geotechnical and structural, performance of energy piles, Performance-based design of case studies (Ch. II). Numerical modelling (Ch. III). The interaction factor method for energy pile groups based on analytical models (Ch. V). The equivalent pier method for energy pile groups (Ch. VII) *Thermo-mechanical performance of energy pile groups*, Ph.D. thesis, EPFL, pp. **37-47, 52-58, 101-103, 185-198, 235-239**.
- [XXXIII] Rowe, R. & Armitage, H. (1987). *A design method for drilled piers in soft rock*. Canadian Geotechnical Journal 24(1): **126-142**.
- [XXXIV] Williams, A. & Pells, P. (1981) Side resistance rock sockets in sandstone, mudstone, and shale. *Canadian Geotechnical Journal* 18(4): **502-513**.
- [XXXV] Zhang, L. & Einstein, H. H. (1998) End bearing capacity of drilled shafts in rock. *Journal of geotechnical and geoenvironmental engineering* 124(7): **574-584**.

Francesco Di Bari

Personal Information:

Permanent address: Via V.lo Boito 11, Andria (BT) - Italy

Mail: f.dibari93@gmail.com

Phone: +39 3382191620

Professional experience and appointments

September 2018 –
March 2019

Research Student, Swiss Federal Institute of Technology in Lausanne (EPFL)

Supervisors: Prof. Lyesse Laloui and Dr. Alessandro Francesco Rotta Loria

Scholarships: Politecnico di Torino and EPFL

Higher Education

March 2016 –
March 2019

M.Sc. in Structural Civil Engineering, Politecnico di Torino

Dissertation: “Procedure and Eurocodes Extension for Geothermal Piles”

Supervisors: Prof. Bernardino M. Chiaia

October 2012 –
December 2015

B.Sc. in Building Engineering, Politecnico di Bari

Dissertation: “Wood: Resistance Verifications and Design Methods”

Supervisor: Prof. Greco Rita

Final grade: 100/110

Fields of interest

Geomechanics; Structural mechanics; Energy; Multiphysical phenomena; Environmental sustainability.

Awards

Scholarships:

- 2013, Politecnico di Bari
- 2014, Politecnico di Bari
- 2015, Politecnico di Bari

Language Skills

- Mother Tongue: Italian
- English: Fluent
- French: Beginner

Organizational / managerial skills

Ability to work in a team, collaborating, sharing and creating in a positive atmosphere. Ability to relate with the public. Ability, curiosity and commitment in the learning processes. Strongly motivated to achieve continuous personal, human and professional growth. Open to different cultures, able to live and work in multicultural environments; inclined to continuous cultural exchange.